Analysis of crosstalk signals in a cylindrical layered volume conductor – Influence of the anatomy, detection system and physical properties of the tissues

by

Suretha Viljoen

Submitted in partial fulfilment of the requirements for the degree

Master of Engineering (Bio-Engineering)

in the

Faculty of Engineering, Built Environment and Information Technology

UNIVERSITY OF PRETORIA

Pretoria

May 2005

Summary

Title: Analysis of crosstalk signals in a cylindrical layered volume conductor – Influence of the anatomy, detection system, and physical properties of the tissues

Author: Suretha Viljoen

Supervisor: Dr. T. Hanekom

Co-supervisor: Prof. Dr. D. Farina

Department: Electrical, Electronic and Computer Engineering

Degree: Master of Engineering (Bio-Engineering)

A comparison of the ability of different spatial filters to reduce the amount of crosstalk in a surface electromyography (sEMG) measurement was conducted. It focused on the influence of different properties of the muscle anatomy and detection system used on the amount of crosstalk present in the measurements.

An analytical model was developed which enabled the simulation of single fibre action potentials (SFAPs). These fibres were grouped together in motor units (MUs). Each MU has characteristics which, along with the SFAPs, are used to obtain the motor unit action potential (MUAP). A summation of the MUAPs from all the MUs in a muscle leads to the electromyogram (EMG) signal generated by the muscle. This is the first model which simulates a complete muscle for crosstalk investigation. Previous studies were done for

single fibres (Farina & Rainoldi 1999; Farina et al. 2002e; Farina et al. 2004a) or MUs (Dimitrova et al. 2002; Dimitrov et al. 2003; Winter et al. 1994). Lowery et al. simulated a complete muscle, but only investigated one spatial filter (Lowery et al. 2003a). This model is thus the first of its kind.

EMG signals were generated for limbs with different anatomical properties and recorded with various detection systems. The parameters used for comparison of the recorded signals are the average rectified value (ARV) and mean frequency (MNF), which describe the amplitude and frequency components of an EMG signal, respectively. These parameters were computed for each EMG signal and interpreted to make recommendations on which detection system results in the best crosstalk rejection for a specific experimental set-up.

The conclusion is that crosstalk selectivity in an sEMG measurement is decreased by increasing the thickness of the fat layer, increasing the skin conductivity, decreasing the fibre length, increasing the interelectrode distance of the detection system, placing the detection electrodes directly above the end-plate area or an increased state of muscle contraction. Varying the contraction force strength or placing the detection electrodes directly above the tendon area has no influence on the crosstalk selectivity.

For most of the conditions investigated, the normal double differential (NDD) detection system results in the best crosstalk reduction. The only exceptions are a set-up with poor skin conductivity where NDD and double differential (DD) performed comparably, and the two simulations in which the muscle length is varied, where the DD filter performed best.

Previous studies have found DD to be more selective for crosstalk rejection than NDD (Dimitrov et al. 2003; Farina et al. 2002a; Van Vlugt & Van Dijk 2000). Possible reasons for the contradictory results are the high value of skin conductivity currently used or influences of the muscle geometry.

Key terms: sEMG, modelling, crosstalk, analytical model, spatial filters, MUAP, ARV, MNF, muscle shortening, increased contraction force.

Opsomming

Titel: Analise van kruisspraakseine in ´n volumegeleier – Invloed van die anatomie, deteksiestelsel en fisiese eienskappe van die weefsel

Outeur: Suretha Viljoen

Studieleier: Dr. T. Hanekom

Mede-studieleier: Prof. Dr. D. Farina

Departement: Elektriese, Elektroniese en Rekenaar-ingenieurswese

Graad: Meestersgraad in Ingenieurswese (Bio-Ingenieurswese)

In die studie word die vermoë van verskillende ruimtelike filters om kruisspraak te verwerp, ondersoek. Die klem val op die invloed wat eienskappe van die spieranatomie en deteksiestelsel op die mate van kruisspraakverwerping in ´n elektromiogram- (EMG) meting het.

´n Analitiese model is ontwerp waarmee enkelvesel-aksiepotensiale (EVAPe) opgewek kan word. Die vesels is saamgegroepeer in motoreenhede (MEe). Elke ME het sy eie eienskappe wat saam met die EVAPe gebruik word om die motoreenheid-aksiepotensiaal (MEAP) op te wek. Die EMG-sein bestaan uit ´n sommasie van al die MEAPe van die MEe in die spier. Hierdie model is die eerste waarin ´n volledige spier gesimuleer word om kruisspraak te ondersoek. Vorige studies is gedoen op enkele vesels (Farina &

Rainoldi 1999) (Farina et al. 2002e) (Farina et al. 2004a) of MEe (Dimitrova et al. 2002) (Dimitrov et al. 2003) (Winter et al. 1994). Lowery et al. het ´n hele spier gesimuleer, maar net die effek van een ruimtelike filter ondersoek (Lowery et al. 2003a). Die huidige model is dus die eerste in sy soort.

EMG-seine is gegenereer vir ledemate met verskillende anatomiese eienskappe en met verskeie deteksiestelsels gemeet. Die parameters waarmee die deteksiestelsels vergelyk word, is die gemiddelde gelykgerigte waarde en gemiddelde frekwensie, wat onderskeidelik die amplitude- en frekwensiekomponente van die sein beskryf. Hierdie parameters is vir elke EMG-sein bereken en geïnterpreteer om uitspraak te lewer oor watter deteksiestelsel die grootste mate van kruisspraakverwerping toon vir ´n spesifieke eksperimentele opstelling.

Die gevolgtrekking is dat die mate van kruisspraakverwerping in ´n oppervlak-EMG-sein verlaag word deur ´n dikker vetlaag, vel met ´n beter geleidingsvermoë, ´n korter vesellengte, ´n deteksiestelsel met ´n groter interelektrode-afstand, plasing van die meetelektrodes reg bo die motorpunt of ´n verhoogde mate van spiersametrekking. Variasie van die krag waarmee die spier saamtrek of plasing van die meetelektrodes reg bo die tendon-area het geen invloed op die mate van kruisspraakverwerping nie.

In die meeste van die situasies wat ondersoek is, het die normaal dubbel-differensiële (NDD) deteksiestelsel die beste kruisspraakverwerping getoon. Die enigste uitsonderings is ´n vel met ´n baie swak geleidingsvermoë, waar die NDD en dubbel differensiële (DD) deteksiestelsels se resultate vergelykbaar is, en die twee simulasies waar die spierlengte verander is. Hier het die DD-stelsel die beste gevaar.

Vorige studies het gevind dat DD meer selektief vir kruisspraakverwerping is as NDD (Dimitrov et al. 2003; Farina et al. 2002a; Van Vlugt & Van Dijk 2000). Moontlike redes vir die verskille is die hoë velgeleiding wat gebruik is of die invloed van die spier-geometrie.

Sleutelterme: oppervlak-EMG, modellering, kruisspraak, analitiese model, ruimtelike filter, motoreenheid-aksiepotensiaal, gemiddelde gelykgerigte waarde, gemiddelde frekwensie, spierverkorting, toenemende saamtrekkrag.

List of abbreviations

1-D	-	one-dimensional
2-D	-	two-dimensional
APs	-	action potentials
ARV	-	average rectified value
AU	-	arbitrary units
CNS	-	central nervous system
CSA	-	cross-sectional area
CV	-	conduction velocity
DD	-	double differential
EMG	-	electromyogram
HSR-EMG	-	high spatial resolution EMG
IB^2	-	inverse binominal filter of the second order
IED	-	interelectrode distance
IPI	-	interpulse interval
IZ	-	innervation zone
LDD	-	longitudinal double differential
MNF	-	mean frequency
Mono	-	monopolar
MUAP	-	motor unit action potential
MUs	-	motor units

MVC	-	maximum voluntary contraction
NDD	-	normal double differential
NMJ	-	neuromuscular junction
NU	-	normalised units
PCSA	-	physiological cross-sectional area
SD	-	single differential
sEMG	-	surface electromyography
SFAP	-	single fibre action potential

Table of contents

1

Introduction

1.1. Problem statement

Electric signals generated from the contraction of muscle fibres can be measured on the skin surface. This is called surface electromyography (sEMG). sEMG measurements can be used in rehabilitation after sports injuries or large operations, for control of myoelectric prosthesis, biofeedback and occupational medicine, to name a few. Because the distance between the source of the electric potential and the detection electrode is relatively large, signal fidelity cannot always be ensured. A signal measured above one muscle may contain components generated by another muscle. This is known as crosstalk, which is one of the major drawbacks of sEMG measurements.

1.2. Research question

Different detection systems can be used to measure sEMG signals. The detection systems have different abilities to reject crosstalk. The response from a certain detection system is also dependent on the characteristics of the limb under study, such as the thickness of the fat layer, conductivity of the skin and the length of the muscle fibres. All these factors influence the amount of crosstalk present in the final measurement.

The question arose whether it was possible to determine the best detection set-up for crosstalk rejection for a specific combination of limb and detection system characteristics. All the possible combinations of parameters influencing crosstalk (as mentioned above) were simulated and the performance of the detection systems to reject crosstalk was compared. The best spatial filter for crosstalk rejection was identified in each situation.

1.3. Hypothesis and approach

The approach followed was to create an analytical model of a limb and include as much anatomical data as possible in the model. This model was then used to simulate all the above-mentioned conditions influencing the performance of the detection systems. Five different detection systems were chosen for sEMG recording, and their performance with respect to crosstalk rejection was compared in each of the situations.

Two-dimensional (2-D) spatial filters are more selective in detecting the response of a single motor unit (MU) or for determining the conduction velocity (CV) of a single MU (Rau et al. 1997; Rau & Disselhorst-Klug 1997). The hypothesis is that they will also be more selective for crosstalk rejection than one-dimensional (1-D) filters. Previous authors reported conflicting results, some stating that the double differential (DD) set-up resulted in the best crosstalk rejection and others preferring 2-D systems such as the normal double differential (NDD) system. The goal was to determine whether 1- or 2-D systems resulted in the highest rate of crosstalk rejection as the distance between the detection system and the electric source increased. The effect of the different anatomical and detection system parameters on the crosstalk rejection was also investigated.

1.4. Research contribution

Crosstalk has been investigated by modelling before, but all of the models had some limitations. This is the first analytical model where single fiber action potentials (SFAPs) are combined into the response of MUs to simulate a complete muscle. The MUs are located at any position in the limb and the resulting EMG signal is measured with different detection systems. It was important to include as much information about the system as possible in the model to ensure that the results obtained were an accurate reflection of an authentic sEMG signal.

Because crosstalk is due to signals generated by muscles other than the desired muscle and usually originates a large distance from the detection electrodes, simulation of a complete muscle as opposed to a single fibre or MU increases the resemblance between the model and a real muscle. MUs of different sizes firing at different time instances increase the randomness of the measured EMG signal. Innervation zone (IZ) and tendon spread were also accounted for. These factors more accurately simulate a physiological EMG signal and test the ability of a detection system to discriminate between true EMG and crosstalk components.

An analytical model simulating the potential generated by a single muscle fibre as detected on the skin surface was developed by Farina et al. (Farina et al. 2004b). This model was used to generate libraries of surface potentials to describe different anatomical conditions (such as fat layer thickness, fibre length, skin conductivity and interelectrode distance).

The potentials from the libraries were used to build a complete muscle consisting of thousands of muscle fibres arranged in different motor units. The parameters describing the MUs (discharge rate, CV, size, etc.) are defined by the user. sEMG signals resulting from the contraction of the total muscle were recorded with different detection systems, and the results were compared with reference to crosstalk rejection.

1.5. Dissertation layout

The first part of the study is a comprehensive literature study on the history and development of EMG in chapter 2, followed by the general methods applied in the study (chapter 3).

Figure 1.1 shows a block diagram of the total EMG research field. The dashed block in the diagram indicates the contribution of this study.

The current study investigates crosstalk in sEMG by using an analytical model. The work can be divided into three sections. In the first section, the simulations were all performed at 100 % maximum voluntary contraction (MVC), while different parameters of the detection system or volume conductor were varied. The effect of different spatial filters on crosstalk was evaluated (chapter 4).

The contraction force was then varied from 10 – 100 % MVC and the performance of the spatial filters with reference to crosstalk was again compared (section 5.1). When the contraction force reduces from 100 % the number of MUs that are activated is reduced. MUs are recruited, starting with the smallest one with the lowest value of CV and the highest discharge rate first. Reducing the number of active MUs thus has an effect on the resultant CV and discharge pattern of the active muscle.

Lastly, muscle shortening was simulated with the objective again being to identify the preferred filter for crosstalk rejection (section 5.2). This was done by reducing the muscle length while increasing the muscle radius (thus maintaining a constant volume). Reducing the muscle length means that the muscle-tendon junction (a high crosstalk area) moves closer to the detection electrodes. Increasing the muscle radius led to an increase in the spacing between different muscle fibres, which means that the distance between the fibres and the detection electrodes was also increased.

A final conclusion on the work done is presented in chapter 6.

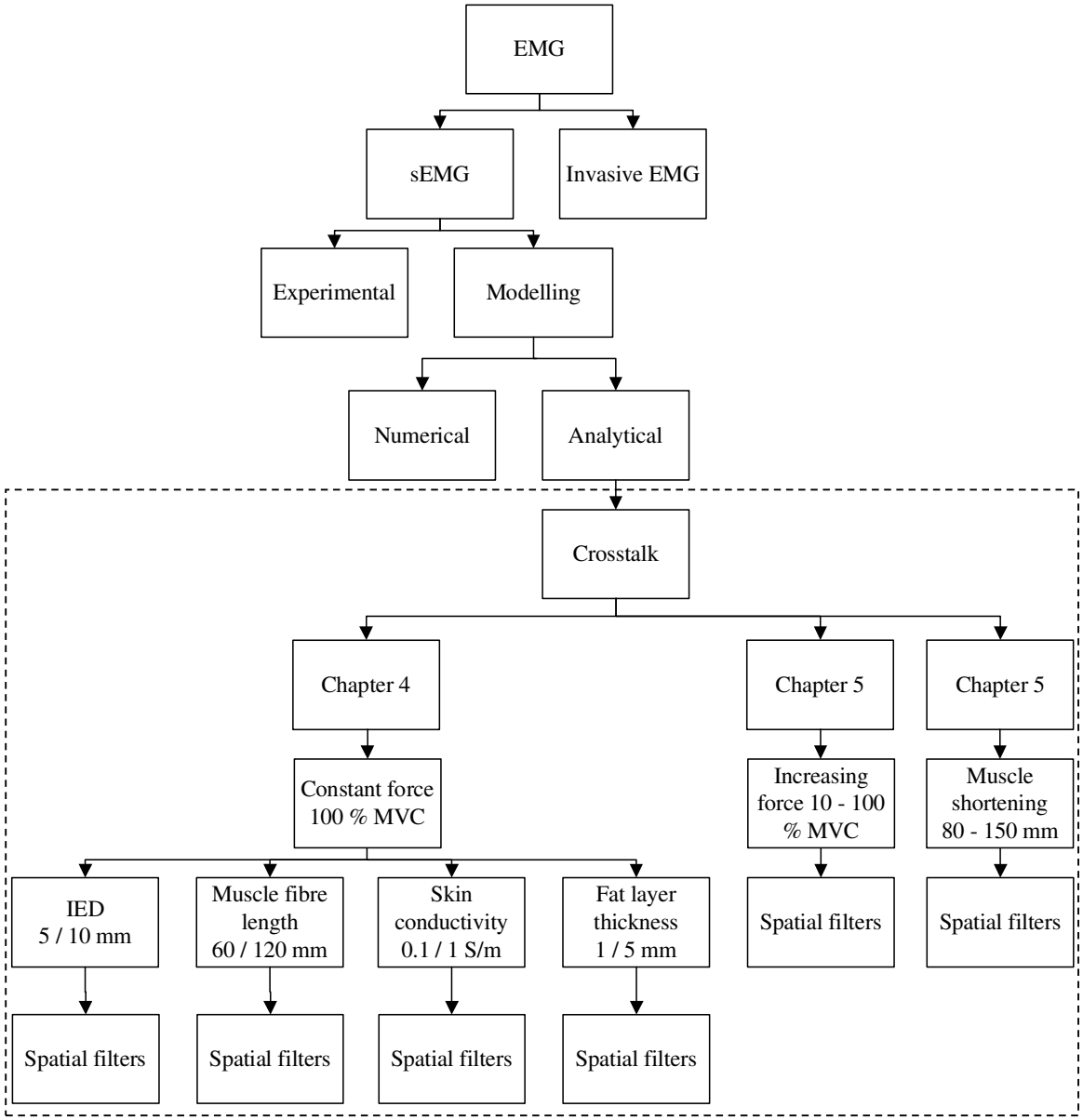

Figure 1.1. A block diagram showing where the current research (indicated with dashed block) fits into the total EMG research field.

2

Literature study

2.1. The origin of EMG signals

Electrical potentials generated inside the body (called biopotential signals) can be detected using electrodes placed on the skin surface. This is because the body acts as a volume conductor, enabling signals to propagate passively through the tissue layers from their source to the skin surface. An example of such an electric potential is the EMG signal, which originates from the contraction of muscle fibres.

The possibility that muscles could generate electricity was already documented in 1666 by the Italian Francesco Redi, who was studying the electric ray (Basmajian & De Luca 1985). Luigi Galvani drew the link between electricity and muscle contraction in 1791 by experimenting with frog legs, and he is seen as the father of neurophysiology. His work was, however, questioned by Alessandro Volta (1793), who proved that a current could also be generated by placing two dissimilar metals in an electrolyte, and it wasn't until 1838 that Carlo Matteucci finally proved that an electric current could originate in a muscle. The first recording of an EMG signal was made by a Frenchman, Du Bois-Reymond, in 1849 (Basmajian & De Luca 1985).

A muscle contraction starts in the brain or spinal cord. Here, a cell body with a long extension (the axon) is located. These two form the motor neuron. The axon divides into numerous branches, each making a neuromuscular junction (NMJ, also called the end-plate) with a single muscle fibre. The part of the muscle in which the NMJs are found is called the IZ. The motor neuron and all the muscle fibres it is connected to, is known as a motor unit (MU) (see figure 2.1) (Basmajian & De Luca 1985; Marieb 1991). The MU is thus the smallest part of a muscle which can be selectively activated by the central nervous system (CNS) (Devasahayam 2000).

Depending on the type and function of a muscle, it may contain 50 – 1500 MUs, consisting of 10 – 2000 fibres each (Merletti & Parker s.a.). Muscles responsible for fine actions and adjustments (such as those controlling the eyes) generally contain only a few fibres per MU, whereas large muscles (such as those of the limbs) have large MUs (Basmajian & De Luca 1985).

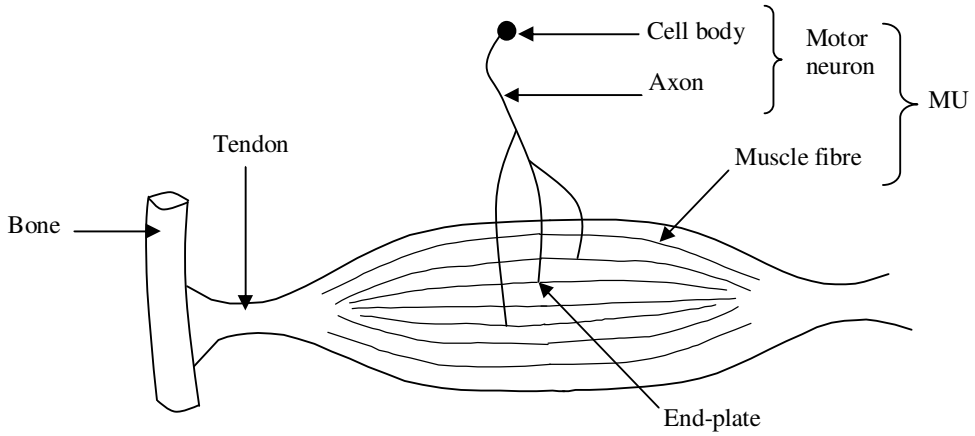

Figure 2.1. The motor unit

The nerve impulse generated by the CNS travels along the axon to the NMJ, at which point two action potentials (APs) are generated. They travel in opposite directions along the muscle fibre and are extinguished at the fibre-tendon endings. These APs are the basic source of an EMG signal, with the response generated by one fibre known as an SFAP (Halyard 2001).

Muscle fibres are divided into two groups on the basis of their physical properties. Type I muscle fibres have a smaller diameter, are more fatigue resistant and produce lower forces than type II fibres (Plonsey & Barr 2000). Since the diameter of a fibre is proportional to

the square of its CV, type I fibres will have a lower value of CV than type II fibres (Basmajian & De Luca 1985; Halyard 2001). It has been shown that MU CV increases with the size of the MU (Andreassen & Arendt-Nielsen 1987; Basmajian & De Luca 1985; Knaflitz et al. 1990), thus implying that larger MUs have a higher percentage of type II fibres (Houtman et al. 2003) and thus a larger CV (Farina et al. 2002c; Sadoyama et al. 1988). The relationship between CV and fibre diameter for the biceps brachii is given by equation 2.1:

$$v = 2.2 + 0.05(d - 25), \qquad (2.1)$$

where v is the CV in m/s and d the diameter of the fibre in µm (Duchêne & Hogrel 2000).

The overall effect is that each MU has a different CV, which determines the velocity with which the AP propagates along the muscle fibre (Masuda & De Luca 1991). The first report of a non-invasive manner in which to record CV was by Lindström et al. (1970). Experimentally determined values of CV are between 2.8 and 6 m/s with a mean of 4 m/s (Andreassen & Arendt-Nielsen 1987; Broman et al. 1985; Lindstrom et al. 1970; Merletti & Parker s.a.; Sadoyama et al. 1988; Troni et al. 1983).

A combination of all the SFAPs originating from fibres belonging to one MU is known as the motor unit action potential (MUAP). Each MU fires a certain number of times per second, resulting in MUAP trains (Basmajian & De Luca 1985; Merletti & Parker s.a.). During a muscle contraction the measured EMG signal is the summation of the MUAP trains of all the MUs active during the contraction. Because of the summation, the contribution of individual MUs cannot be identified anymore, and the signal is called the interference pattern (Webster 1998).

2.2. EMG detection

2.2.1 Electrodes

An EMG signal is detected by using electrodes to convert the current carried by ions inside the body to a current carried by electrons for use in an electric circuit. This means that a chemical reaction must take place at the electrode-tissue interface (Day). Electrodes can be placed either on the skin surface (sEMG) or inside the active muscle (needle or wire

EMG). The area of the electrode that makes contact with the tissue is known as the detection surface (Basmajian & De Luca 1985). The impedance between the detection surface and the tissue has to be minimised to ensure maximum fidelity of the recorded signal. With surface electrodes this can be accomplished by applying an electrolytic gel to the skin, or vigorously rubbing the skin to remove the external layer (Webster 1998). Invasive electrodes can be treated through an electroplating process to enlarge the detection area, thus decreasing the impedance (Basmajian & De Luca 1985).

The simplest detection system consists of one electrode that detects the electric potential at the recording site with respect to a reference point. The reference point is another electrode placed in a location that is electrically quiet, or contains electrical signals that are unrelated to the ones recorded by the detection electrode. This is a monopolar set-up (Basmajian & De Luca 1985; Merletti & Parker s.a.). This set-up records all activity in the vicinity of the detection electrode, whether it is generated by the desired muscle or not.

2.2.2 Surface EMG vs. invasive EMG

EMG detection can be used for the analysis of single MU potentials. Because an MU is the smallest part of a muscle that can be selectively activated, information about the neuromuscular system, neuronal excitation patterns, excitation spread and the function or anatomy of muscles can be obtained from an MUAP (Basmajian & De Luca 1985). In the past, identification of single MUs was only possible by making use of invasively recorded EMG signals using a wire or needle electrode (Merletti & Parker s.a.). Because these signals are obtained over a smaller detection area (thus a more selective measurement) and the distance between the electrode and the MU is short, it is possible to identify the activity of a single MU. The disadvantage of invasive measurements is that the electrode is inserted into the muscle region, thus penetrating the skin. This leads to discomfort for the patient and introduces the risk of infection. It is not possible to observe the spread of the excitation wave from invasive measurements or to perform long-duration monitoring. Repeatability of experiments is also not very good. Insertion of the steel needle influences the excitation waveform, making accurate recordings of the MUAP difficult (Disselhorst-Klug et al. 1999b). Although wire electrodes reduce the discomfort, they migrate within the muscle during contraction (Mogk & Keir 2003). They are, however, useful for recording the activity of deep muscles even during dynamic contractions (Rau & Disselhorst-Klug 1997).

Surface electrodes overcome most of the above-mentioned restrictions of invasive detection. They are more practical to use, especially for repeated or long-duration recordings, inexpensive and provide a global estimate of the underlying potentials (De Luca & Merletti 1988). Application of the electrodes is simple and can be done without medical supervision, and because the electrode is non-invasive, accurate MUAP recording is possible (Dimitrova et al. 2002; Rau & Disselhorst-Klug 1997; Zwarts et al. 2000). When using multiple electrodes it is possible to investigate different sites in the muscle (Merletti & Parker s.a.; Roeleveld et al. 1998). The disadvantage of sEMG is that the resulting signal is a blurred average of all the constituent potentials. This is because of the large area over which the signal is detected as well as the large distance between the electrode and the MUs. This means that it is difficult to identify the response of a single MU from an sEMG recording because of the low-pass filtering effect of the separating tissues (Farina et al. 2002e; Farina & Rainoldi 1999; Rau & Disselhorst-Klug 1997). It is also very difficult to identify the activity of very small or deep muscles (Basmajian & De Luca 1985) and muscle characteristics such as excitation spread or innervation pattern (Rau et al. 1997). To overcome these limitations, active electrodes (Basmajian & De Luca 1985; Bhullar et al. 1990; De Luca 2002) and spatial filters (Disselhorst-Klug et al. 1999a; Farina et al. 2003a; Rau & Disselhorst-Klug 1997) have been implemented to increase the selectivity of sEMG measurements. Selectivity refers to the sensitivity of a detection system to a certain variable. When comparing amplitude selectivity (for instance), a more selective detection system will have a larger decrease in amplitude as the distance between the source and the detection electrode increases than a less selective one. The fact that a small change in the detection set-up (distance between source and detection electrode) causes a significant change in the measured value (amplitude) is called selectivity.

A passive detection configuration is usually employed for sEMG detection, which means that the recording electrodes are connected to the signal processing unit and amplifiers through leads. These leads may present a high capacitance to the recorded signal, resulting in a degraded signal at the input of the signal-processing unit. In an active electrode configuration, the first amplifier is an integral part of the detection electrode. Because of this high input impedance, low output impedance amplifier the capacitance seen by the electrode is virtually zero (Bhullar et al. 1990). This means that the influence of the skin-electrode interface impedance is minimised. The active electrode technique improves spatial resolution and enables the detection of very low signal amplitudes (Basmajian & De

Luca 1985; Rau & Disselhorst-Klug 1997). They have also been implemented to detect single MUAPs at up to 20 % maximum contractions (Bhullar et al. 1990).

2.2.3 Spatial filters

The scattered position of the MUs, volume conduction of the potentials and the electrode area all result in the low-pass filtering effect of the resulting EMG signals (Dimitrova et al. 2002; Farina et al. 2004c; Lindstrom & Magnusson 1977; Stegeman et al. 2000). To counteract this low-pass filtering phenomenon, the same principles as applied to image theory are incorporated. In image theory high-pass filtering is used to enhance the edges of images and to focus contours by enhancing the contrast (Hall 1979). Edges in image processing correspond to amplitude steps in EMG signal analysis. The principle is thus applied in EMG analysis through spatial filtering to reduce the spread of potentials, thus leading to better localisation of the sources. Spatial filtering thus has a high-pass filtering effect and is performed by the weighted summation of signals detected by electrodes arranged in specific configurations. Since it implies a reduction of the detection volume, the number of contributing sources (MUs) is reduced (Farina et al. 2003c; Reucher et al. 1987a).

The first spatial filter was proposed and implemented by Bryan Matthews (1934). He noticed that the electrocardiogram measurement from a frog's heart and liver are of almost equal size when the measurement is made simultaneously from both sites with the electrodes referenced to ground. Since this was highly improbable, he tried referencing the electrode pairs to each other. The signal measured on the liver disappeared while the one from the heart was smaller and a more accurate indication of the heart's activity. The reason for this was that the electrodes referenced to ground in the first case were interconnected through the common ground terminal, while the second set-up ensured that only changes between the two electrode pairs were displayed as resulting potentials. This was the birth of the single differential filter.

A single differential filter consists of two monopolar electrodes, which record the underlying potential with respect to a reference node. The signals detected at these two electrodes are subtracted from each other, resulting in the difference between the two signals and rejection of the common mode present between them (De Luca 2002). This is

the lowest order of spatial filtering, with the potential distribution in the direction of the electrode configuration being differentiated (Rau et al. 1997). This filter is known as a bipolar or single differential (SD) filter with the distance between the two recording electrodes known as the interelectrode distance (IED) as can be seen from figure 2.2. As the IED increases, the area of detection increases (Merletti & Parker s.a.), leading to a decrease in selectivity (Koh & Grabiner 1992). It is not practically possible to reduce the IED of bipolar electrodes enough to enable the detection of single MU activity at high contraction forces (Disselhorst-Klug et al. 1999b; Rau & Disselhorst-Klug 1997).

Double differentiation (DD) detection was introduced by Broman et al. (1985) and further described and implemented by Reucher et al. (1987a), De Luca & Merletti (1988), and Koh & Grabiner (1992). The detection system consists of three electrodes and three differential amplifiers (see figure 2.2). The signal is detected by two SD systems with the output of each SD system connected to one input of another differential amplifier. This amplifier differentiates the signal for the second time and its output is known as the double differential recording of the input signal. The DD signal is thus the difference between the two SD signals, and it results in cancellation of the signal simultaneously present on all three electrodes. A signal travelling just below the skin surface, thus arriving at the electrodes at different times, will be displayed while one originating from far away and seen simultaneously on all three electrodes will be rejected. The recording system can be placed with its main axis positioned either longitudinally or transversally with respect to the fibre direction. Longitudinal DD (LDD) is normally used to estimate the delay a signal experiences while travelling down a muscle fibre, while transversal DD is useful for examining the discharge pattern of different adjacent MUs or the decrease of the signal amplitude with increasing distance from the source (Merletti et al. 2003; Reucher et al. 1987a).

Each of the three spatial filters mentioned thus far, monopolar, SD and DD, have different strong points. Monopolar detection is best for obtaining information about the tendon area, SD for IZ and fibre length estimates and DD for CV estimation (Merletti et al. 1999b).

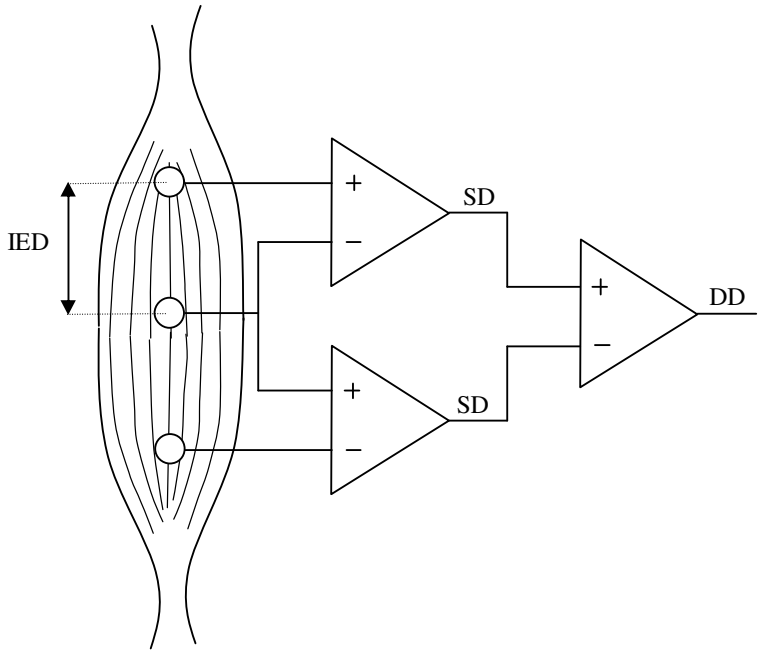

Figure 2.2. SD and DD recording set-up. The IED is also shown.

Reucher et al. (1987a; 1987b) introduced the first two-dimensional filter. It consists of five electrodes arranged in a cross (see figure 2.3), and is known as a normal double differentiating (NDD) filter. Owing to its improved spatial selectivity, the detection of single MU activity becomes possible even at 100 % MVC (Reucher et al. 1987a). Other groups also implemented 2-D filters (Disselhorst-Klug et al. 1997; Rau & Disselhorst-Klug 1997; Rau et al. 1997).

The NDD filter was found to be isotropic for wavenumbers lower than half the maximum wavenumber. The wavenumber of a signal is defined as 2π divided by the wavelength of the signal, with the maximum wavenumber given by the Nyquist Theorem (2π divided by twice the distance between two adjacent spatial samples). The question arose whether it was possible to develop another filter that could have an isotropic transfer function for a larger range of values. The inverse binominal filter of the second order (IB^2) was incorporated, and its transfer function was found to be isotropic for most wavenumbers (Disselhorst-Klug et al. 1997). It consists of nine electrodes (see figure 2.3) and was found to be the most selective in identifying single MUAPs.

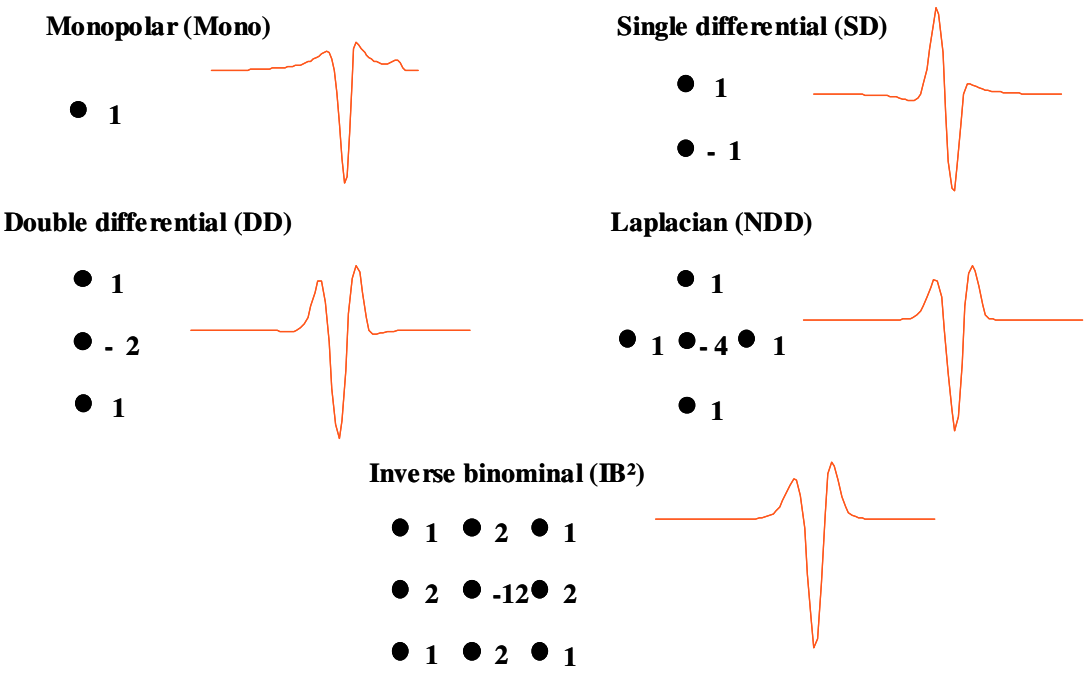

Figure 2.3. The weights used for the different detection systems. The same inter-electrode distance of 5 or 10 mm is used in all instances.

Figure 2.3 shows an example of the spatial filters implemented in the current study, as well as an SFAP detected with each one. Both the SD and DD detection systems were placed with their main axis longitudinally with respect to muscle fibre direction.

Concentric electrodes were theoretically proposed by Kossev et al. (1988) and Van Steenwijk (1986), implemented by Bhullar et al. (1990) and expanded to the 2-D spatial frequency domain and multiple-ring systems by Farina and Cescon (2001). The system consists of a central point electrode and one or more concentric rings. If the thickness of the rings are minimised, they can be considered as circumferences, thus neglecting the effect of electrode size. This system showed higher selectivity with respect to detecting single MU sources than the above-mentioned systems, with selectivity increasing as the number of concentric rings increased. Also, since it is an isotropic system, it is not affected by rotation, and the problem of electrode location with respect to fibre orientation is eliminated (Farina & Cescon 2001).

Two-dimensional detection of EMG signals is known as high spatial resolution EMG (HSR-EMG) (Rau & Disselhorst-Klug 1997). HSR-EMG is the only non-invasive way to determine the CV of a MU, even at maximum levels of muscle contraction (Rau & Disselhorst-Klug 1997). The higher spatial resolution is gained at the cost of more detection electrodes as well as more complex signal analysis. These two factors are played off against each other when choosing a detection system. The goal of this study is to help quantify the gain in resolution to assist in making the choice. To understand spatial selectivity fully, it is necessary to evaluate the propagating and non-propagating parts of the signal individually.

2.2.4 Propagating and non-propagating components

When an EMG signal is measured with an electrode array placed in the direction of the muscle fibres (longitudinal), it is clear that a portion of the signal is travelling (measured at a different time on each electrode), and another portion is non-travelling (occurs at the same time on all electrodes) (Merletti & Parker s.a.). In figure 2.4 two non-travelling parts can be seen at about 23 and 31 ms, while the main waveform can be seen to propagate from electrode 1 to 10. The non-propagating part of an SFAP is clearly visible in the monopolar configuration in figure 2.3 (the small bump just after the main signal). In the SD recording it is barely visible while it completely disappears with any higher order of measuring set-up. This illustrates the variance in sensitivity of different spatial filters for different signal components.

As the distance between the fibre and the detection electrode increases, the non-travelling components become the dominant part of the detected signal (Farina et al. 2002a). These non-travelling components are also known as far-field potentials, and are defined by the fact that they maintain their latency, amplitude, morphology and polarity even when the recording is made a whole body length away (Stegeman et al. 1997). Figure 2.5 shows the near- and far-field components of a dipolar source when the reference electrode is positioned to the left of the source in the far-field region.

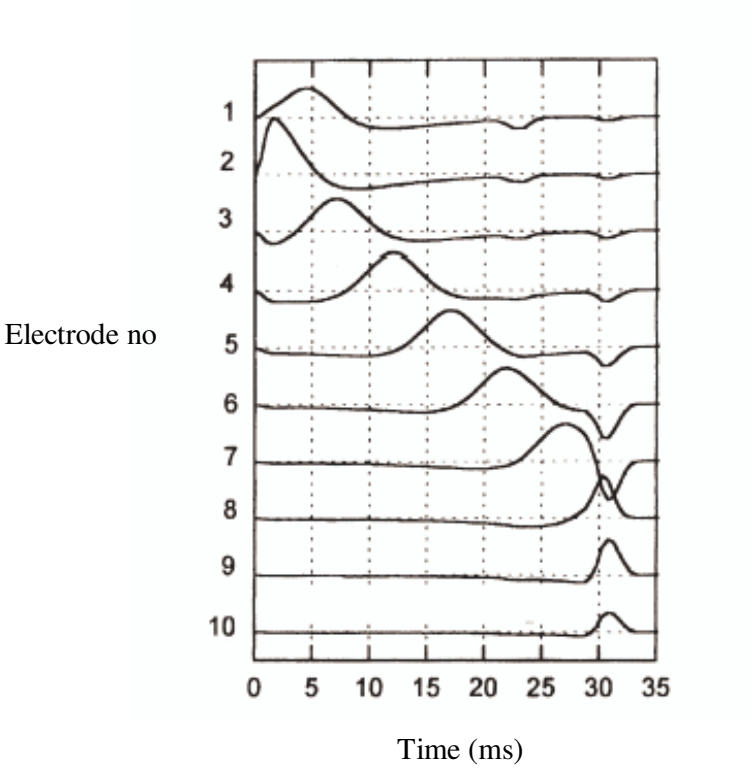

Figure 2.4. Propagating and non-propagating components of an EMG signal (with permission: Merletti et al. 1999a).

A propagating AP can be described by the summation of two equal "back-to-back" dipoles (+ - - +), resulting in an effective quadripole. Because the dipoles can be considered as superimposed (+ = +), the resulting potential resembles a tripole (+ - +), as seen in figure 2.6.

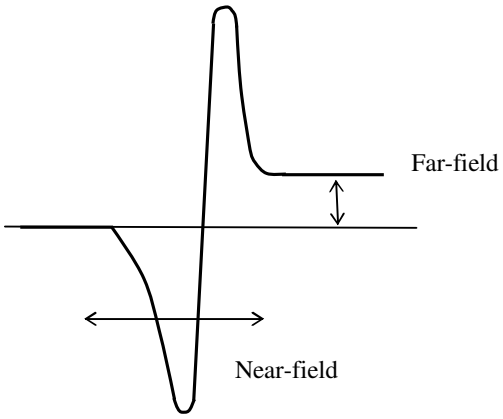

Figure 2.5. Near- and far-field components of a dipolar source

Most models of EMG generation use this tripole description as the source of the EMG signal (Roeleveld et al. 1997a).

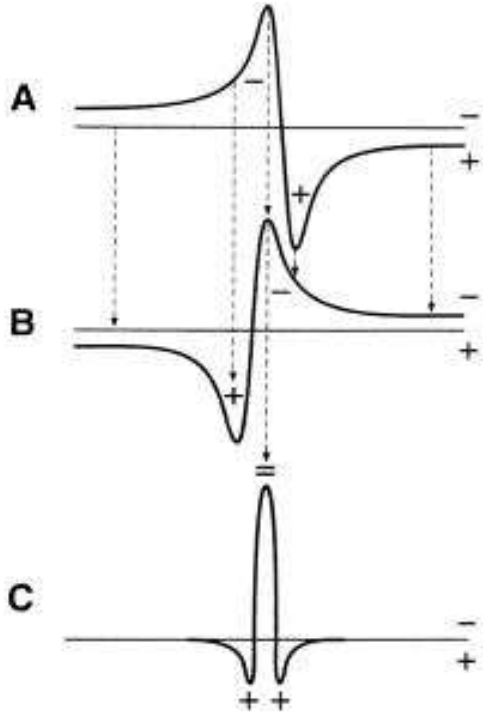

Figure 2.6. Summation of two equal and opposite dipoles resulting in a tripole with only near-field distribution (with permission: Stegeman et al. 1997).

From figure 2.6 it is clear that the far-field potentials of the two dipoles cancel each other, resulting in the tripolar shape with only a near-field distribution. When the AP encounters an inhomogeneity or disturbance (for instance the end-plate or muscle-tendon junction), the quadripolar source can become unbalanced, resulting in the generation of a net dipolar source. The near-field components of this source may be similar to the ones produced by the quadripolar source, but there will now also be a resultant far-field potential (see figure 2.7) (Dimitrova et al. 2002; Stegeman et al. 1997).

The fact that a propagating AP does not have a net dipole component explains why the travelling components can only be measured a few millimetres away from their origin. Attenuation of the propagating components as the distance increases is thus larger than that of the non-propagating components. This is why non-travelling components (describing the generation and extinction of an AP) can be measured at a distance far from their origin as long as the reference and recording electrode is on different sides of the source (Roeleveld et al. 1997a; Roeleveld et al. 1997b). This is the primary source of crosstalk.

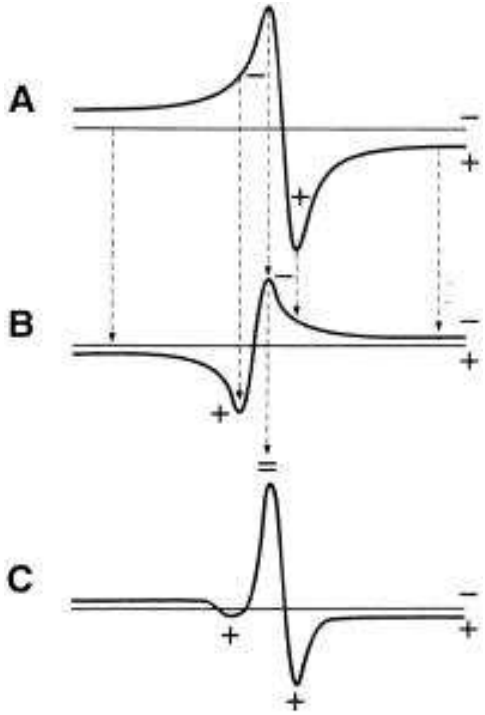

Figure 2.7. Summation of two unequal dipoles resulting in a tripole with near- and far-field distribution (with permission: Stegeman et al. 1997).

2.2.5 Crosstalk

When the measured response of one muscle contains signal components generated by other muscles, those undesired components are called crosstalk. Morrenhof et al. were some of the first to identify this phenomenon (Morrenhof & Abbink 1985), with De Luca and Merletti (1988) providing the first quantitative information about it. The larger the detection volume, the greater the chance of including crosstalk in measurements (De Luca 2002; Merletti & Parker s.a.). Dimitrova et al. (2002) showed that crosstalk is caused by muscles located not only under, but also beyond the muscle of interest, and that the contribution of the latter muscles might even be higher. Because these components travel a larger distance through the volume conductor than those describing the activity of the underlying muscle activity, they will be composed of mostly far-field signals. This has been proven through simulations and experiments by Farina et al. (2004c). A true EMG signal contains mostly near-field signals, with far-field components describing only the generation and termination phases of the potentials (Farina et al. 2002e). To ensure effective signal processing it is necessary to minimise the amount of crosstalk present in a measurement. Crosstalk has been investigated by experimental means (De Luca & Merletti 1988; Farina et al. 2002e; Farina et al. 2004a; Koh & Grabiner 1992; Mogk &

Keir 2003; Morrenhof & Abbink 1985; Perry et al. 1981; Solomonow et al. 1994; Van Vlugt & Van Dijk 2000; Winter et al. 1994) and modelling approaches (Dimitrova et al. 2002; Dimitrov et al. 2003; Farina & Rainoldi 1999; Farina et al. 2002e; Farina et al. 2004a; Farina et al. 2004c; Lowery et al. 2003a; Winter et al. 1994). De Luca and Merletti (1988) measured a signal above an unstimulated peroneal muscle with an amplitude equal to 16.6 % of that of the stimulated tibial muscle. Solomonow et al. (1994) detected EMG signals originating from an active muscle above a denervated cat leg. Several methods have been proposed to quantify and reduce crosstalk, but a conclusion on which one performs best has not been reached yet.

The cross-correlation between recorded signals has been used to identify the amount of crosstalk present in a recording (Mogk & Keir 2003; Morrenhof & Abbink 1985; Winter et al. 1994). The values for crosstalk predicted in this way were substantially lower than those determined by experimental measurements, leading to an investigation of the feasibility of the method. The conclusion was that the cross-correlation between two signals cannot be used as a measure of crosstalk. Broman et al. (1985) proved that the phase relationship of volume-conducted signals might change, thereby changing the amount of correlation between signals. Common drive (the simultaneous fluctuations in the mean discharge rates of different MUs in pairs of muscles during synergistic and antagonistic muscle co-activation (Basmajian & De Luca 1985; Lowery et al. 2003a)) and MU synchronisation (increased tendency of MUs to fire within a few milliseconds of one another (Lowery et al. 2003a)) will also lead to a higher value of correlation between signals generated by different muscles, falsely leading one to interpret it as crosstalk (De Luca & Merletti 1988; Farina et al. 2002e; Lowery et al. 2003a). The fact that the dominant components in crosstalk and true EMG signals differ also eliminates the use of the cross-correlation coefficient (Farina et al. 2004a).

Winter et al. (1994) proposed that mathematical differentiation of a mono- or bipolar detected signal should reduce the amount of crosstalk. Dimitrova et al. (2002) proved this statement to be incorrect, as differentiation increases the frequency of the components responsible for crosstalk.

Another method is to compare the ratio between surface and intramuscular recorded EMG signals (Perry et al. 1981). Because of the difference in detection volumes present between these two measurements, this technique is not very reliable (Farina et al. 2002e).

When electrical stimulation is employed to evaluate crosstalk (De Luca & Merletti 1988; Farina et al. 2002e; Koh & Grabiner 1992; Koh & Grabiner 1993; Solomonow et al. 1994; Van Vlugt & Van Dijk 2000), care should be taken to ensure only the desired muscle is stimulated. Unintentional stimulation of nearby muscles will lead to higher crosstalk estimates. The ratio between the amplitude detected above the stimulated and unstimulated muscle is usually used as a measure of the crosstalk present. Intramuscular EMG of the neighbouring muscles is often used to ensure selective stimulation of the desired muscle, but because of the selectivity of the measurement absence of EMG is not proof of absence of muscle activity or crosstalk (Farina et al. 2002e). It is thus possible that certain MUs in a neighbouring muscle might be active without being detected by the invasive EMG because of its small detection volume. It is always important to keep in mind that the order of recruitment may be reversed when electrical stimulation is implemented. In a voluntary contraction, the smallest MUs are recruited first with the size increasing until the required muscle force is reached. When electrical stimulation is applied directly to the nerve (with an implanted electrode), the largest MUs are recruited first, with progressively smaller MUs recruited as the stimulation intensity is maintained (Koh & Grabiner 1992). If surface electrodes are used for stimulation, this is not necessarily the case (Knaflitz et al. 1990). Another difference between a voluntary and an elicited contraction is the fact that MUs are recruited synchronously (all at the same time) when stimulated (Lowery et al. 2003a).

Since the volume conductor and electrode area can be modelled as a low-pass filter, it has been suggested that the frequency content of a signal should be dependent on the distance it has travelled from its origin (Basmajian & De Luca 1985; Lindstrom & Magnusson 1977). This implies that crosstalk signals will contain mainly low-frequency components, and that temporal high-pass filtering will eliminate these unwanted components. It has, however, been proved (experimentally and in simulation) that crosstalk signals may contain frequency components higher than those detected directly above a stimulated muscle (Dimitrova et al. 2002; Farina et al. 2002e). This can again be explained by the fact that crosstalk signals are non-propagating, and are thus not affected by the low-pass filtering of the volume conductor as the propagating components are. The use of a high-pass filter to reduce crosstalk is thus not always reliable (Farina et al. 2004a).

Since spatial filters increase the selectivity of a measurement, it has been proposed that a more selective filter will reduce the amount of crosstalk (Disselhorst-Klug et al. 1997).

This statement has, however, been contradicted by several authors (Farina & Cescon 2001; Farina et al. 2002a). The objective of the current study was to investigate the validity of the above statement through a modelling approach.

2.3. Previous models for SFAP generation

A number of different models have been implemented to study the generation and propagation of SFAPs inside the volume conductor. The different layers included in the model have been studied by Roeleveld et al. (1997a) and Farina et al. (2004b), and it has been found that inclusion of the muscle, fat and skin layer is necessary to obtain results that are similar to those obtained from measurements. The inclusion of more layers results in a larger spread of the potentials because of an increase in the distance between the source and detection system, as well as the effect of different conductive properties of the layers (fat and skin) compared to that of the muscle layer.

Analytical models make use of mathematical expressions to describe the volume conductor, sources and co-ordinate system for the simulation (Blok et al. 2002; Duchêne & Hogrel 2000; Farina & Merletti 2001; Farina et al. 2004b; Gootzen et al. 1991; Lindstrom & Magnusson 1977; Roeleveld et al. 1997a; Stegeman et al. 2000). They provide an easy interpretation of the dependence of signal features on system parameters and are computationally efficient. Some models focus only on the response of a single fibre or MU (Disselhorst-Klug et al. 1997; Duchêne & Hogrel 2000; Farina & Merletti 2001; Farina et al. 2004b; Reucher et al. 1987b), while others incorporate the total muscle response (Farina et al. 2002b; Farina et al. 2002c; Gootzen et al. 1991). It is, however, difficult to describe complex geometries with analytical equations. When this is the case, numerical methods must be used (Lowery et al. 2002; Lowery et al. 2003b; Mesin 2005; Schneider et al. 1991).

2.3.1 Numerical models

When using a numerical model to describe a system, the volume and its boundary must be divided into small, well-described elements, which can then be solved with a finite or boundary element method. Complex geometries and inhomogeneous materials can be included with relative ease. It has been noted that the location of the bone inside the volume conductor has a pronounced influence on the detected potential (Lowery et al.

2002). In most analytical models, the bone is located in the centre of the limb for simplicity. To alter this location would be very time-consuming and complicated, as all the equations would have to be adapted. In a finite element model it is relatively simple, as different elements only have to be selected to represent the bone.

2.3.2 Analytical models

An analytical model was generated by Farina et al. (2004b), which facilitates the simulation of SFAPs. These SFAPs correspond to the potential detected on the surface of the volume conductor owing to the propagation of an intracellular action potential (IAP) along a fibre inside the volume conductor.

Source description

The IAP can be described in the spatial domain by equation 2.2:

$$V_m(z) = \begin{cases} Az^3 e^{-z} + B, z > 0 \\ 0, z \le 0 \end{cases}, \qquad (2.2)$$

with V_m the potential, z the distance travelled along the fibre, A = 96 mV/mm^3 (a suitable constant to model the amplitude of the AP) and B = 90mV (the resting potential of the cell membrane) (Farina & Merletti 2001). The transmembrane current density source is proportional to the second derivative of $V_m(z)$ and is given by

$$i(z,t) = \frac{d}{dz}\left[\psi(z - z_i - vt)\, p_{L_1}(z - z_i - \frac{L_1}{2}) - \psi(-z + z_i - vt)\, p_{L_2}(z - z_i - \frac{L_2}{2})\right], \qquad (2.3)$$

where v is the conduction velocity of the source, $\psi(z)$ is the first derivative of $V_m(z)$, $p_L(z)$ is a function that equals 1 for $-L/2 \le z \le L/2$ and 0 otherwise, z_i is the end-plate position and L_1 and L_2 the semi-lengths of the fibre from the end-plate to the right and left tendon, respectively (Farina & Merletti 2001). The current density source is thus described as two waves travelling in opposite directions from the end-plate to the tendon at a certain CV, where each wave has a triphasic shape.

Plonsey (1984) derived an equation describing the potential field detected on the outside of an unbounded conducting medium due to a circular cylindrical source by solving Poisson's equation:

$$\nabla^2 \phi = -\frac{\rho}{\varepsilon}, \tag{2.4}$$

where ∇ is the divergence, Φ the potential field, ρ the charge density and ε the permittivity of the material. This dielectric principle can be applied to conducting media by the principle of duality. This states that the permittivity can be considered as conductivity (σ) and the charge density as a current density (J) (Plonsey 1984). It is also known that the following relationships exist between the current density in the volume conductor, J, the density current of the source, I, the electric field, E and the potential, Φ (Farina & Rainoldi 1999):

$$\begin{aligned} \nabla \cdot J &= I \\ J &= \sigma E \\ E &= -\nabla \Phi \end{aligned}, \tag{2.5}$$

Farina and Rainoldi (1999) obtained the current density of the source by substituting these relations into the Poisson equation, resulting in the partial differential equation:

$$-\sigma_x \frac{\partial^2 \phi}{\partial x^2} - \sigma_y \frac{\partial^2 \phi}{\partial y^2} - \sigma_z \frac{\partial^2 \phi}{\partial z^2} = I, \tag{2.6}$$

where the muscle fibre is parallel to the z-axis and the skin is in the x-z plane (see figure 2.8). Equation 2.6 is valid for the muscle layer because it contains the source, but for the fat, skin and air layer the right-hand side is set equal to zero. Because the potential must decay to zero as y increases to infinity, the current density must be continuous in the y direction and the electric field is continuous in the x and z planes. This leads to a set of boundary conditions which can be used in solving the equations.

When equation 2.6 is transformed to the spatial frequency domain by taking the Fourier transformation, an ordinary differential equation is obtained for each layer of the volume conductor. From these equations it is possible to determine the transfer function of each of the layers. The transfer function of the total volume conductor (including muscle, fat and skin) is given in equation 2.7:

$$H_{vc}(k_x,k_z,y_0)=\frac{2}{\sigma_{2a}}e^{-k_{ya}|y_0|}\frac{1}{(1+R_c)\cosh\left[k_y(h_1+d)\right]\alpha(k_y(h_1+d))+(1-R_c)\cosh\left[k_y(h_1-d)\right]\alpha(k_y(h_1-d))}\,,$$

(2.7)

with $k_x = 2\pi f_x$ and $k_z = 2\pi f_z$ the angular frequencies, $d = h_1 - h_2$, $k_y = (k_x^2+k_z^2)^{0.5}$, $k_{ya} = (k_x^2+R_a \cdot k_z^2)^{0.5}$ and $\alpha(s) = k_{ya} + k_y.R_m \cdot tgh(s)$ (Farina & Rainoldi 1999). The rest of the definitions can be found in figure 2.8.

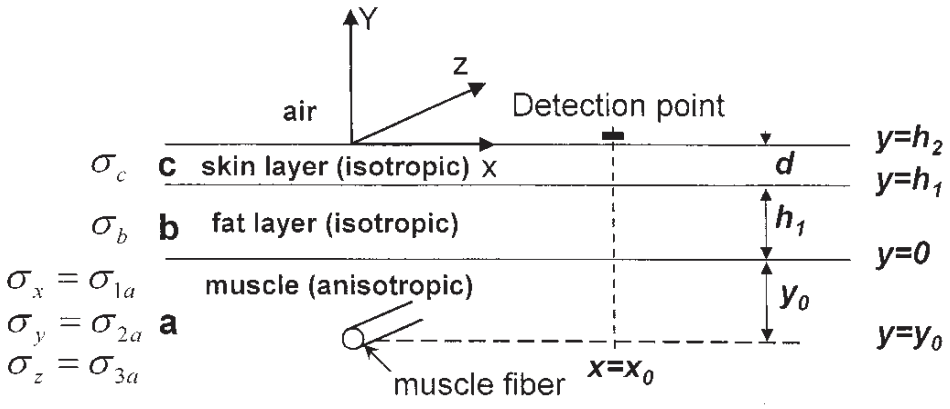

d = thickness of the skin layer
h_1 = thickness of the fat layer
y_0= depth of the current density source in the muscle
$h_2=h_1+d$

$$R_c=\frac{\sigma_c}{\sigma_b} \qquad R_m=\frac{\sigma_b}{\sigma_{2a}} \qquad R_a=\frac{\sigma_{3a}}{\sigma_{2a}} \qquad \sigma_{1a}=\sigma_{2a}$$

Figure 2.8. Model of the volume conductor showing the different layers (with permission: Farina & Merletti 2001).

Farina and Merletti (2001) computed the transfer function of the detection electrodes ($H_{ele}(k_x,k_z,\theta)$), including the effect of electrode size, configuration and inclination of the fibres with respect to the detection system. The potential detected on the skin surface can now be computed by taking the inverse Fourier transform of the product of the transfer function of the volume conductor, the electrodes and the Fourier transform of the source, $I(k_z)$:

$$\phi(z) = \Im^{-1}\left\{ I(k_z)\frac{1}{2\pi}\int_{-\infty}^{\infty} H_{vc}(k_x,k_z)H_{ele}(k_x,k_z,\theta)e^{jk_x x_0}\,dk_x \right\}, \qquad (2.8)$$

$I(k_z)$ is equal to the Fourier transform of equation 2.3. To compute the potential detected at a certain position z_0 as a function of time, the above equation is solved at each instant of time. This is the first model in which the source can be located in any one of the volume conductor's layers. The generation and extinction of the source is modelled as a gradual appearance and disappearance of the derivative of the IAP at the end-plates and tendon area (Farina et al. 2004b).

Model description

The layers included in the model are bone, muscle, fat and skin. They are homogeneous and may also be anisotropic. The anatomical data of the limb and muscle fibres can be specified, as well as the parameters for the detection system. Figure 2.9 shows a three-dimensional view of the simulated limb with the different layers and detection electrodes. The physical parameters used in constructing the model were obtained from anatomical data to ensure accuracy of the simulated potentials (see section 2.4). Chapter 3 contains a detailed description of the implementation of the model and its parameters.

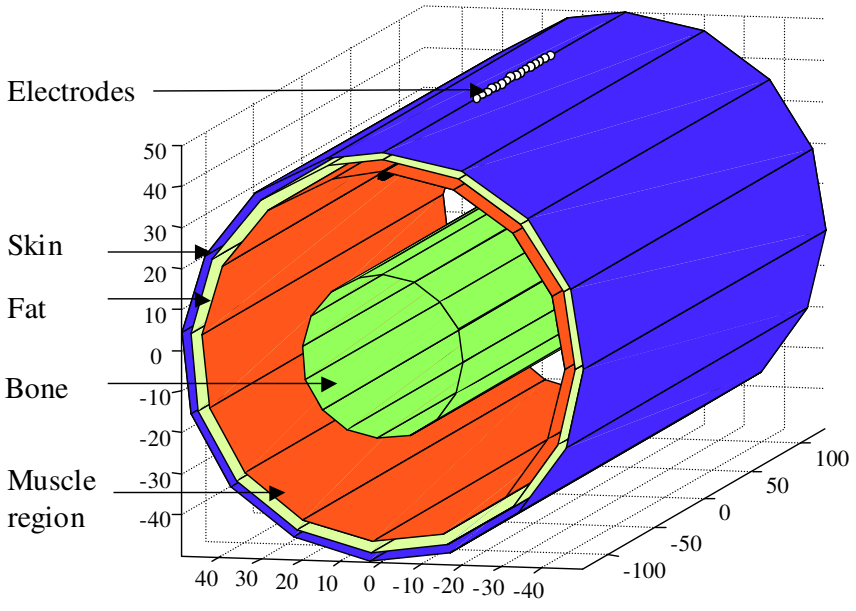

Figure 2.9. The analytical model used to generate the SFAPs.

2.4. Anatomical data

As indicated by Farina et al. (2004b), the parameters used for the volume conductor model has a large influence on the results obtained for selectivity of different spatial filters. The best filter for a certain anatomy may give the poorest results for another anatomy. Since the goal of the study is to determine the best spatial filter for rejecting crosstalk on the biceps brachii muscle, it is important to use experimentally obtained anatomical data in the construction of the model.

Table 2.1 shows the anatomical data obtained for the biceps brachii muscle. The physiological cross-sectional area (PCSA) (also see figure 3.2) of the muscle was one of the first parameters used to determine the volume conductor properties. Table 2.2 shows some global data obtained for the upper arm.

Table 2.1. Anatomical data for biceps brachii muscle

Variable	Value	Reference
PCSA (mm²)	590	Garner & Pandy 2003
Fibre length (mm)	143	Garner & Pandy 2003
Fibres / muscle	234 000 - 270 000	Klein et al. 2003) (Sale 2002
MU / muscle	300	Sale 2002
	774	The Baltimore Longitudinal Study of Aging 1998
Fibres / MU	500 - 750	Sale 2002; Maurel 1998
Fibre density (fibres/mm²)	400 - 460	Computed
Muscle conductivity (longitudinal)	0.5 S/m	Foster & Swan 1986; Geddes & Baker 1967
Muscle conductivity (radial + angular)	0.1 S/m	Foster & Swan 1986; Geddes & Baker 1967
IZ spread	10 mm	Merletti et al. 1999a
Tendon spread	10 mm	Merletti et al. 1999a

Table 2.2. Anatomical data for upper arm

Variable	Value	Reference
Humerus radius	13.5 mm	Orcholl et al.
	9.25 mm	Bullen et al.
Bone conductivity (isotropic)	0.02 S/m	Foster & Swan 1986; Gabriel et al. 1996
Upper arm radius	51.07 mm	Miyatani et al. 2001
Fat layer conductivity (isotropic)	0.05 S/m	Foster & Swan 1986; Geddes & Baker 1967
Fat layer thickness	2.2 ± 2.1 mm	Farina et al. 2003c
Skin conductivity	$2 \cdot 10^{-5}$ – 20 S/m	Gabriel et al. 1996
Skin thickness	1 mm	Zhao et al. 2004

The final values used in the model can be found in table 3.1. These values are taken from averages of the above data. The selected muscle is approximated by an ellipse with semi-axis lengths of a = 15 mm and b = 12.7 mm. These values were chosen to obtain the desired muscle PCSA of 600 mm².

3

Methods

In figure 3.1 a diagrammatic overview of the model developed in the study is given. The analytical model consists of four different layers, describing the bone, muscle, fat and skin layer of the limb. The simulations were done in Matlab on a Pentium 4 computer with 128 MB RAM. This model was used to generate eight libraries containing the SFAPs of the muscle fibres in the muscle region. The eight libraries describe eight different situations with different characteristics for the limb and detection systems. The desired simulation is defined by choosing which of the eight libraries to use, as well as specifying the characteristics of the active muscle to be simulated. The muscle characteristics include the muscle size and depth under the fat layer, the number of MUs in the muscle, the number of fibres per MU and the placement of the active muscle in the muscle region of the limb.

The necessary SFAPs are then loaded from the correct library and summed to form the MUAPs. The characteristics of the MUs (including the MU discharge rate and CV) are combined with the MUAPs to form the MUAP trains. According to the type of detection system used and the IED of the system, the MUAP trains are summed to result in the sEMG signal. The detection systems are located circumferentially around the limb.

The results obtained with the different detection systems are compared with the objective to identify the system that results in the highest rate of crosstalk rejection for a specific experimental set-up. A detailed explanation of the development process follows.

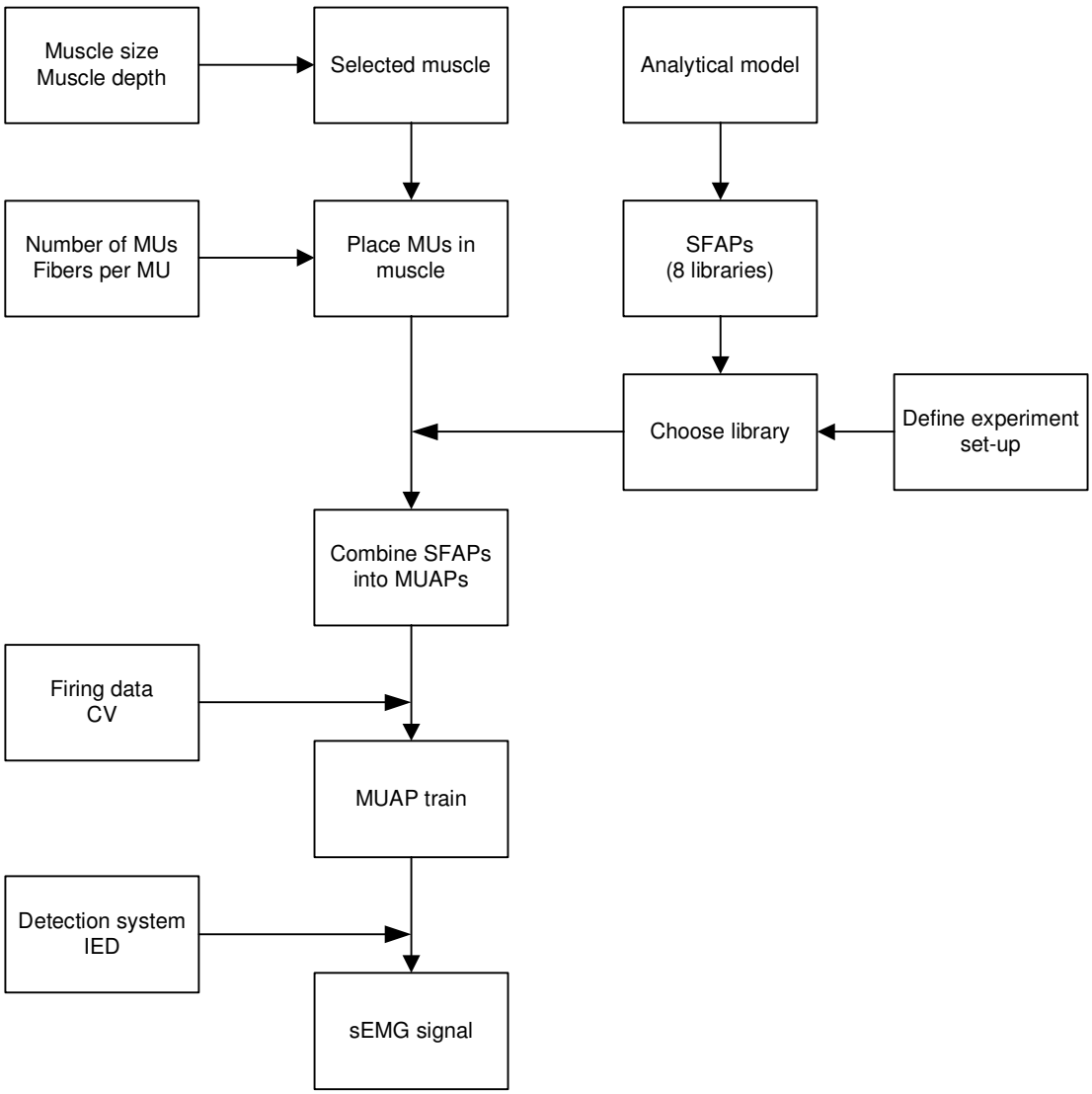

Figure 3.1. A block diagram of the work done in the present study

3.1. SFAP libraries

A muscle's EMG signal consists of the summation of all the SFAPs of the fibres constituting the muscle. The first step of the model was to generate these SFAPs. One potential was generated for each muscle fibre in the muscle region of the limb.

The analytic model developed by Farina et al. (Farina et al. 2004b) was used to generate eight libraries of SFAPs. "Library" is the term used to define a set of data that contains one SFAP for each muscle fibre in the total muscle region of the limb. Each library contains the potentials generated for a specific limb and detection system set-up. The parameters that characterised the limb and that were fixed for all the libraries can be found in table 3.1. The parameters were obtained from the anatomical data for the biceps brachii as specified in section 2.4.

The muscle fibres were arranged by depth below the fat layer (dy) and by angle (dx) between the fibre and the y-axis (0 °, see figure 3.3). The SFAPs were detected with an array of 11 monopolar point electrodes, where the centre of the array was placed halfway between the end-plate and tendon area of the muscle (see figure 2.9). Tendon and IZ spread was accounted for.

The parameters that were varied between the libraries can be seen in table 3.2. The values were again based on anatomical data for the biceps brachii muscle (see section 2.4). The fibre semi-length is the distance from the end-plate region to the muscle-tendon junction, thus approximately half the total length of the muscle fibre. Because IZ and tendon spread was accounted for, the final two fibre semi-lengths were not always equal. These libraries enable one to simulate different conditions encountered in experimental recordings.

Because the potential detected by an electrode is only dependent on the absolute distance between the muscle fibre it originated from and the detection electrode, it is sufficient to simulate SFAPs for one half (0 – 180 °) of the fibres in the muscle region. When a potential originates from the other half (180 – 360 °), the distance between the source fibre and the detection electrode is computed and the potential from the fibre located at the same distance from the electrode but in the 0 – 180 ° half is used. This means that the libraries contain 60 000 SFAPs, while the muscle region has 120 000 fibres, resulting in a fibre density of 20 fibres/mm^2 (Farina et al. 2002b; Farina et al. 2002c; Fuglevand et al. 1993).

Table 3.1. Fixed parameter values used for simulation of the libraries. Values obtained from anatomical data for biceps brachii (see table 2.1)

Variable	Value
Limb radius	50 mm
Bone radius	15 mm
Skin thickness	1 mm
Fibre density	20 fibres/mm²
Angle between fibres	0,41 °
Depth between fibres	0,22 mm
Conductivity of bone (isotropic)	0,02 S/m
Conductivity of fat (isotropic)	0,05 S/m
Conductivity of muscle (radial + angular)	0,1 S/m
Conductivity of muscle (longitudinal)	0,5 S/m
Interelectrode distance	5 mm
Detection type	Monopolar
Innervation zone spread	10 mm
Tendon spread	10 mm
Electrode type	Point
Sampling frequency	4096 Hz

Table 3.2. Variable parameters used for simulation of the libraries

Library	Fat layer thickness (mm)	Skin conductivity (S/m)	Fibre semi-length (mm)
1	1	1	60
2	5	1	60
3	1	0,1	60
4	5	0,1	60
5	1	1	30
6	5	1	30
7	1	0,1	30
8	5	0,1	30

3.2. Generation of MUAPs from SFAP libraries

An MUAP is the total response of one MU, which means that all the SFAPs of the fibres in an MU are summed together. Each MU has different characteristics, which influence the MUAP. The construction of the MUAPs was the next step.

Using each library it was possible to create a muscle and simulate the total response of all the muscle fibres contracting together. A certain part of the muscle region is specified as the active muscle for a simulation. The active muscle is approximated by an ellipse, and the length of the two semi-axes, as well as the depth of the active muscle under the fat layer, can be specified. Table 3.3 shows the fixed parameters that were used for the simulations.

Table 3.3. Fixed parameters used for simulations. Values based on anatomical data for the biceps brachii (see table 2.1)

Variable	Value
Depth of muscle under fat layer	0 mm
Fibres / MU	50 – 1000
MU / muscle	200
PCSA of selected muscle	600 mm²
Maximum force exerted by muscle	100 % MVC
% MVC where all MUs are recruited (*RR*)	85 %
IPI variability (*ipi_var*)	15 %
Variation in discharge rate with force (*sl_dis*)	0.3 pps/%MVC

To minimise signal degrading, the active muscle is placed directly underneath the fat layer. It is, however, possible to move it deeper into the muscle region. The number of fibres per MU is uniformly distributed between 50 and 1 000 (Gootzen et al. 1991), while the muscle always contains 200 MUs. The PCSA of a muscle is the area obtained when the muscle is cut at a right angle with respect to its fibres. This is the same value as the cross-sectional area (CSA) for muscles with parallel fibres, but pennated muscles (oblique muscle fibres attached to a central tendon, resembling a feather) have a larger value of PCSA than CSA,

see figure 3.2. Since the biceps brachii muscle has parallel fibres, its PCSA and CSA values are equal.

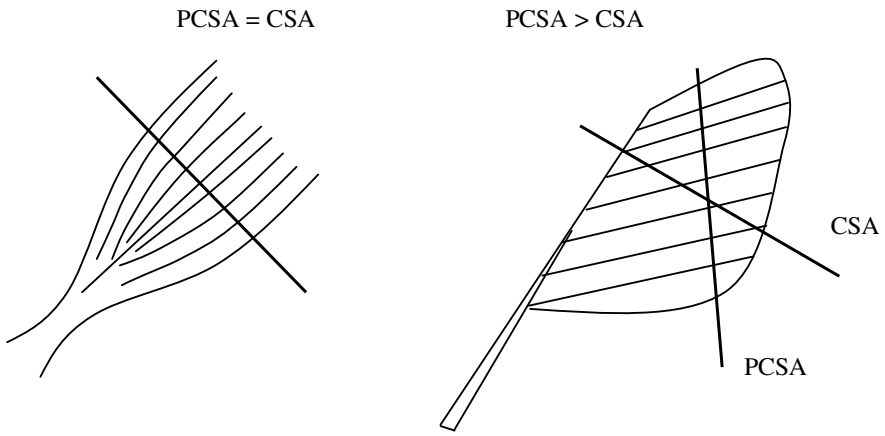

Figure 3.2. The difference between the CSA and PCSA for a muscle with parallel fibres (left) and a pennated muscle (right).

The force exerted by a muscle is measured as a percentage of the maximum possible force the muscle is capable of. This force is called the maximum voluntary contraction, or MVC. To increase the force produced by a muscle, the CNS can employ one of two mechanisms. The first involves activation of more MUs, called recruitment (Farina et al. 2002c; Fuglevand et al. 1993). When all the MUs have been recruited, the second method is implemented: increasing the discharge rate of the MUs already active (Devasahayam 2000). This is called rate coding. The percentage MVC at which all MUs have been recruited differs for different muscles (Basmajian & De Luca 1985; Elfving et al. 2002), and is denoted by the parameter RR.

When a 100 % MVC contraction is simulated, all the MUs are recruited and discharging at a certain discharge rate. The term rate is used instead of frequency, as the latter implies a discharge pattern that is invariable with time. The time between two successive MU discharges is called the interpulse interval (IPI). The discharge rate is equal to the inverse of the IPI. Because of the pseudorandom nature of the IPIs, the discharge rate will differ when calculated from different IPIs, and it is thus necessary to obtain an average IPI before calculating the discharge rate. This difference in time between the actual discharge and the expected discharge is called jitter (Basmajian & De Luca 1985). The interpulse interval variability determines the amount of jitter present in the discharge pattern of MUs. The

value given in table 3.3, *ipi_var*, is the variability in the interval between two successive pulses given as a percentage of the IPI.

The MU centres are placed at random locations inside the active muscle, and the closest N fibres to each centre are assigned to that MU, with N denoting the number of fibres in the MU. This ensures that each MU has a circular territory as defined by Stalberg and Antoni (1980) and Gootzen et al. (1991). Figure 3.3 shows a section through the limb showing the different layers, active muscle, MU location and area. The location of the detection system centres is also shown.

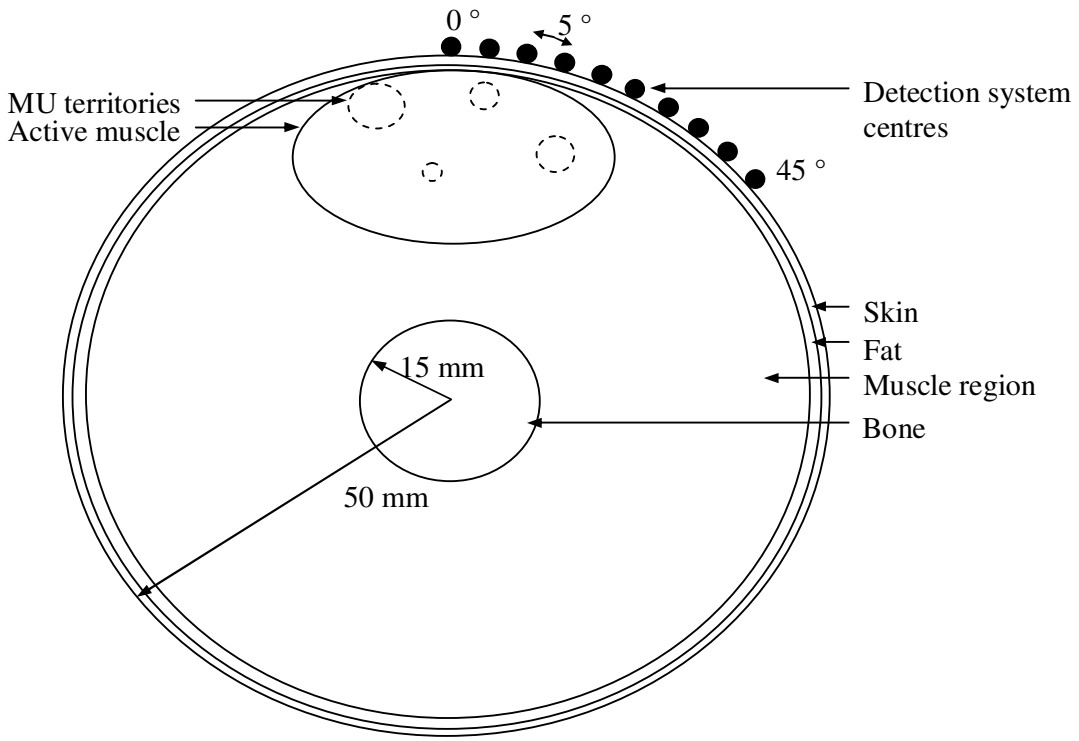

Figure 3.3. The created model of the limb with different layers, the active muscle, the location and territory of the MUs. The location of the detection system centres (M, SD, DD, NDD, IB ^{2}, see figure 2.3) is also shown.

Each MU is assigned a CV, with the smallest CV assigned to the smallest MU (Farina et al. 2002c). The CV has a Gaussian distribution (Lange et al. 2002) with a mean of 4 m/s and a variance of 0.3 m/s. The CV is limited between 2 and 7 m/s, which agrees to experimental findings (Andreassen & Arendt-Nielsen 1987; Broman et al. 1985; Lindstrom

et al. 1970; Lindstrom & Magnusson 1977; Merletti & Parker s.a.; Sadoyama et al. 1988; Troni et al. 1983).

The potentials contained in the libraries were all simulated at a CV of 4 m/s, which means that a SFAP has to be scaled to the correct CV of the MU it belongs to prior to adding it to the MUAP. Figure 3.4 shows an example of a SFAP that has been scaled to different values of CV. It is clear that the potential not only occurs at a later time when the CV decreases, but that the signal morphology also changes (Merletti et al. 1999a). This is because the whole generation and extinction process is sped up or slowed down by the scaling.

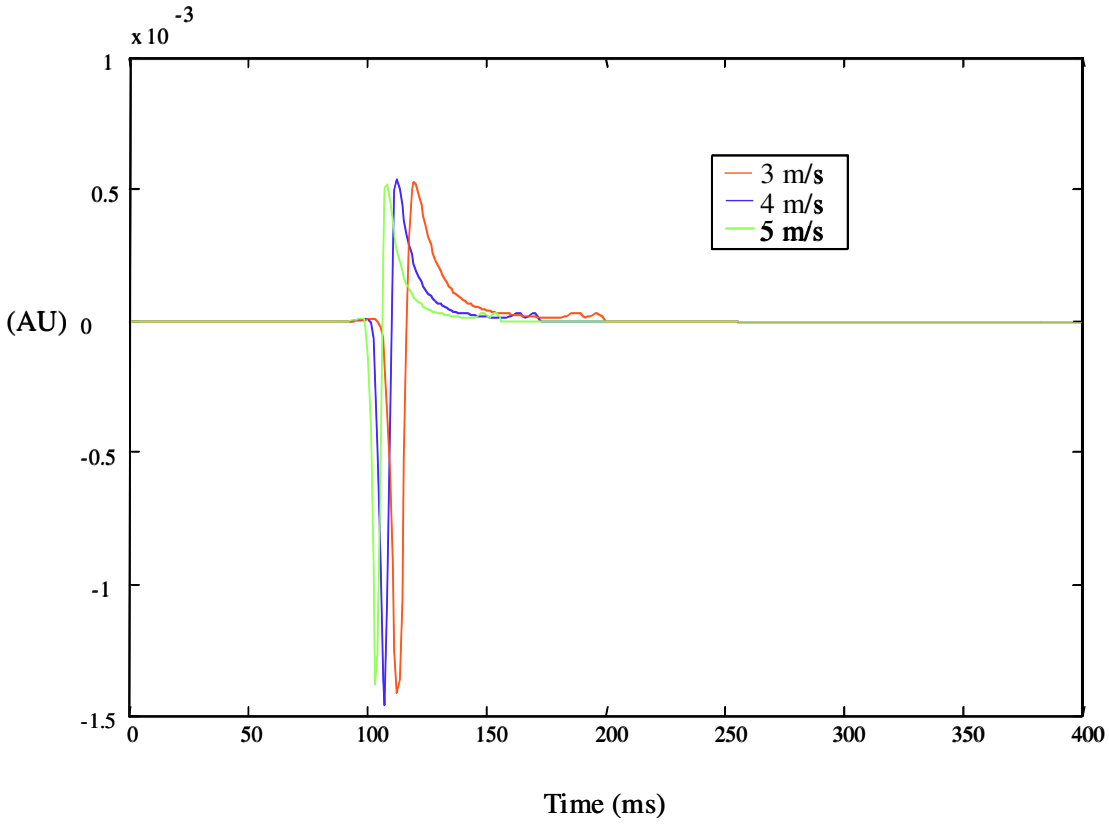

Figure 3.4. An SFAP scaled to different values of CV than the simulated value of 4 m/s.

The SFAPs of all the muscle fibres belonging to a certain MU are summed to result in the MUAP of that MU. An approximation incorporated to reduce the simulation time is that the same fibre can be shared by more than one MU. Its SFAP will, however, be scaled to the correct CV value for the specific MU before adding it to that MU's MUAP.

3.3. Motor unit discharge patterns

Once the MUAPs have been generated, they are combined with the discharge data of the MUs to create the MUAP trains. A MUAP train describes the regular discharge pattern of the whole MU as a function of time.

For the current simulation the MUs in the muscle were all assumed to be active, simulating a maximal force contraction. It was assumed that the force increases linearly from 0 to 100 % in 3 s. The duration of time in which a certain contraction strength is reached is given by

$$t_{\%MVC} = \frac{\%MVC}{100} \cdot 3, \tag{3.1}$$

where $t_{\%MVC}$ is the time duration in seconds, %MVC is the desired contraction strength (100 % MVC in this case), 100 denotes the maximum contraction and 3 specifies the time of maximum contraction. The MU discharge rate was computed on the basis of the MU recruitment threshold, described by equation 3.2:

$$RTE(i) = e^{\ln(RR)i/n}, i = 1,2,3..., \tag{3.2}$$

where *RTE* denotes the recruitment threshold excitation (% MVC where MU_i is recruited), *RR* the percentage MVC where all MUs are recruited (85 % for current simulation), *i* the number denoting the MU and *n* the total number of MUs in the active muscle (Fuglevand et al. 1993). By specifying the time when MVC is reached (t_{MVC} = 3 s for the current simulation), *RTE* can be converted to time units:

$$RTE\_time(i) = t_{\%MVC} - \frac{RTE(i)}{100} \cdot t_{MVC}, \tag{3.3}$$

It is clear that *RTE_time* can have negative values if the required contraction strength is reached before all MUs have been recruited ($t_{\%MVC}$ smaller than t_{MVC}). MUs with a negative value of *RTE_time* have thus not been recruited yet and will have a discharge rate

of zero. Because a contraction strength of 100 % MVC is currently simulated, this did not occur. The discharge rate of the recruited MUs is computed with the following equation:

$$f\_rate(i) = f_{\min} + sl\_dis \cdot (100 - RTE(i)), \qquad (3.4)$$

with f_{min} = 8 pulses per second (pps) and *sl_dis* the variation in discharge rate with a force equal to 0.3 pps/%MVC. The upper limit of MU discharge rate was set to 35 pps, corresponding to experimental measurements (Farina et al. 2002c; Fuglevand et al. 1993).

The largest discharge rate was assigned to the first MU recruited. The order of recruitment of MUs follows the Henneman size principle, which states that the smallest MUs are recruited first (Basmajian & De Luca 1985; Fuglevand et al. 1993; Knaflitz et al. 1990; Stegeman et al. 2000) . The principle has been observed practically by Sun et al. (1999). The discharge rates have thus been assigned in inverse order of MU size. Figure 3.5 shows the discharge rate assigned to each MU at 100 % MVC, RR = 85 % with the largest discharge rate assigned to the smallest, first recruited MU. The smallest MU has also been assigned the lowest value of CV (Masuda et al. 1996).

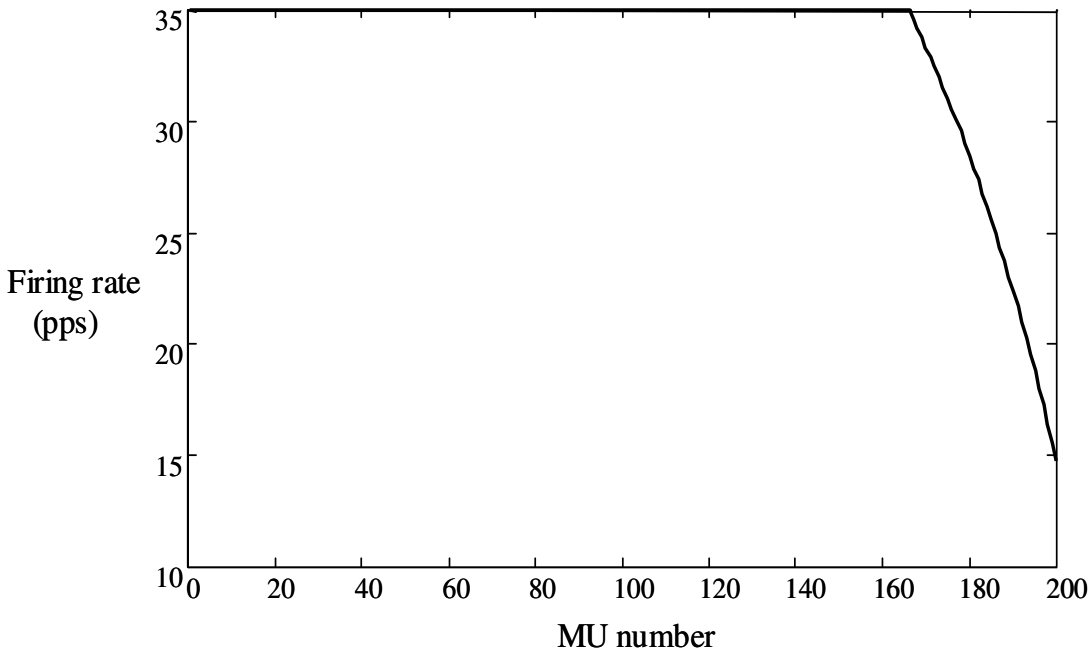

Figure 3.5. The discharge rate assigned to each of the 200 MUs at 100 % MVC.

IPI variability following a Gaussian distribution was added to each discharge to generate the final MU discharge pattern. The standard deviation of the IPI variability was 15 % of the IPI for all MUs.

The discharge pattern of eight MUs can be seen in figure 3.6. MU 1 (top row) is recruited first and MU 200 (bottom row) last. The discharge pattern indicates the instances in time when a certain MU fires. Discharging implies that a nerve impulse is generated in a cell body located in the brain or spinal cord. This results in the generation of an AP on each muscle fibre innervated by the motor neuron originating from that cell body. Each time an MU fires, it will thus generate an MUAP, which shows the total response of all the fibres in the MU contracting together.

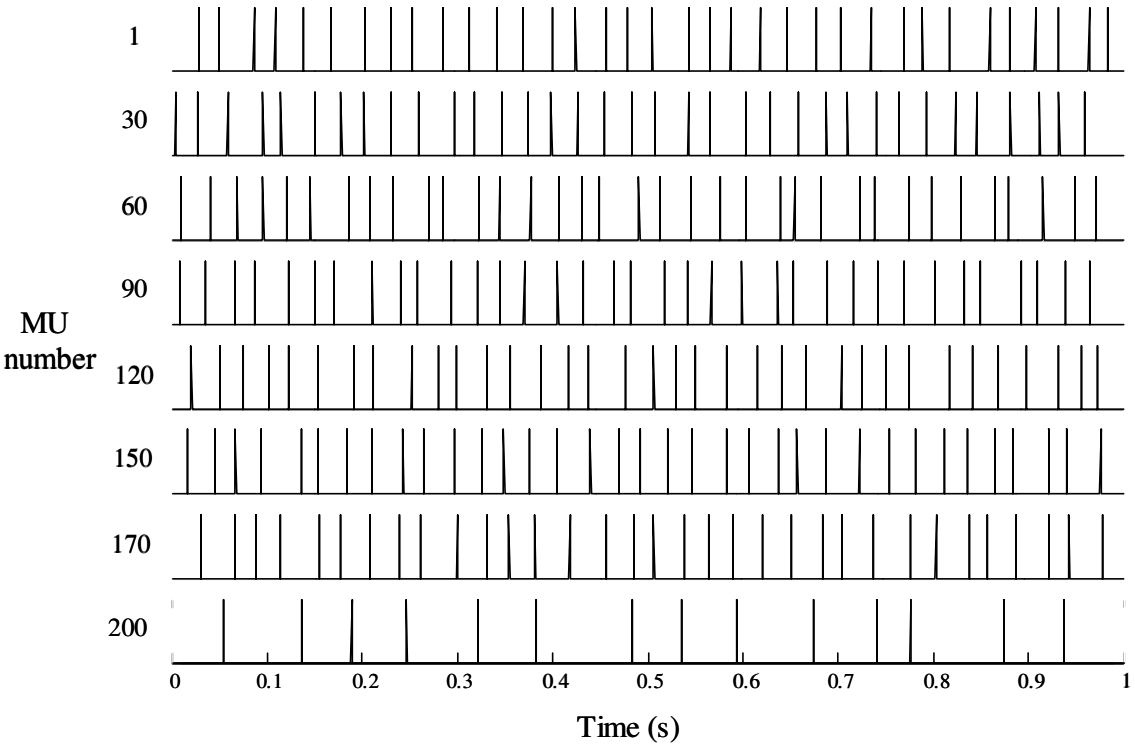

Figure 3.6. The discharge pattern of eight different MUs at 100 % MVC. Each time an MU fires it generates an MUAP. MU 1 is the first recruited MU and 200 the last.

The convolution of the MUAP of a certain MU and its discharge pattern results in the EMG signal detected on the surface of the skin due to that MU (Stegeman et al. 2000), as shown by equation 3.5:

$$S(i) = discharge\_pattern(i) * MUAP(i), \quad (3.5)$$

where *S(i)* is the MUAP train generated by MU(i), *discharge_pattern(i)* is the discharge pattern of MU(i) as can be seen in figure 3.6 and *MUAP(i)* is the MUAP of MU(i). A resulting MUAP train can be seen in figure 3.7. The summation of the MUAP trains of all the MUs in the active muscle leads to the EMG signal generated by the muscle.

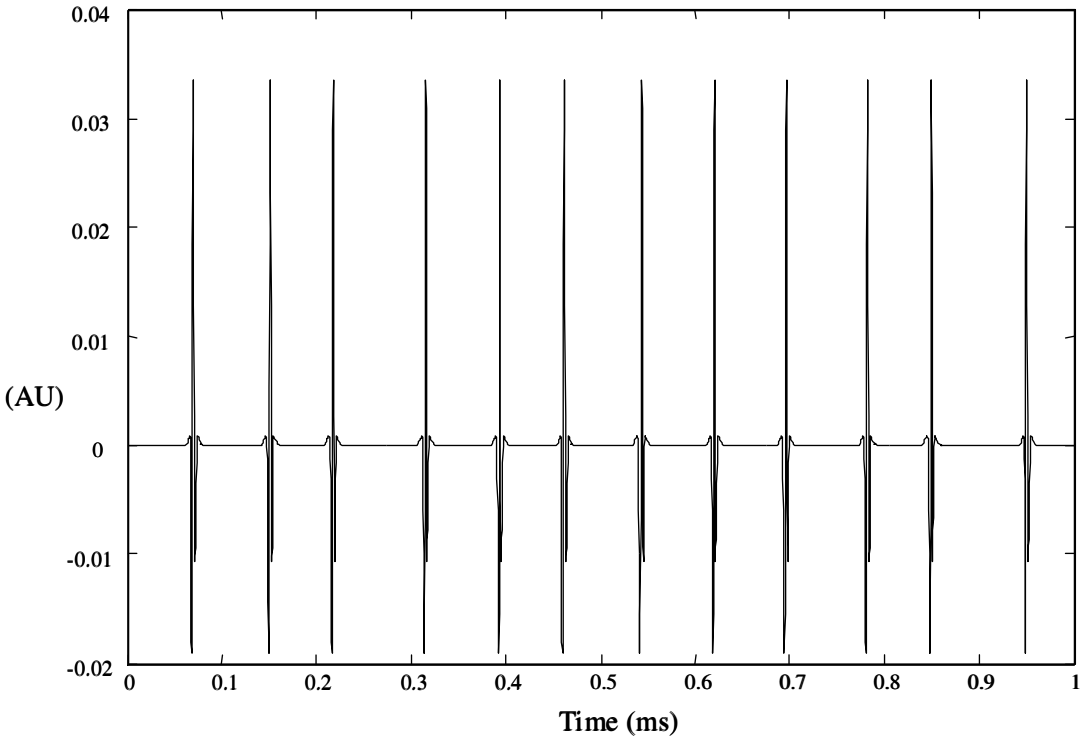

Figure 3.7. The MUAP train of a single MU containing 30 fibres.

3.4. Detection of the simulated sEMG signal

Once all the MUAP trains have been computed, they can be summed to obtain the EMG signal generated by the active muscle. This signal can then be detected with different electrode configurations located on the skin surface.

The signal was recorded with 10 detection systems placed circumferentially around the arm with their centres from 0 ° - 45 ° (see figure 3.3). Each detection system consists of a matrix of nine detection electrodes with an IED of either 5 or 10 mm. Depending on the

kind of spatial filter desired, different electrodes can be included in the summation to obtain the EMG signal detected on the skin surface. The weights assigned to the different electrodes are determined by the transfer function of the spatial filters (see figure 2.3). The resulting EMG signal detected at different angles around the limb with different detection systems can be seen in figure 3.8.

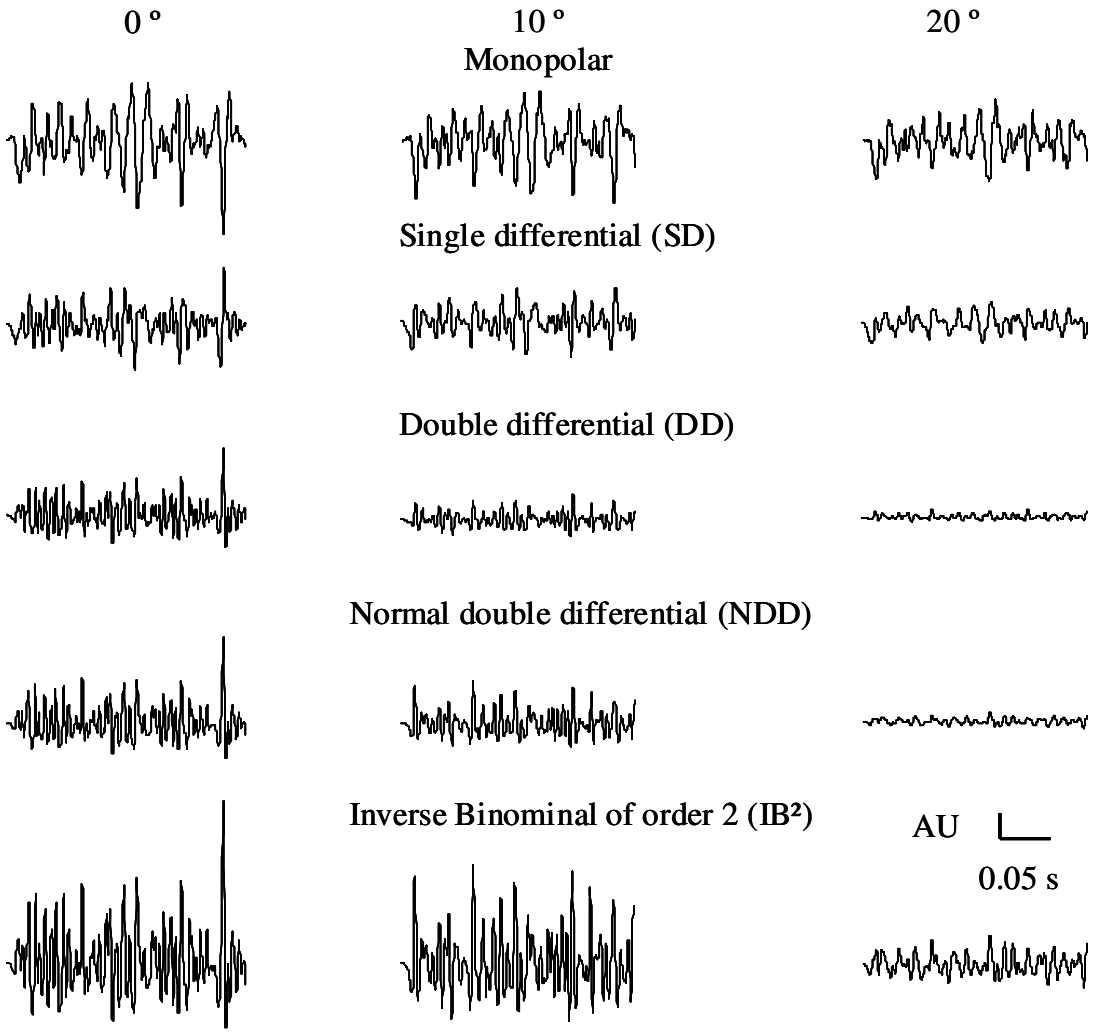

Figure 3.8. The simulated EMG signal detected on the skin surface at different angles using different detection systems.

The location of the detection system with respect to the innervation and extinction zones has been investigated before (Basmajian & De Luca 1985; De Luca 2002). Because non-propagating potentials have their origin at the end-plate or tendon area in the muscle, in practice it is usually preferred not to measure on these sites (Schulte et al. 2004). The muscle morphology also changes as one moves closer to the tendon area (De Luca 2002).

All the simulations comparing the effects of the limb and detection system parameters on crosstalk were performed with the detection systems placed halfway between the innervation and tendon area of the muscle. A separate simulation was done to establish what the effect of these areas of high crosstalk was on the different detection systems. In this simulation the detection system centres were placed directly above the IZ or tendon area.

The signals obtained with different spatial filters and originating from different libraries can now be compared to address the issue of crosstalk reduction.

3.5. Measures for evaluation of crosstalk reduction

The resultant EMG signals are evaluated to compare the performance of the different spatial filters for different simulation conditions. Two parameters that have been studied extensively and have been found to be appropriate indicators of the amplitude and frequency components (respectively) of an EMG signal are the average rectified value (ARV) and mean frequency (MNF) (Basmajian & De Luca 1985; De Luca & Merletti 1988; Farina & Merletti 2000; Merletti & Parker s.a.; Merletti et al. 1990; Merletti et al. 2001).

The ARV is related to the area under the rectified signal (De Luca 2002) and its decrease with increasing distance from the active muscle provides an indication of filter selectivity with respect to crosstalk. MNF defines the frequency component that carries the largest weight (centre of gravity) and thus gives information on the frequency content of detected signals. These can be obtained from equations 3.6 and 3.7:

$$ARV = \frac{1}{N}\sum_{i=1}^{N}\left|x_i\right|, \tag{3.6}$$

$$MNF = \frac{\sum_{i=1}^{M} f_i P_i}{\sum_{i=1}^{M} P_i}, \tag{3.7}$$

where N is the number of EMG samples in the chosen epoch, x_i are the EMG signal samples, f_i is the frequency, M is the highest harmonic considered and P_i is the i^{th} line of

the power spectrum. The signals used were 1 s long and sampled at a frequency of 4 096 Hz.

As stated in section 2.2.4, the propagating components, which form the main part of an EMG signal, are attenuated rapidly with increasing distance. Crosstalk signals propagate with less attenuation and can thus be measured at a larger distance from their origin. The detection system that shows the best suppression of amplitude content (a reduction of ARV) as the distance increases will thus be preferential for crosstalk reduction. Also, because travelling components are low-pass filtered by the volume conductor, the frequency content of true EMG signals should decrease with increasing distance from the source. This is reflected as a decrease in MNF with increasing distance. ARV is thus used to specify the selectivity of a system, while MNF provides information about the crosstalk signal.

Figure 3.9 shows representative graphs of the ARV and MNF values obtained with a monopolar (Mono) and DD detection system. The values are shown for an increasing distance between the detection electrodes and the source. Because the DD system shows a larger decrease in amplitude value (ARV) with increasing distance, its amplitude selectivity is said to be higher than that of the Mono system. This results from the higher order filtering and increased spatial selectivity of the DD system compared to Mono. Higher amplitude selectivity thus means better crosstalk rejection.

From a comparison between the MNF of Mono and DD it is apparent that DD contains lower frequency components than Mono because of the lower MNF value of DD. The DD signal was thus influenced more by the low-pass filtering effect of the volume conductor, and thus comprised mostly travelling components. Because Mono is only slightly affected by the low-pass filtering of the volume conductor, the non-travelling components contribute to a larger degree in the Mono signal.

The increase in frequency components at large distances reflects the increasing contribution of non-travelling components with increasing distance. Because the non-travelling components are not subject to the low-pass filtering of the volume conductor, and because their contribution to the final EMG signal increases with increasing distance, the MNF of the signal increases with the distance between the source and the detection electrodes.

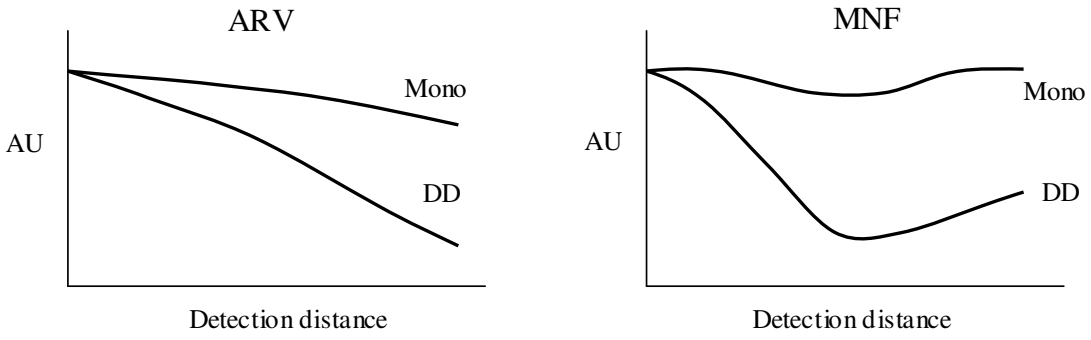

Figure 3.9. Representative curves showing the ARV and MNF values for increasing distance between the source and detection electrodes. Values have been normalised with respect to the first value and are thus shown in arbitrary units (AU).

Chapter 4

The effect of anatomical and detection system parameters on crosstalk

The objective of the study is to compare the ability of different spatial filters to reject crosstalk in different conditions. Chapter 3 describes the model that was developed for this purpose. In chapter 4 the results obtained from the different simulations are presented to determine the individual effect of each of these parameters on crosstalk. The influence of MU position and size is considered in section 4.1 while sections 4.2 – 4.5 focus on the different anatomical (fat layer thickness, skin conductivity and fibre length) and detection system (IED) parameters. Section 4.6 compares the difference in crosstalk when the detection system is located above either the IZ or the tendon area.

All the figures shown in this section are normalised with respect to the value obtained with the detection system located at 0 ° (see figure 3.3). This location minimises the distance between the active muscle and the detection system and thus results in the maximum amplitude EMG signal. Each detection system is normalised with respect to itself because

the goal of the study is not to quantify which situation results in the least amount of crosstalk, but rather which detection system shows the highest rate of crosstalk reduction. A logarithmic scale was used for the y-axis to accentuate the difference in spatial filter performance as the distance between the source and detection electrodes increases.

4.1. Influence of the location and size of the MUs on the sEMG signal

The location of the MUs in the active muscle is chosen randomly. This means that the user has no control over the placement of the largest or first recruited MU, since it is varied randomly between simulations. To determine if this random placement of MUs has an effect on the sEMG signal, 10 simulations were done in which the only variable was the location of the MUs in the active muscle.

4.1.1 Results and discussion

Figure 4.1 shows the mean and standard deviation of the ARV and MNF obtained from 10 simulations. It is clear that the random placement of the MUs results in a variation of the ARV and MNF values. The standard deviation is, however, sufficiently small for the response of different systems to be identified from one another and does not overlap for the largest part of the simulation.

Because the volume conductor acts as a low-pass filter (De Luca & Merletti 1988; Farina et al. 2004c; Lindstrom & Magnusson 1977; Stegeman et al. 2000), it has a smoothing effect on the EMG signals. The signals originating from different MUs will undergo different amounts of smoothing because of the varying depth of the MUs in the muscle. The more the response from an MU is smoothed, the smaller its contribution to the final EMG signal will be. Deeper MUs thus have a smaller contribution to the final EMG signal than more superficial ones.

It is clear that the two 2-D filters (NDD and IB^2) have a very similar response. This was observed in all the simulations performed in the total study.

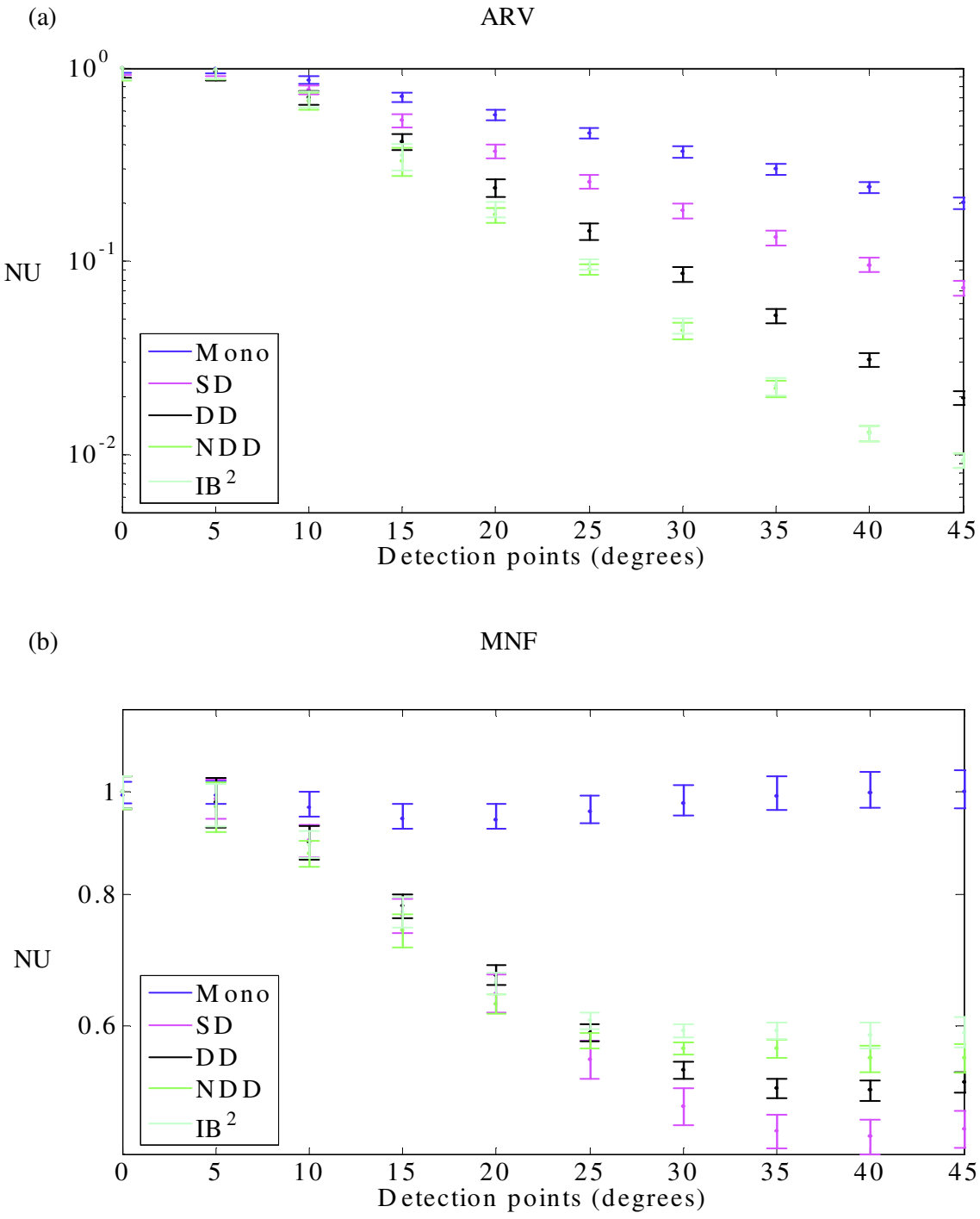

Figure 4.1. Mean and standard deviation of the ARV (a) and MNF (b) for 10 simulations. Fat layer = 1 mm, IED = 5 mm, fibre length = 60 mm, skin conductivity = 1 S/m.

4.1.2 Conclusion

Despite the variations observed between the simulations, it is possible to discriminate visually between the different spatial filters and to compare their performance with respect to crosstalk rejection. The trends followed by the computed variables are also clear. It may, however, be incorrect to base any conclusions on a single simulation.

All the results shown in the rest of the study are thus the average value obtained from 10 simulations with the only variable being the random location of the MUs. Standard deviation is excluded from any further figures to ensure ease of discernment between the different detection systems.

Since NDD and IB^2 gave similar results, IB^2 is omitted from the rest of the figures for clarity. All the comments and conclusions for NDD also hold true for IB^2.

4.2. Influence of fat layer thickness

Because the fat layer is anisotropic and a poor conductor, an increase in its thickness influences the spatial spread of the potentials more than a mere increase in fibre depth does (Roeleveld et al. 1997a). The filtering properties of fat and muscle tissue are also different (Farina et al. 2002a). A study was done to determine what effect the increase in fat layer thickness from 1 to 5 mm has on the performance of the different detection systems.

4.2.1 Results

The increase in fat layer thickness leads to an overall decrease in amplitude selectivity, as can be seen in figure 4.2 (a). When the distance between the detection system and the muscle is small, the results obtained by all the detection systems are comparable, but they start to diverge as the distance increases. NDD becomes the most selective filter, followed by DD, then SD and lastly Mono. The order remains the same when the fat layer thickness is increased.

The characteristics of the crosstalk signals can be seen from the MNF values (figure 4.2 [b]). At first, the frequency content of SD, DD and NDD decreases with increasing

distance. It then shows a flattening and eventually an increase in value. The increase is much

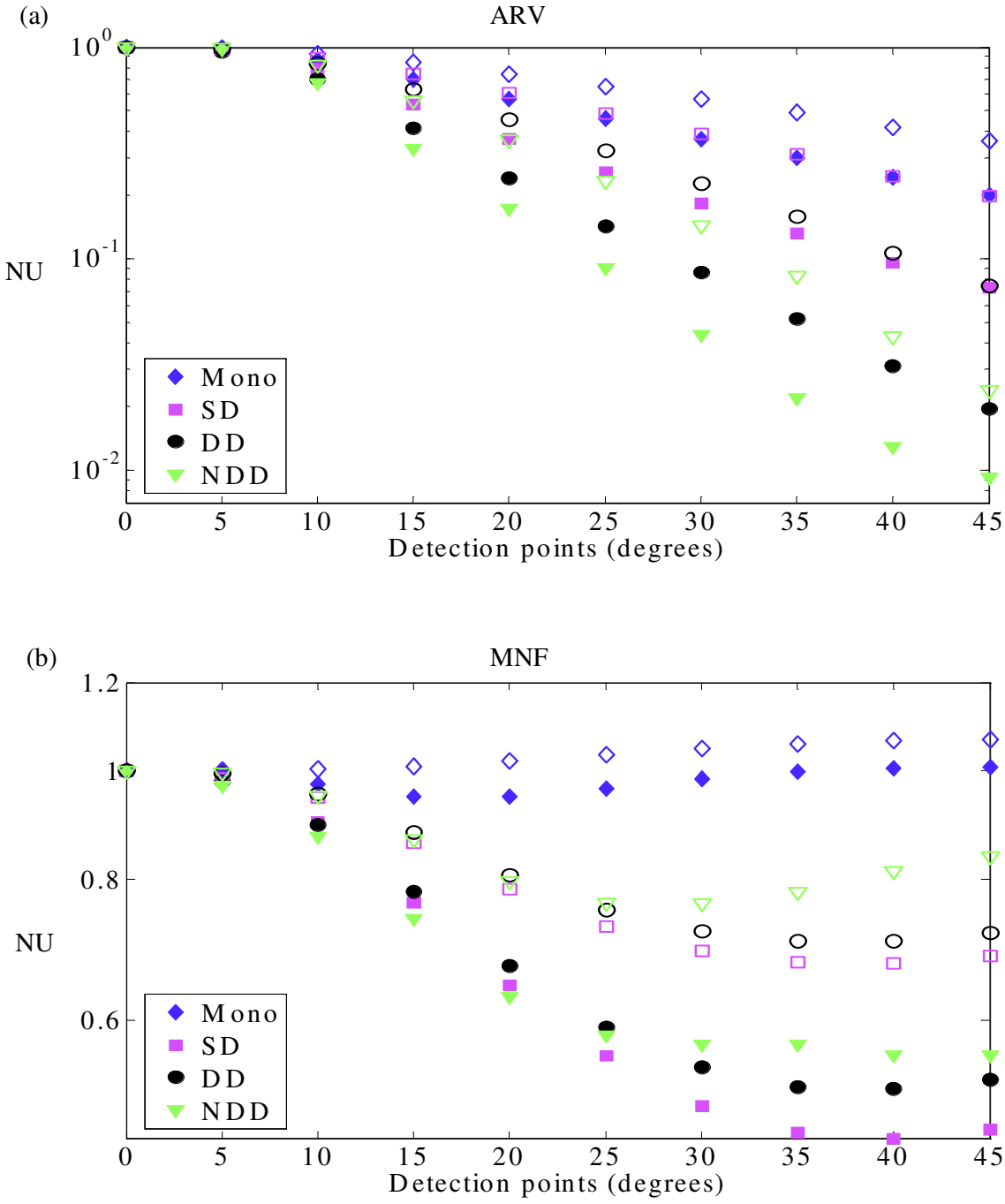

Figure 4.2. The ARV (a) and MNF (b) of library 1 (filled markers, fat layer = 1 mm) and 2 (open markers, fat layer = 5 mm), IED = 5 mm, fibre length = 60 mm, skin conductivity = 1 S/m.

more evident in NDD than the other two. A thicker fat layer leads to a smaller reduction in frequency components in all the investigated detection systems, and an even sharper increase for the NDD system. Mono shows only a slight decrease in MNF before it starts to increase to an even higher value than that at 0 °. This effect is again more evident in the case of a thick fat layer.

4.2.2 Discussion

An increase in fat layer thickness has a number of influences on the potentials detected on the skin surface. Firstly, it leads to an increase in the distance between the source and the detection electrodes. Since the total distance is increased, the relative variation in distance between the detection electrode and propagating waveform is reduced. A more similar EMG signal is thus observed from the different detection points (Lowery et al. 2002). The fat layer increase furthermore causes the volume of muscle contributing to the sEMG to increase (Lowery et al. 2003b). This means that signals originating from far away (crosstalk) are more likely to be included in the EMG measurement.

The result of the above-mentioned effects is that the true EMG signal and the crosstalk portion contribute in more equal parts to the detected EMG signal as the fat layer thickness increases. As Merletti et al. stated: components resulting from deeper MUs carry a larger relative weight in the measured EMG signal as the distance between the source and detection electrodes increases (Merletti et al. 1999a). A higher signal amplitude is thus observed at the same distance from the active muscle when a thick fat layer is present compared to the presence of a thin fat layer (as seen in figure 4.2 [a]). This means that the amount of crosstalk increases with an increase in fat layer thickness. This increase in crosstalk and decrease in selectivity with increasing fat layer thickness is confirmed by other groups (De Luca & Merletti 1988; Farina et al. 2002a; Farina & Merletti 2003; Lowery et al. 2003a; Lowery et al. 2003b; Roeleveld et al. 1997a; Solomonow et al. 1994).

The frequency components of the crosstalk signals indicate that high-pass filtering of the detected EMG signal might partly reduce the crosstalk in an SD or DD detected signal. This is, however, not the case for a signal detected with the NDD system. The increase in frequency with increasing distance might be explained by the fact that non-travelling components are not affected by the low-pass filtering effect of the volume conductor

(Dimitrova et al. 2002; Farina et al. 2002a), and that they will have a higher frequency content than the true EMG signal.

When the performance of the different spatial filters is compared, DD and NDD show similar results at first. As the distance between the source and detection electrode increases, NDD results in better crosstalk rejection. This is the case for both thick and thin fat layers.

The inability of Mono to reject crosstalk is clear from the fact that almost no amplitude selectivity is present. The ARV and MNF values both stay approximately the same with increasing distance from the active muscle. This means that signals originating from far away will contribute to the final signal with the same weight as a signal from a nearby location. The crosstalk signal will contain higher frequency components than the true EMG signal.

Farina et al. recently found contradictory results when comparing the SFAP from deeper fibres measured with NDD and DD systems (Farina et al. 2004c). Their conclusion was that NDD is less selective than DD and SD with respect to fibre depth. This can be attributed to the fact that they used only single fibres for their simulations and the depths compared were 1 mm and 5 mm. Since the current study used a muscle consisting of between 10 000 and 200 000 fibres arranged at depths from 1 to 27.4 mm below the skin surface, it is difficult to draw a direct comparison between the two studies. Also, as stated before, an increase in depth in the muscle layer and an increase in depth due to a thicker fat layer will not yield the same results.

4.2.3 Conclusion

An increase in fat layer thickness leads to an overall decrease in selectivity for all the spatial filters tested. This means that better crosstalk selectivity is possible with decreasing fat layer thickness. The best detection system to use for crosstalk rejection with either a thick or thin fat layer is the NDD set-up.

4.3. Influence of skin conductivity

It has been shown that the effect of the fat layer on surface potentials is only accurately modelled if a highly conductive skin layer is also present (Farina & Rainoldi 1999; Roeleveld et al. 1997a). It is not possible to model the experimentally observed lateral spread of potentials without inclusion of this layer. Because of the low conductivity of the fat layer, it limits the flow of current from the high conductivity muscle region to the skin surface. The addition of a high conductivity skin layer shunts the fat layer, thus causing potentials to show a more realistic decrease with increasing distance. Two values of skin conductivity were simulated to examine the effect it has on crosstalk reduction.

4.3.1 Results

From figure 4.3 it is clear that the reduction in skin conductivity leads to an overall increase in selectivity. As seen in the previous figure, the results obtained with all the detection systems are comparable for small distances between the muscle and detection system, while NDD becomes the most selective filter as the distance increases. It is followed by DD, then SD and lastly Mono. When the skin conductivity is decreased, the amplitude response of NDD and DD are comparable and eventually almost equal, with DD performing slightly better.

The MNF again shows a decrease and flattening off. SD results in the largest decrease in frequency components, followed by DD, then NDD and lastly Mono. A decrease in skin conductivity does not change this order.

4.3.2 Discussion

Because the skin is a complex structure that is highly affected by factors such as temperature, humidity, stress level, etc. it is still not clear exactly what value of skin conductivity to use in simulations. The value currently used (1 S/m) is higher than the conductivity of muscle or fat. This is based on the observation that a high conductivity layer is necessary to explain the lateral spread of potential found experimentally (Roeleveld et al. 1997).

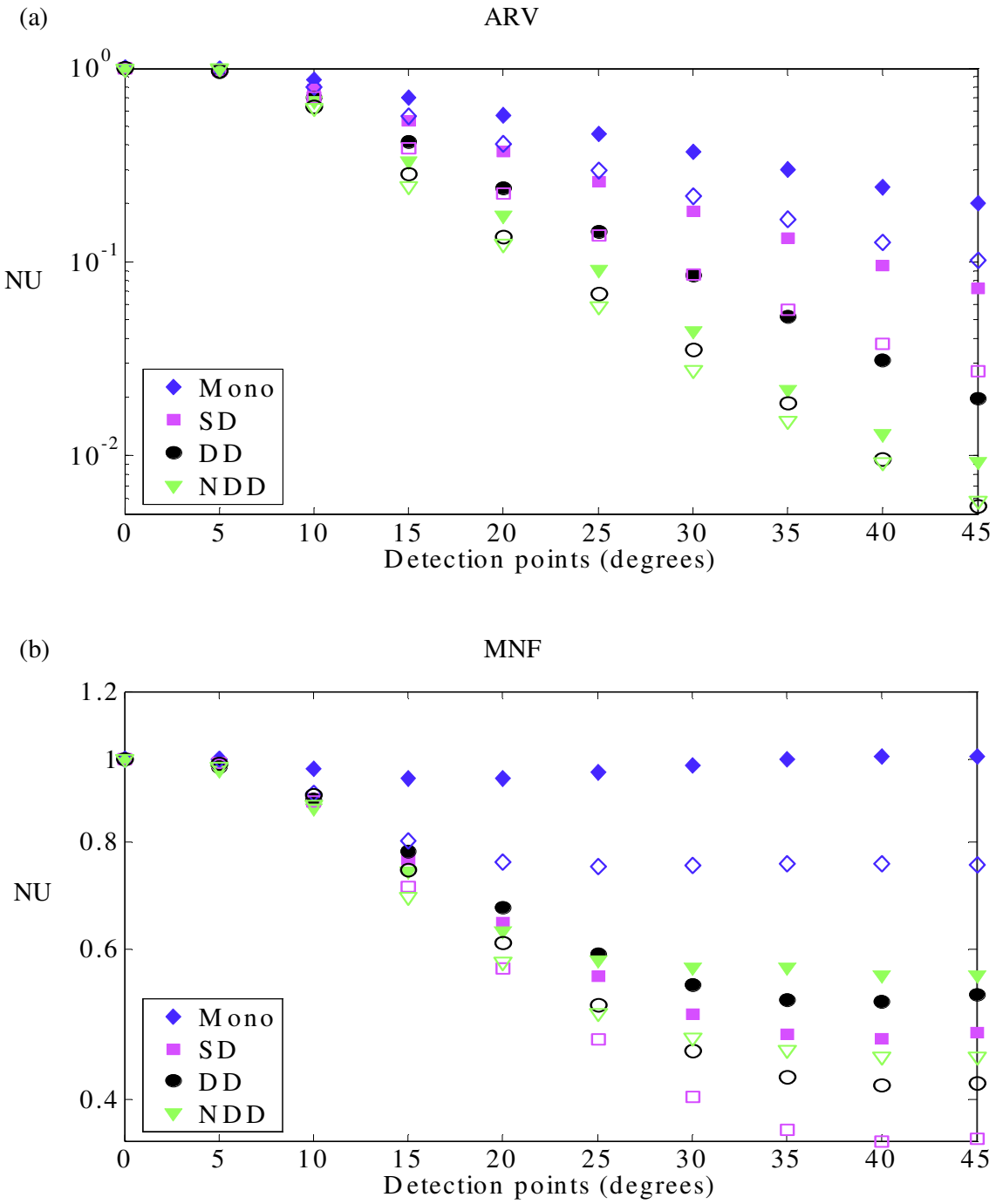

Figure 4.3. The ARV (a) and MNF (b) of library 1 (filled markers, skin conductivity = 1 S/m) and 3 (open markers, skin conductivity = 0.1 S/m), IED = 5 mm, fibre length = 60 mm, fat layer = 1 mm.

When electrodes are applied to the skin surface, the normal practice is to lower the skin impedance by abrasion or by applying a conductive gel to the skin. This maximises the quality of the recorded EMG signal. From figure 4.3 [a] it is clear that a more conductive skin layer leads to higher amplitude values at increasing distance from the source. This means that crosstalk increases with skin conductivity. Lowery et al. (2003a) confirms this observation. If skin conductivity is decreased, selectivity is increased, which means that better crosstalk reduction is obtained.

When skin conductivity is high (close to 1 S/m), NDD results in the best measurements, affected least by crosstalk. When it is reduced, NDD and DD perform basically equally. It is thus clear that the performance of the DD system is greatly enhanced with respect to NDD as skin conductivity is reduced.

4.3.3 Conclusion

A decrease in skin conductivity leads to an increase in selectivity, and better crosstalk reduction is thus possible because the contribution from far away sources decreases. The most effective spatial filter for crosstalk reduction with high skin conductivity is NDD, while DD and NDD perform comparably when skin conductivity decreases.

4.4. The effect of different fibre lengths

The non-propagating components originate approximately at the centre (IZ) and end (muscle-tendon junction) of a muscle fibre. These components play an important role in the crosstalk signal. Since the objective of the study is to reject crosstalk, it was necessary to investigate what effect the distance between these sites and the detection electrodes had on crosstalk. Two fibre semi-lengths of 30 and 60 mm were simulated and the sEMG signal recorded with different detection systems. The detection electrode array was always placed halfway between the IZ and muscle-tendon junction.

4.4.1 Results

From figure 4.4 [a] it is clear that the amplitude selectivity of NDD and DD is increased with decreased fibre length. The selectivity of SD is initially decreased, but from a certain point it increases, while that of Mono is always decreased. In both cases NDD shows the

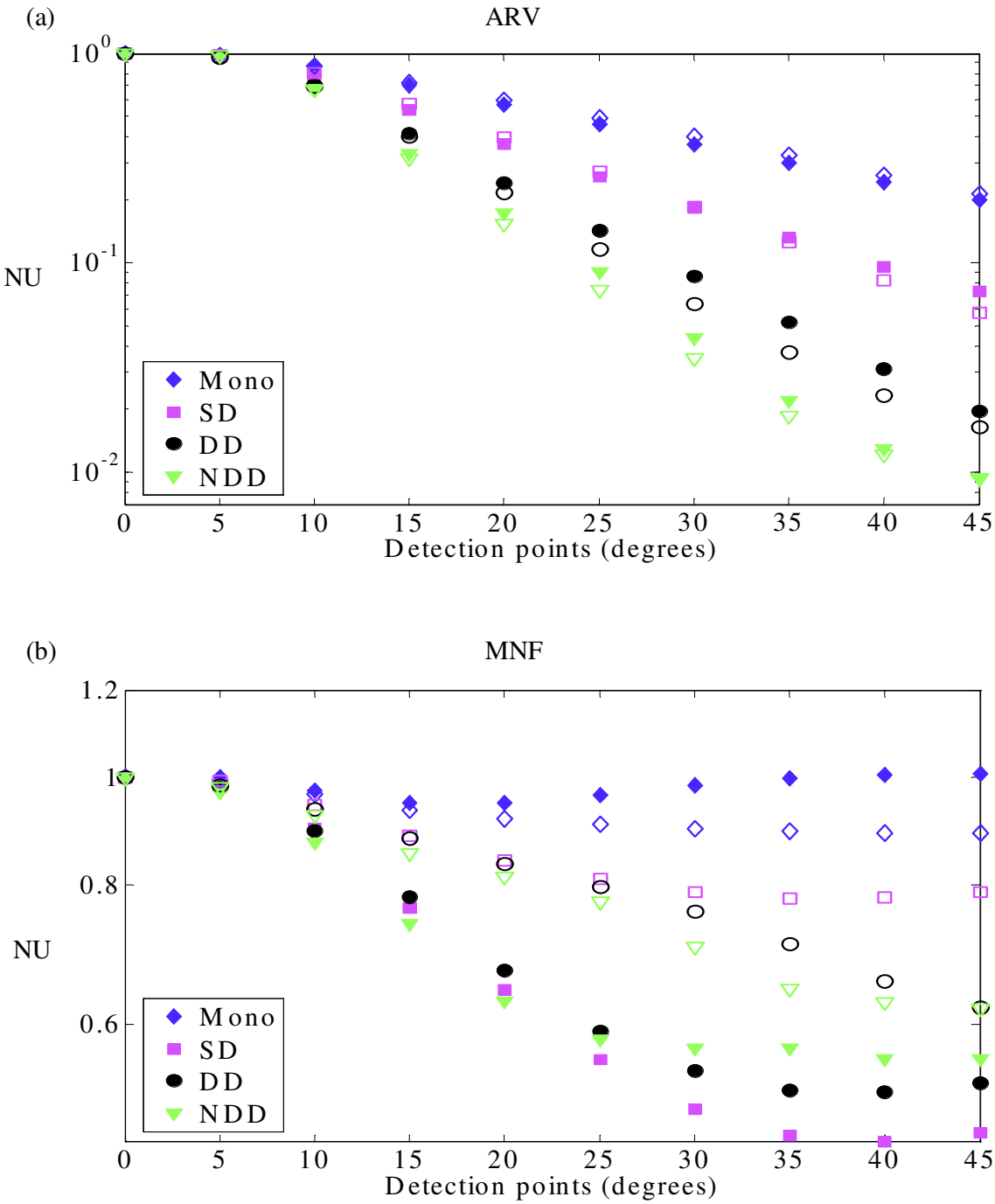

Figure 4.4. The ARV (a) and MNF (b) of library 1 (filled markers, fibre semi-length = 60 mm) and 5 (open markers, fibre semi-length = 30 mm), IED = 5 mm, fat layer = 1 mm, skin conductivity = 1 S/m.

most selective measurements. A decrease in fibre length does not influence the order in which the detection systems are ranked with respect to amplitude selectivity.

For short fibres NDD has the most selective frequency response, followed by DD, SD and lastly Mono (figure 4.4 [b]). The MNF of SD, DD and NDD increases when the fibre length is decreased, while that of Mono decreases.

When longer fibres are simulated, NDD again shows the lowest MNF value at first, but SD overtakes it as the distance increases. There is a large increase in frequency components with a decrease in fibre length. Mono again shows almost no amplitude or frequency selectivity for either fibre length.

4.4.2 Discussion

As stated before, non-propagating components originate at the IZ and muscle-tendon junction (Roeleveld et al. 1997a; Roeleveld et al. 1997c). At the IZ two APs travelling in opposite directions are generated. This means that there are two dipoles located close to each other, resulting in a partial cancellation of their effect. The non-propagating components originating from the IZ thus do not have a large influence on the surface potential. This means that the main contribution of non-propagating components will be from the muscle-tendon junctions (Gootzen et al. 1991). The shorter the fibre length, the closer these junctions are located to the IZ, and thus to the detection electrodes.

When the fibre length is decreased, the tendon regions move closer to the detection electrodes. This means that the non-propagating components become a more dominant part of the detected signal. The necessity to reject these components and ensure signal fidelity is thus further increased for short fibre lengths.

From figure 4.4 [a] it is clear that NDD results in the most selective amplitude response for both long and short fibres. This is desirable, because it means that signal components originating from far away (crosstalk) will be suppressed most.

The increase in MNF when a shorter fibre is simulated clearly shows the increased weight of the non-travelling components that are not low-pass filtered by the volume conductor. This means that shorter fibres result in higher crosstalk values.

For longer fibres, NDD has the highest frequency components, followed by DD and then SD. For shorter fibres, NDD has the lowest frequency components, followed by DD and then SD. It is thus clear that the fibre length has a large influence on the characteristics of the crosstalk signals in EMG measurements, especially for the SD system.

Because of the low selectivity of Mono, it always leads to the highest crosstalk values.

4.4.3 Conclusion

A decrease in fibre length causes an increase in the amount of crosstalk present in the measurements. It does, however, result in an increased rate of crosstalk rejection with increasing distance. To ensure maximum rejection of these undesirable components, the NDD detection system should be used for both long and short fibre lengths. Differences in fibre length greatly influence the characteristics of the crosstalk signal.

4.5. The effect of varying IED

IED defines the distance between two adjacent detection electrodes. The potential detected by a detection system is the summation of all the potentials within the pick-up volume of the system. A larger IED implies a larger pick-up volume (Merletti et al. 1999a). The best IED value to use for the biceps brachii has been specified as 5 mm by Reucher et al. (1987b). To investigate the effect of IED on crosstalk, a simulation was performed in which the IED of the different detection systems was set to 5 and 10 mm, respectively.

4.5.1 Results

Figure 4.5 shows the results obtained for long muscle fibres with a semi-length of 60 mm. The amplitude selectivity of SD, DD and NDD is reduced with increasing IED (figure 4.5 [a]). Because the monopolar set-up consists of only one electrode, it is not possible to change its IED. For both values of IED, NDD results in the most selective measurements.

Changing the IED does not significantly change the order of most selective to least selective filter, meaning NDD stays the most selective filter with an IED of either 5 or 10 mm, followed by DD, then SD and lastly Mono.

An increase in IED shows an increase in main frequency components contributing to the detected signal (figure 4.5 [b]).

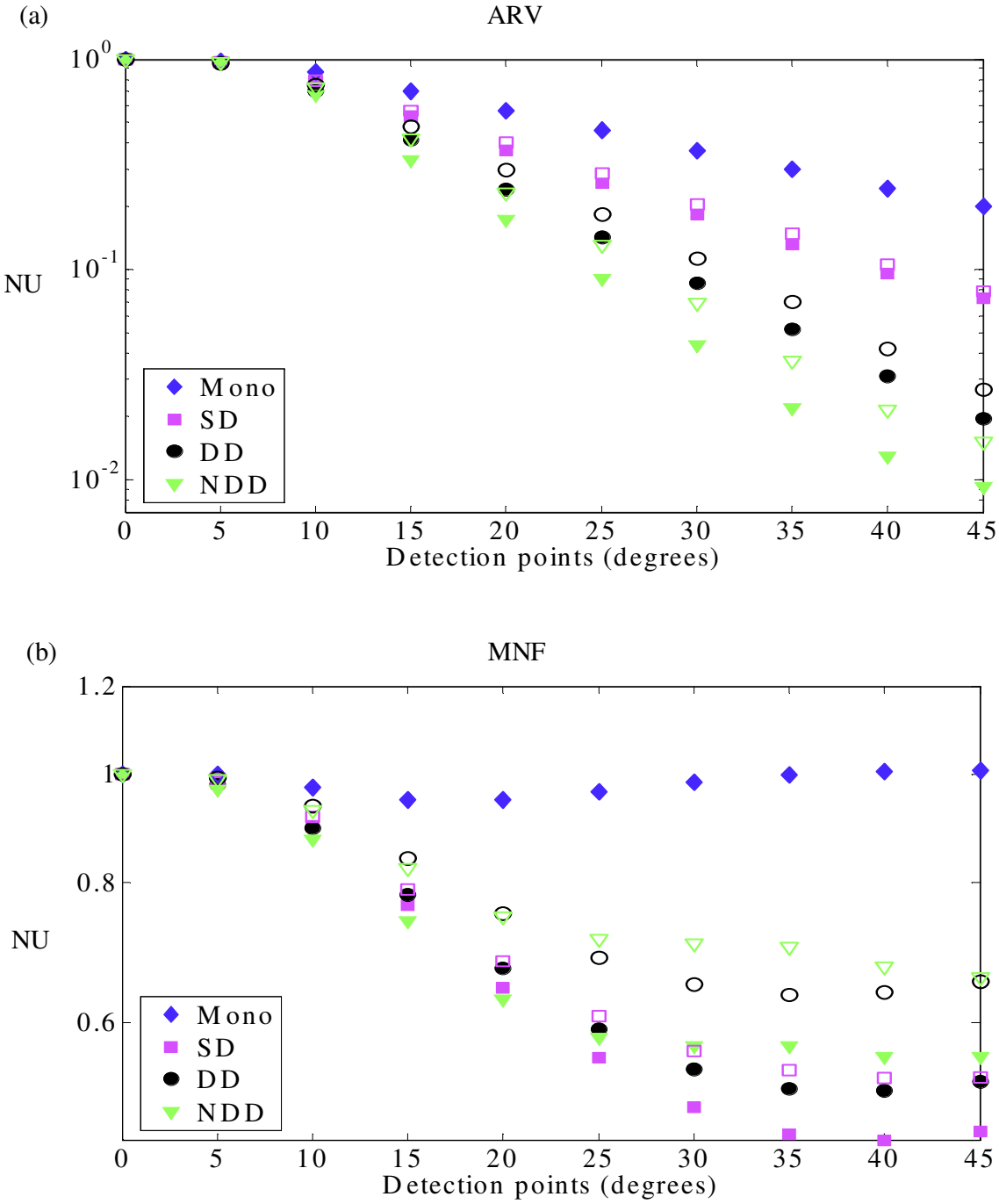

Figure 4.5. The ARV (a) and MNF (b) of library 1 with an IED of 5 mm (filled markers) and IED = 10 mm (open markers) fibre semi-length = 60 mm, fat layer = 1 mm, skin conductivity = 1 S/m.

The frequency selectivity is thus also reduced with increasing IED. In both cases, SD results in the highest frequency suppression followed by DD and then NDD. This occurs at a smaller distance with the larger IED.

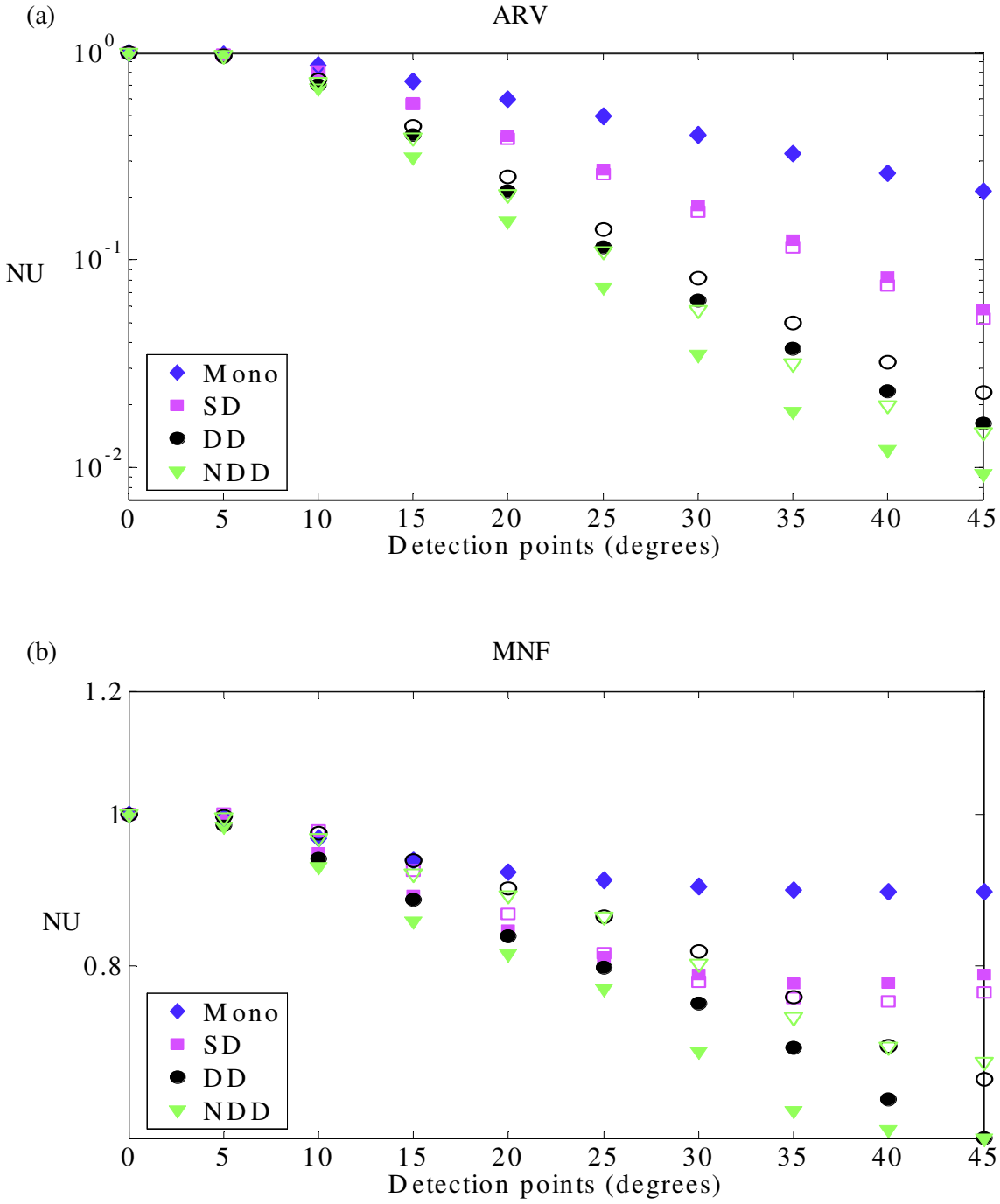

Figure 4.6. The ARV (a) and MNF (b) of library 5 with an IED of 5 mm (filled markers) and IED = 10 mm (open markers) fibre semi-length = 30 mm, fat layer = 1 mm, skin conductivity = 1 S/m.

Schulte et al. (2004) stated that the effect of IED on estimates of MNF is larger when a short fibre length is used. It appears that short fibres need a smaller IED value to ensure correct estimation of MNF, while IED values from 2.5 to 10 mm all yield accurate estimates with longer fibres (75 mm total fibre length). Even though the current study does not focus on the accuracy of the estimates, Schulte's results lead to an investigation on the combined effect of fibre length and IED on crosstalk. The previous simulation was repeated with a fibre semi-length of 30 mm, and the results can be seen in figure 4.6.

A comparison of figures 4.5 and 4.6 shows that the amplitude content (part a of both figures) is not significantly influenced by a reduction in fibre length. The main difference is the fact that SD shows slighty decreased selectivity for the longer fibre length and increased selectivity for the shorter fibre length.

An analysis of the frequency content reveals more differences. It is clear that the longer fibres lead to a larger reduction of frequency components than the shorter fibres (part b of both figures) in all cases except for the monopolar set-up. Monopolar measurement yields higher frequency components when a longer fibre length is simulated. It is also obvious that MNF varies less with IED when a shorter fibre length is used.

The frequency performance of the SD filter deteriorates most when the fibre length is reduced. Its results change from containing lowest frequency components at 60 mm to containing the second highest at 30 mm. It is the only filter that shows a more selective response with an IED of 10 mm than 5 mm as distance increases.

4.5.2 Discussion

Farina et al. (2002d) recorded signals from the trapezius muscle using a SD set-up and found that increasing IED led to an increase in amplitude value. Merletti did modelling experiments (Merletti et al. 1999a) in which he found an increase in ARV for increasing IED values. This can be explained by the fact that the electrode pick-up area increases with the IED. A larger pick-up area means more SFAPs will be summed to obtain the resulting signal, and it will thus have a larger amplitude. This also implies that crosstalk will be increased with increasing IED. This effect is seen in figure 4.5 and 4.6, where the amplitude selectivity of NDD and DD decreases with increasing IED. This means that

fibres further away make a large contribution to the final signal. The only exception is SD when a short fibre length is simulated. At first the two IED values result in the same amplitude selectivity, but at some stage the larger IED becomes a little more selective. Similar results were obtained by Farina et al. (2002a), who state that a reduction in IED is not an effective way to reduce crosstalk for SD systems. The result thus implies that an IED of 10 mm results in greater selectivity with respect to crosstalk when an SD system is used in an area which is known to contain significant crosstalk than in the case of an IED of 5 mm. It should, however, be noted that the difference is very small, and that both IED values give comparable results.

Farina et al. (2002a) and Koh and Grabiner (1993) found much less variation in crosstalk measurement when varying the IED of the SD set-up than when that of DD was varied. Figures 4.5 [a] and 4.6 [a] confirm this result, showing that SD measurements vary very little as IED changes, when compared to DD and NDD.

In general, an increase in IED leads to a decrease in selectivity and thus to an increase in crosstalk, irrespective of the detection system used. This is confirmed by some other authors (Farina et al. 2002a; Lowery et al. 2003a), and is seen for both long and short fibre lengths.

When comparing the frequency components it is again clear that an increase in IED causes an increase in MNF value. The only exception is again SD with a short fibre length (figure 4.6 [b]), where MNF is seen to decrease with increasing IED. Merletti et al. (2003) found similar results when taking measurement from the trapezius muscle. Changing the length of the muscle fibres has the largest influence on IED variations for the SD system.

4.5.3 Conclusion

An increase in IED value generally leads to a decrease in selectivity, and thus to an increase in crosstalk. The NDD filter results in the best measurements for crosstalk rejection for both long and short fibres, with an IED of either 5 or 10 mm. The conclusion of Reucher et al. (987b) that an IED of 5 mm is preferred for the biceps brachii is confirmed. Lastly, the SD set-up proves to be influenced least by changes in IED, but most by changes in fibre length.

4.6. The effect of electrodes located on end-plate or tendon area

It has been stated that the characteristics of a measured signal are dependent on the position of the detection electrodes with reference to the IZ and tendon area. As this is the origin of the non-propagating components, more crosstalk will be detected when the signal is measured directly above one of these sites (Basmajian & De Luca 1985; De Luca 2002; Merletti et al. 1999a; Schulte et al. 2004). To examine the performance of the detection systems in these high-crosstalk areas, electrodes were placed directly above these sites and the resulting signals compared to those measured above the electrically more quiet locations.

4.6.1 Results

Figure 4.7 [a] shows a comparison between a signal measured above the IZ and one measured halfway between the IZ and tendon area. NDD, DD and SD all show higher amplitude selectivity when measured above the IZ. Mono is the only system that is less selective when placed above the IZ. NDD is the most selective filter to use for both electrode placements.

The frequency content of NDD and DD shows a sharp decrease with increasing distance from the active muscle when measured above the IZ (figure 4.7 [b]). Mono also has a slight decrease in MNF, while that of SD increases.

Figure 4.8 shows the results when the detection systems are placed above the tendon area and halfway between the IZ and tendon area. Placement of the detection electrodes above the tendon area appears to have a smaller effect on the measurements than placement above the IZ has. The amplitude content shows very little difference for the two electrode locations, with NDD again being the most selective filter.

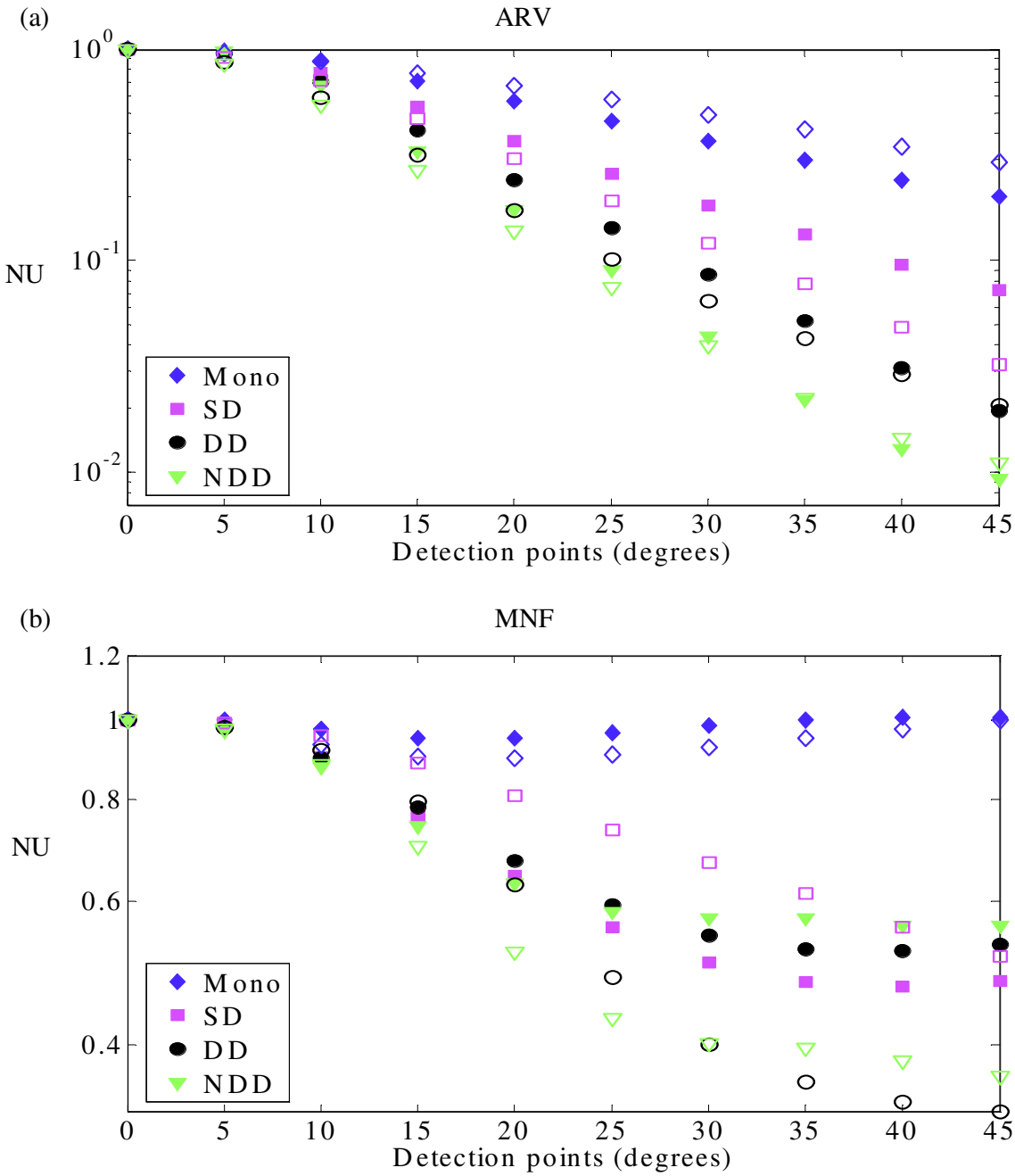

Figure 4.7. The ARV (a) and MNF (b) of library 1 detected halfway between the IZ and tendon (filled markers) and above the IZ (open markers). Fibre semi-length = 60 mm, fat layer = 1 mm, skin conductivity = 1 S/m, IED = 5 mm.

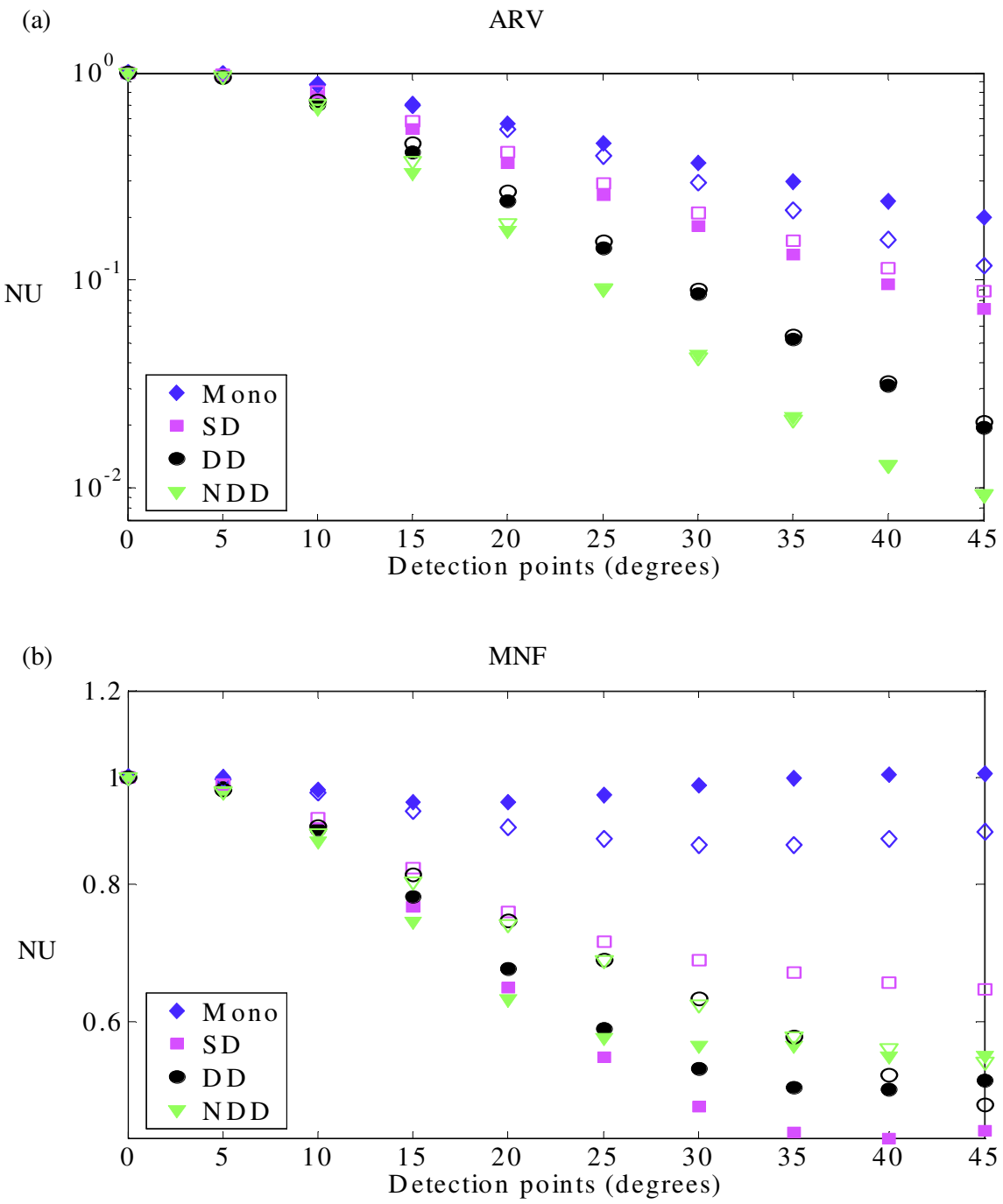

Figure 4.8. The ARV (a) and MNF (b) of library 1 detected halfway between the IZ and tendon (filled markers) and above the tendon area (open markers). Fibre semi-length = 60 mm, fat layer = 1 mm, skin conductivity = 1 S/m, IED = 5 mm.

All the detection systems except for Mono show an increased MNF when the detection electrodes are placed above the tendon area. NDD and DD show a very similar

performance, with DD resulting in lower values than NDD at large distances. SD is affected most by the shift in electrode positions.

4.6.2 Discussion

Since many of the non-propagating components present in an sEMG signal originate at the IZ or tendon area (see section 3.4), these are good sites to test the performance of different spatial filters with respect to crosstalk reduction.

A comparison of the figures above clearly shows that NDD results in the best crosstalk reduction for measurements taken at any of the three locations. It always results in the most selective measurements, irrespective of the amount of crosstalk present.

As stated by De Luca (2002), more crosstalk is present in measurements made directly above the IZ or tendon area. These sites are thus not preferred for sEMG detection. It should be noted that figures 4.7 and 4.8 are normalised with respect to the value detected at 0 °, and do not show the absolute amount of crosstalk present. Although the IZ has a more selective NDD response than halfway between the IZ and tendon area, it does not mean that there will be a smaller amount of crosstalk present at the first site mentioned.

It is thus preferable to obtain an sEMG measurement from a location halfway between the IZ and tendon area. If a situation should arise in which it is necessary to perform a measurement on the IZ or tendon area, the NDD set-up will ensure maximum signal fidelity in the presence of crosstalk.

It should also be noted that the IZ and tendon area are not the only sources of crosstalk in a real EMG measurement. Most of the crosstalk originates from adjacent muscles. It is thus impossible to determine the exact location of the detection electrodes with respect to these sources of crosstalk. The study was merely a theoretical one in which the influence of different detection electrode placements on crosstalk was investigated.

4.6.3 Conclusion

NDD results in the most selective measurements and will ensure minimal interference from crosstalk signals, for any detection location along the length of the muscle. It is, however,

recommended always to place the detection electrodes halfway between the IZ and tendon area. The SD system is influenced most by the different placement of the detection electrodes.

4.7. General conclusions

Different spatial filters have been compared before on theoretical (Disselhorst-Klug et al. 1997; Reucher et al. 1987b), modelling (Reucher et al. 1987b; Dimitrov et al. 2003) and experimental grounds (Disselhorst-Klug et al. 1997; Farina et al. 2003b; Farina et al. 2003c; Van Vlugt & Van Dijk 2000). Each method has different strengths and limitations. A theoretical comparison of the transfer functions may give results far from those obtained in practice. Modelling allows for comparison of various situations under controlled circumstances, but any model remains a simplification of reality. An experimental comparison leads to accurate results, but there may be uncontrollable variables and also obvious practical limitations. The approach followed in this study was to develop a more anatomically correct model than was available before and to compare the simulated results with experimentally obtained ones. The main objective of the study was to determine whether a more selective spatial filter results in a larger reduction of crosstalk with increasing distance from the active muscle.

Farina et al. (2002a) proposed that 2-D systems lead to higher attenuation of the propagating components of an EMG signal with increasing distance from the source, while non-propagating components are rejected to a lesser degree. They based their conclusion on the fact that the characteristics of a filter are determined by its transfer function, and its spatial selectivity by it spatial cut-off frequency (Disselhorst-Klug et al. 1997). The transfer function is derived in the spatial domain, with CV being the link between the time and spatial domains (Farina & Merletti 2003). When one considers a stationary part of the signal, it obviously has no CV. This means that the transfer function of the spatial filter cannot be used to make any conclusions on the selectivity of the filter with respect to the non-travelling components (Disselhorst-Klug et al. 1997; Farina & Cescon 2001; Farina et al. 2002a; Farina et al. 2003a; Farina et al. 2003c).

As stated in section 2.2.4 crosstalk consists mostly of non-propagating components. Farina et al. (2002a; 2002e) showed that 2-D systems have a lower reduction of non-propagating components than 1-D systems and that NDD is less selective for non-propagating

components than LDD and SD (Farina et al. 2004c). Similar results have been found experimentally by Van Vlugt and Van Dijk (2000).

The above conclusions from modelling experiments were drawn from studies performed with SFAPs or single MUAPs. Although this is a good starting point, results obtained with a simplified model do not always correctly predict results for a more complicated situation. The current model incorporated a complete muscle, consisting of different MUs and thousands of fibres, and is thus a more realistic representation of a real muscle.

The only simulation in which DD was more selective than NDD is the one where skin conductivity was reduced. Skin conductivity is a difficult parameter to determine, as it is affected by many external factors (such as humidity, stress, etc.). The current value used in the other simulations may be higher than physiological values obtained in sEMG measurements. This may explain the difference in crosstalk selectivity when the current model is compared to experimental results.

The influence of anatomical parameters on the results is clear from the current study. This model is more complete than a model simulating only SFAPs or MUAPs, and leads to different conclusions than previous, more simplified models. It remains, however, a model and thus a simplified representation of a real muscle. Further expansion of the model may again lead to different conclusions about the selectivity of spatial filters with respect to crosstalk. As stated by Farina et al., one should always specify selectivity with reference to travelling or non-travelling components, and also that results obtained for SFAPs are not always true for MUAPs (Farina et al. 2002a).

The conclusion from these simulations is that NDD results in the highest crosstalk rejection as long as a high value of skin conductivity is maintained. If the skin conductivity is lowered, DD becomes comparable to NDD.

Crosstalk rejection was in general reduced for a thicker fat layer, increased skin conductivity, a shorter fibre length and an increased IED. A greater reduction of crosstalk is also possible above the muscle end-plates than above the tendon area.

5

The effects of dynamic contraction parameters on crosstalk

5.1. The effect of muscle shortening on crosstalk

The muscle contractions simulated up to this point have all been isometric, isotonic contractions. Isometric means that the muscle fibre length was kept constant as the muscle contracted, and isotonic that the contraction force was constant. It was thus a completely static contraction. Generally, muscle contractions are dynamic, with muscle fibre length decreasing as the contraction force increases. To evaluate the effect this has on crosstalk, these two parameters were investigated separately in the following chapter. Muscle shortening was first incorporated in the contraction.

5.1.1. Methods

Three libraries of APs were simulated using the same analytical model as described in chapter 3. The libraries contain one AP for each muscle fibre in the total muscle region. The muscle fibre length was changed between the libraries to simulate muscle shortening. A constant muscle volume was maintained by increasing the limb and active muscle radius while decreasing the fibre length. The distance between the centre of the active muscle and the centre of the bone remained constant (30 mm, see figure 5.1).

The muscle shape can be described by a Gaussian function (also called a bell-shaped curve, see figure 5.2), given in equation 5.1:

$$r(z) = A \cdot \exp\left(\frac{-z^2}{2 \cdot w^2}\right), \tag{5.1}$$

where A defines the maximum radius of the active muscle, z is the longitudinal distance along the axis of the muscle and w defines the contraction width. The higher the value of w, the more contracted a muscle is.

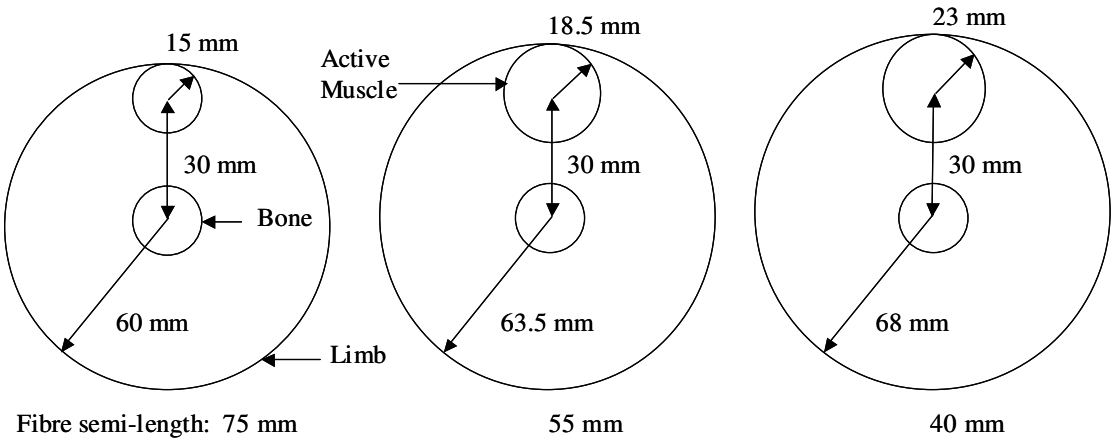

Figure 5.1. The muscle geometries used for incorporating muscle shortening. Increasing limb and muscle radius with decreasing muscle fibre length can be seen. The parameters describing the muscle geometry for libraries 9 (left), 10 (centre) and 11 (right) can be found in table 5.1.

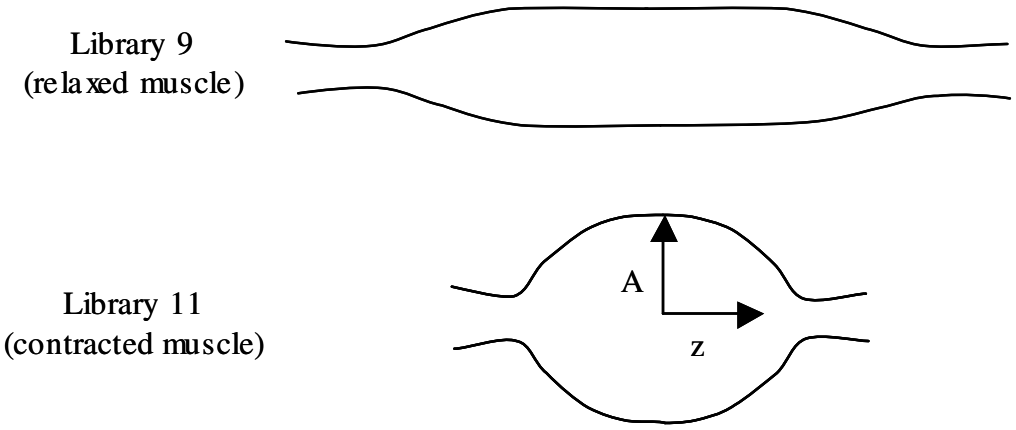

Figure 5.2. A side view of the muscle geometries showing a relaxed muscle (top, library 9) and a contracted muscle (bottom, library 11). A = maximum radius of the active muscle, z = longitudinal distance along the axis of the muscle.

The relation between muscle volume and muscle shape is:

$$V = \int_{-d}^{d} \pi \cdot (r(z))^2 .dz \ , \qquad (5.2)$$

with d the muscle fibre semi-length. A muscle volume of 83.2 cm^3 and maximum fibre semi length of 75 mm was obtained from Garner and Pandy (2003) and used for library 9 (the relaxed muscle). A fully contracted biceps brachii muscle can reduce its length to half of that in the relaxed state (Garner & Pandy 2003). Library 11's fibre semi-length was thus selected as 40 mm, with library 10 given a value between the other two.

The limb radius was obtained by adding all the radii of the components (bone, 30 mm spacing and active muscle). A numerical process was then implemented to obtain the best values of muscle radius (A) and contraction width (w) to ensure a constant muscle volume. The complete process is described by Mesin (2005). The values obtained can be found in table 5.1. Because the number of fibres in the active muscle stays constant as the area increases, the fibre density decreases. This is displayed by the increased depth between fibres with increasing contraction force.

Table 5.1. Variable parameters used for simulating libraries 9 – 11

Library no	Limb radius (mm)	Fibre semi-length (mm)	Muscle radius (A) (mm)	Width (w) (mm)	Depth between fibres (dy) (mm)
9	60	75	15	83.29	0.29
10	63.5	55	18.5	49.58	0.31
11	68	40	23	30.99	0.34

The parameters that were constant for the simulation of libraries 9 - 11 are shown in table 5.2. The same steps as described in sections 3.2 – 3.4 were followed in creating the libraries, detecting the sEMG signal and comparing the results. Any parameters not shown in table 5.1 had the same value as in libraries 1 – 8 (tables 3.1 and 3.3). The detection electrodes were placed in the centre of the muscle in all three cases.

Table 5.2. Fixed parameter values used for simulation of libraries 9 – 11

Variable	Value
Bone radius	15 mm
Maximum force exerted by muscle	100 % MVC
% MVC where recruitment stops (RR)	85 %
IPI variability	15 %
Angle between fibres (dx)	0.41 °
Depth of muscle under fat layer	0 mm
Skin thickness	1 mm
Interelectrode distance	5 mm
CV	4 ± 0.3 m/s

5.1.2. Results

Figure 5.3 shows the results obtained from the simulation of all three libraries. From the amplitude contents it is clear that library 9 (relaxed muscle) always resulted in the most selective measurements, followed by library 10 and then 11. The only exception is NDD, where library 10 is more selective than library 9 at large distances.

NDD is the most selective filter at first for all three libraries, but right at the end DD overtakes NDD in all the investigated cases.

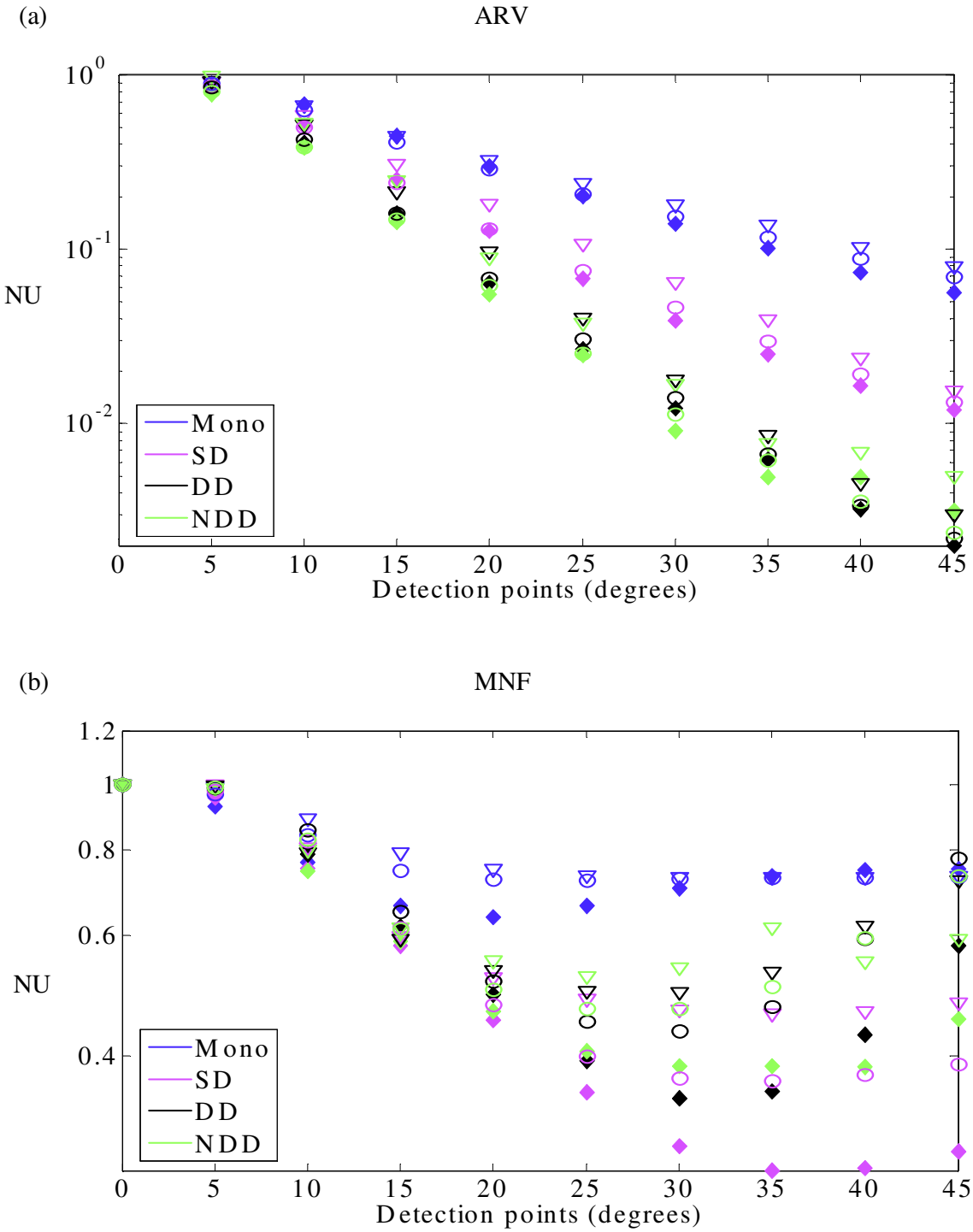

Figure 5.3. The ARV (a) and MNF (b) of libraries 9 (♦, relaxed muscle), 10 (o) and 11 (∇, contracted muscle) with an IED of 5 mm, fat layer = 1 mm, skin conductivity = 1 S/m.

Library 9 (relaxed muscle) results in the lowest values of MNF, followed by library 10 and then 11. At large distances library 11 has a lower MNF than library 10 for DD and NDD detection systems.

The SD system always has the most selective frequency response. For libraries 9 and 10 NDD has the second lowest MNF values, but it is then overtaken by DD. In the end the MNF of NDD is again lower than that of DD. For library 11 DD has a lower MNF than NDD right from the start, but NDD overtakes it at large distances.

NDD thus has the lowest MNF values for all three libraries at large distances. The last time it overtakes DD happens at the same distance for all three libraries.

5.1.3. Discussion

The aim of the experiment was to establish the relationship between limb geometry and crosstalk selectivity. When a dynamic contraction is elicited, the muscle geometry changes along with other muscular properties (including CV, discharge rate and location of the IZ). Since these changes all occur simultaneously, it is very difficult to ascribe a change in the measured sEMG signal to a change in a single muscular property. By changing only the geometrical properties, the influence this has on crosstalk can be investigated directly.

When a muscle contracts the location of the IZ and tendon area can slide with respect to the skin and detection electrodes. Rainoldi et al. (2000) showed that this sliding effect could result in EMG amplitude changes in excess of 200 %. This may falsely be interpreted as an increase in muscle activity. Saitou et al. (1990) observed a shift in biceps brachii IZ position of between 1 and 4 cm with changes in elbow angle, while Ghori et al. (1995) confirmed the fluctuations in EMG amplitude with changing knee angles. When an increase in amplitude is observed along with muscle shortening, it is thus not clear which part of the amplitude change is due to shifting of the IZ underneath the detection electrodes and which part (if any) is due to the muscle shortening. A simulation enables one to change selected variables and keep the rest constant, investigating the individual effect of each one on the selected parameter. Figure 5.3 shows the effect that geometrical changes in the muscle and limb have on EMG parameters.

Crosstalk is mainly caused by the non-travelling components of an EMG signal (Farina et al. 2004a). These components originate at the tendon area and to a lesser degree at the end-plate region (Gootzen et al. 1991). When shortening of the muscle fibre occurs, the IZ and tendon area move closer to the centre of the muscle. This means that the non-travelling components originate closer to the detection electrodes. One would thus expect to see an increase in crosstalk as the muscle fibres decrease in length.

Library 9 simulates a relaxed muscle, with the tendon area the furthest away from the detection electrodes. From figure 5.3 it is clear that library 9 always results in the best crosstalk suppression, as expected. Furthermore one would expect to see more crosstalk in library 10 and most in library 11 (increasing crosstalk as the tendon area moves closer to the detection areas). This can be seen for the Mono, SD and DD systems, and also for most of NDD. At some stage, however, library 10 results in a more selective amplitude response than library 9 (NDD detected). This might be due to the decreasing fibre density with decreasing muscle length.

In all situations the MNF is seen to decrease and then increase with distance. It is thus clear that high-pass filtering will not reduce the crosstalk in any of the measurements when the muscle length is decreasing.

Okada (1987) and Dimitrova et al. (1991) both link increasing muscle length to a decrease in spectral frequencies, while Kamen et al. (1996) confirm that the non-travelling components will have a smaller influence with increasing muscle length because of the increased distance between the source and detection electrodes. As stated by Schulte et al. (2004), MNF estimates are greatly influenced by muscle fibre shortening and are also dependent on the detection system being used. This is clear from figure 5.3 [b], especially when noting the fluctuations in NDD MNF.

5.1.4. Conclusion

The amount of crosstalk present in an sEMG measurement is expected to increase with decreasing muscle length because of the decrease in distance between the detection electrodes and the tendon area. The effect of geometrical changes of the muscle and limb on crosstalk selectivity was investigated through simulation. The results showed that DD

is the most selective filter for crosstalk rejection in all three the investigated situations, followed by NDD, SD and then Mono. Changes in the muscle and limb geometry clearly affected the MNF estimates of sEMG signals.

High-pass filtering will not reduce the amount of crosstalk present in an sEMG measurement when the muscle length is decreasing.

5.2. The effect of increased contraction force on crosstalk

The second effect of a dynamic contraction that was investigated is the effect of increased contraction force on crosstalk. Variability in contraction force can be modelled as a change in the number of recruited MUs, their discharge rate and CV. This was done for six states of muscle contraction, and the resulting influence on crosstalk signals was analysed.

5.2.1. Methods

Six simulations were performed in which the contraction force was increased from 10 to 100 % MVC. Since the biceps brachii is still the muscle under investigation, the value at which all MUs are recruited (RR) remained 85 % MVC. This means that for a contraction force with a value of less than 85 % (i.e. 30 % MVC), all the MUs will not have been recruited yet. At 85 % MVC all the MUs are recruited, and their discharge rate will then be increased (up to the maximum of 35 pps) to obtain a higher contraction force value.

Figure 5.4 shows the discharge pattern of eight MUs when a 10 % MVC is simulated. The discharge rate is clearly lower than it was with 100 % MVC (see figure 3.6). Number 1 (top row) is the first recruited MU (with the highest discharge rate) and number 103 the last. There is a total of 200 MUs in the simulated muscle, which means that 97 MUs are not recruited when a contraction of 10 % MVC is simulated.

Library 1 was used to simulate the increased contraction force, which means that the fat layer thickness was equal to 1 mm, the fibre semi-length 60 mm and the skin conductivity 1 S/m. An IED of 5 mm was used for all simulations.

Since the smallest MU is recruited first, and CV increases with MU size, the large MUs with high values of CV will not be recruited at low values of contraction force. The result is a decrease in the mean CV with decreasing contraction force. This has been observed by several authors (Hogrel et al. 1998; Knaflitz et al. 1990; Masuda & De Luca 1991; Merletti et al. 2001).

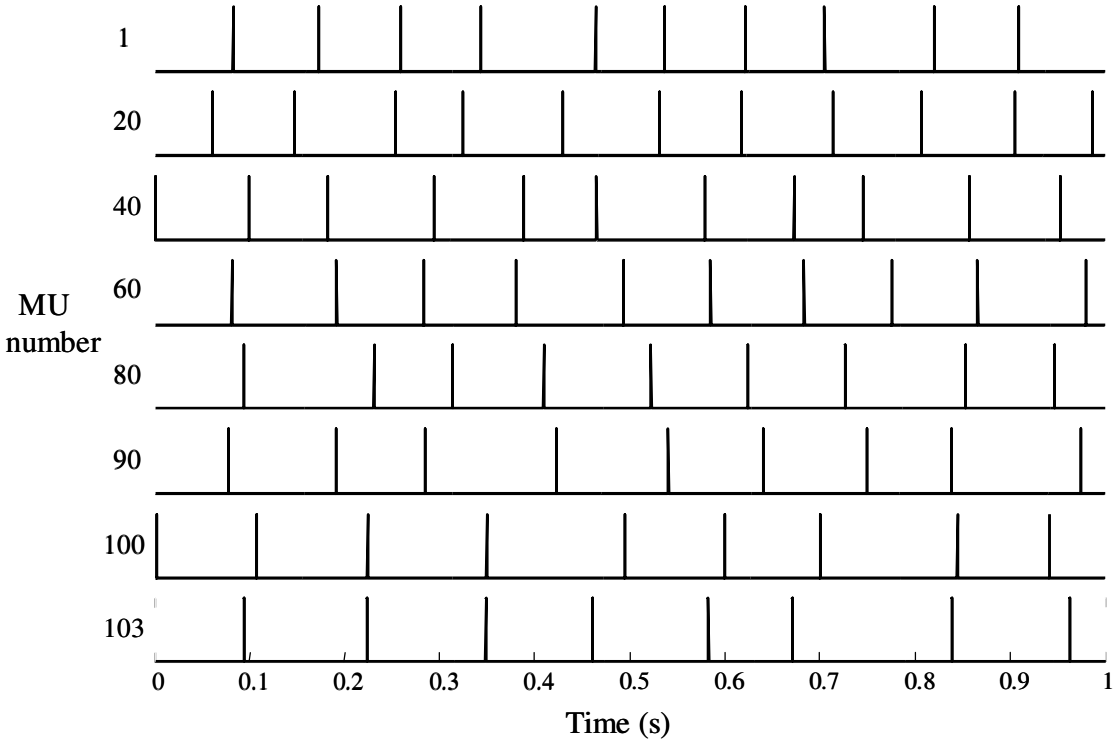

Figure 5.4. The discharge pattern of eight MUs at 10 % MVC. The decrease in discharge rate is evident when this figure is compared to the one generated at 100 % MVC (see figure 3.6).

Table 5.3 shows the parameter values that were used in the simulations. The contraction force was increased in steps from 10 to 100 % MVC. Each contraction force step was evaluated as an isometric, isotonic contraction.

As stated before, the standard equation assumes that the force increases linearly from 0 to 100 % MVC in 3 s. When a lower contraction force is simulated, it will be reached in a shorter time than 3 s. The time, $t_{\%MVC}$, can be computed from equation 5.3:

$$t_{\%MVC} = \frac{\%MVC}{100} \cdot 3 \cdot \quad (5.3)$$

The percentage MVC at which an MU is recruited can be found from equation 3.2, repeated here for convenience:

$$RTE(i) = e^{\ln(RR)i/n}, i = 1,2,3... \ . \quad (5.4)$$

Because the value of $t_{\%MVC}$ is lower than 3s, *RTE_time* can now assume negative values:

$$RTE\_time(i) = t_{\%MVC} - \frac{RTE(i)}{100} \cdot t_{MVC} \quad . \quad (5.5)$$

MUs with negative *RTE_time* values have not yet been recruited at the time that the desired contraction strength is reached. Their discharge rate is thus set equal to zero. A discharge rate is computed for every MU with a positive recruitment time from equation 5.6:

$$f\_rate(i) = f_{\min} + sl\_dis \cdot (100 - RTE(i)) \ , \quad (5.6)$$

with f_{min} = 8 pulses per second (pps) and *sl_dis* the variation in discharge rate with force equal to 0.3 pps/%MVC. The number of MUs recruited for each contraction force value is shown in table 5.3.

The mean and standard deviation of CV is computed from a summation of those CV values assigned to the recruited MUs. As stated, the smaller MUs with lower CVs will be recruited first. From table 5.3 the increase in CV with contraction force ranging from 10 to 50 % MVC is more significant than when the force increases above 50 % MVC. This agrees with experimentally determined values of CV increase with contraction force (Rainoldi et al. 1999).

Table 5.3. Variable parameters for simulating increasing contraction force

Contraction force (% MVC)	Recruited MUs	Max discharge rate (pps)	Mean CV (m/s)	CV Std dev (m/s)
10	103	10.86	3.77	0.18
30	153	17.22	3.88	0.22
50	176	23.59	3.93	0.25
70	191	29.95	3.97	0.27
90	200	35	4	0.3
100	200	35	4	0.3

When comparing the variables used for a 90 and 100 % MVC in table 5.3, the two simulations seem identical. The average discharge rate of the MUs will, however, be lower for a 90 % contraction than when it is simulated at 100 % MVC. The number of MUs discharging at the maximum rate of 35 pps will thus be lower for 90 % MVC than for 100 % MVC.

5.2.2. Results and discussion

Figure 5.5 acts as a validation of the model. It shows the initial value of ARV and MNF as obtained with the different detection systems for different values of contraction force. ARV is strongly dependent on contraction force, while MNF varies only slightly when the contraction force increases. Both graphs are normalised with respect to the values obtained at 10 % MVC.

ARV can be seen to increase with increasing contraction force. The increase can be explained by the fact that more MUs are recruited as the contraction force increases. Since an EMG signal is the summation of the contributions of all the active MUs, it should increase in amplitude as more MUs become active. The values measured at 25 ° (open markers) show a slightly larger increase than those measured at 0 ° (filled markers).

Rainoldi et al. (1999) performed a similar study in which the contraction force was increased with the same steps as in the current study, and the ARV and MNF were

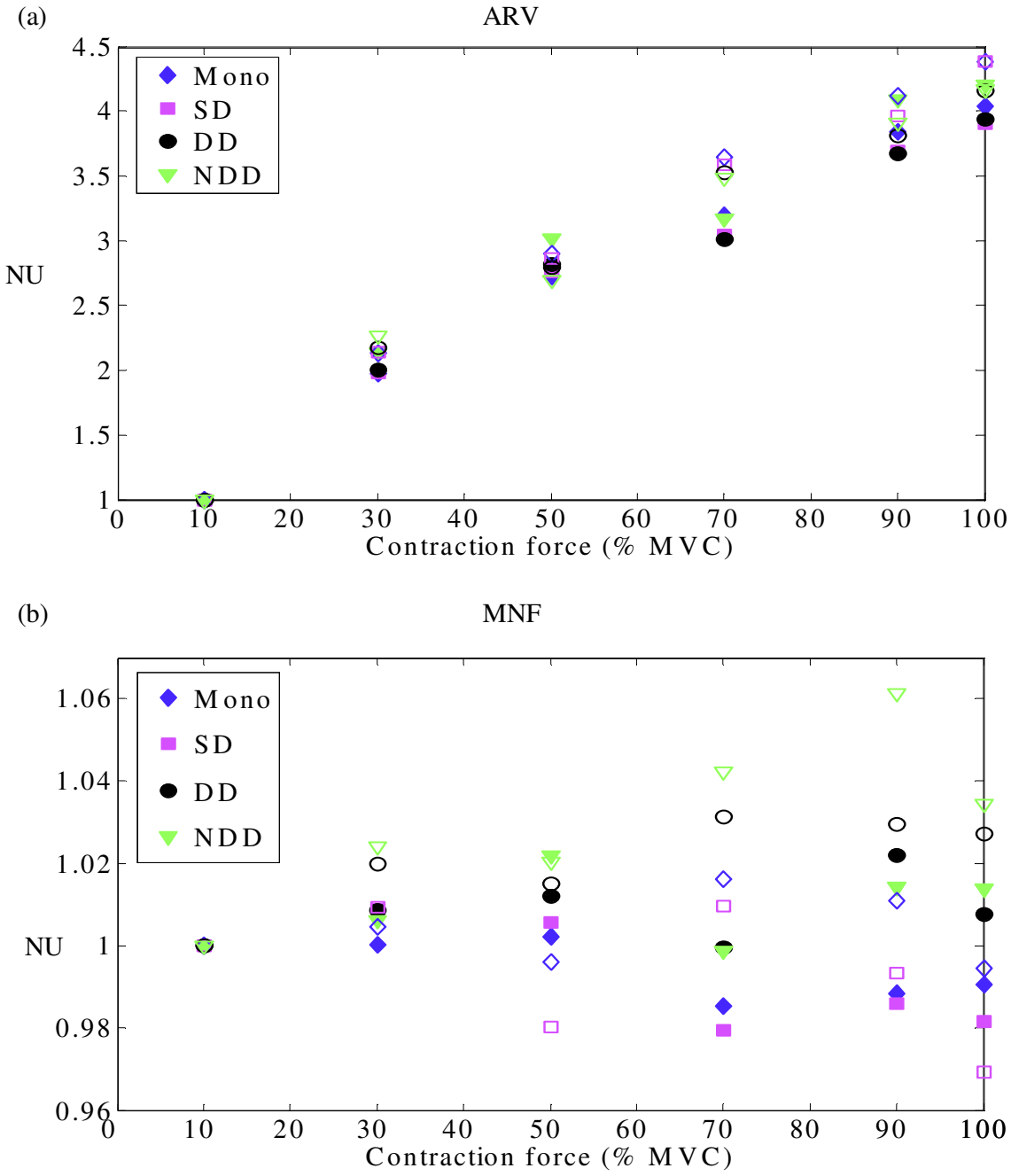

Figure 5.5. The initial values of ARV (a) and MNF (b) of library 1 as detected at different contraction force levels at 0 º (filled markers) and 25 º (unfilled markers), fibre semi-length = 60 mm, fat layer = 1 mm, skin conductivity = 1 S/m, IED = 5 mm.

experimentally determined. He reported that the influence of contraction force on the initial value of the MNF in the biceps brachii is small, and possibly masked by other factors. When comparing the results obtained by other authors on MNF and contraction force, it is difficult to draw any conclusion, as the results vary quite a lot from one simulation to the next. MNF variation with contraction force increase depends on the muscle being studied, the IED and the transfer function of the underlying tissue layers (Elfving et al. 2002; Hogrel et al. 1998). For the current simulation (biceps brachii muscle, IED = 5 mm, skin layer = 1 mm and fat layer = 5 mm) the MNF does not vary significantly with increasing contraction force. The variations do, however, appear to be very random in nature. This observation is independent of the circumferential position of the detection system. The same is thus seen at 0 ° and 25 °.

Figure 5.6 shows the ARV and MNF values obtained from a 10 % and 100 % MVC. The values for ARV and MNF obtained for the other contraction force strengths lie between the 10 and 100 % MVC results. The first observation is that neither the amplitude nor the frequency selectivity of the various detection systems is significantly affected by the difference in contraction force strength.

When comparing the ARV values, Mono, SD and DD show a very slight increase in selectivity with decreasing contraction force, while that of NDD remains constant.

The MNF values of Mono, SD and DD remain mostly unchanged for a 100 % or 10 % contraction. The decrease of NDD, DD and SD MNF with distance asymptotes at 30 ° for both values of contraction force. DD and NDD have slightly lower frequency components for 10 % MVC as compared to 100 % MVC.

NDD is the preferred detection system to use for crosstalk selectivity for all of the contraction force strengths studied.

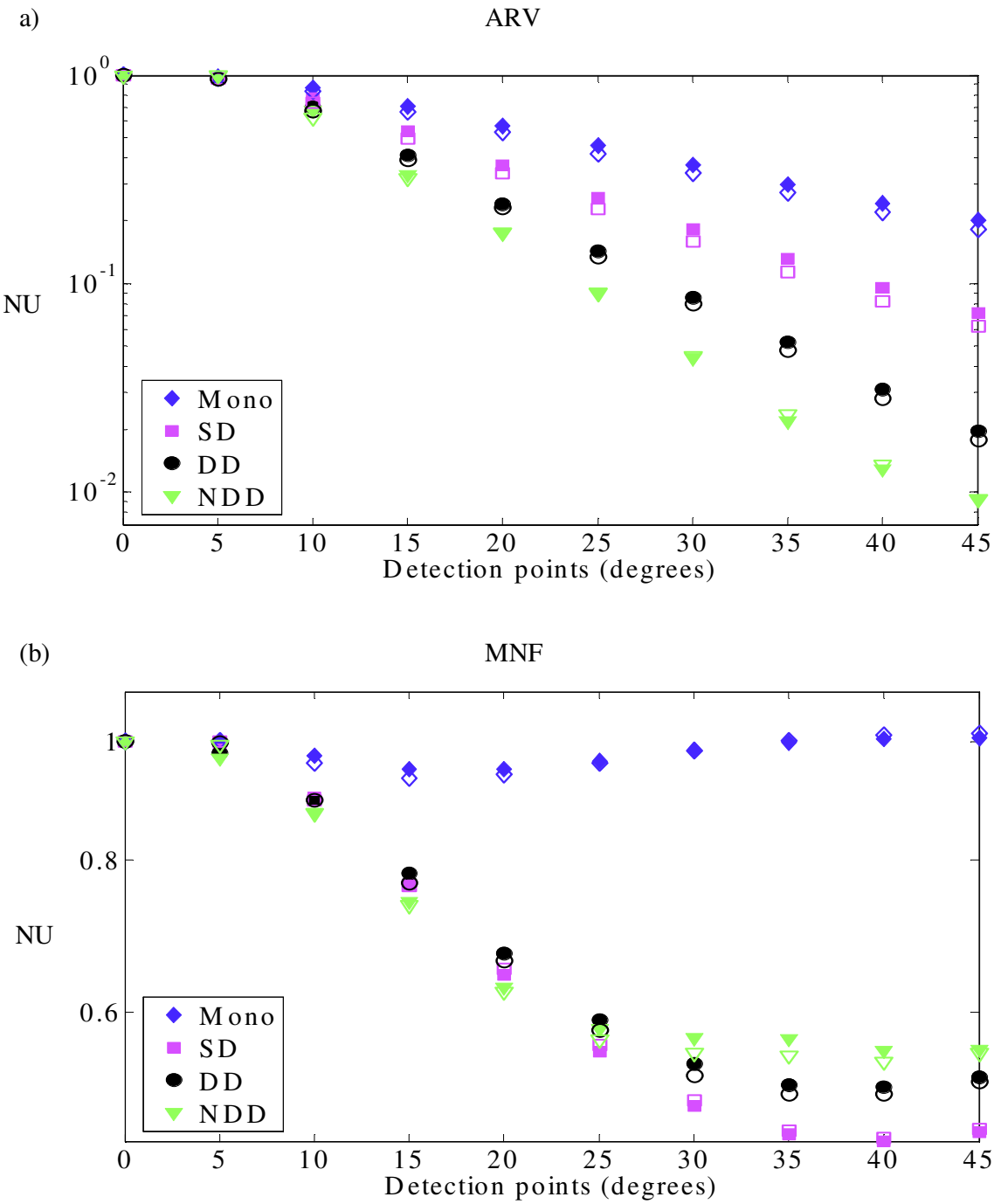

Figure 5.6. The ARV (a) and MNF (b) of library 1 with a contraction force of 100 % (filled markers) and 10 % (open markers), fibre semi-length = 60 mm, fat layer = 1 mm, skin conductivity = 1 S/m, IED = 5 mm.

5.2.3. Conclusion

The influence of increasing contraction force of the biceps brachii muscle on the ARV and MNF of the detected signal was assessed using the model developed in chapter 3. The MNF shows no significant response to increasing contraction force, remaining relatively constant for all detection angles on the limb. The ARV increases with increasing contraction force.

With respect to crosstalk, NDD results in the best crosstalk suppression for all the contraction force strengths studied. The selectivity of the detection systems is not significantly influenced by the variation in contraction force strength.

Lastly the results indicate that crosstalk is not significantly influenced by variations in the contraction force strength.

5.3. General conclusion

In this chapter the effects of dynamic contraction parameters on crosstalk were evaluated seperately. It is concluded that the DD results in the best crosstalk rejection for the different muscle geometries simulated. It is followed closely by the NDD system.

With increasing contraction force simulations, NDD results in the best crosstalk rejection. Crosstalk selectivity is not significantly influenced by changes in contraction force, while changes in muscle geometry do influence it. Changes in crosstalk selectivity in dynamic contractions are thus more likely to be caused by the changing muscle geometry than by the changing contraction force.

6

Conclusion

6.1. Brief summary

A study was performed to determine which spatial filter results in the best crosstalk suppression for different anatomical and detection system properties. It is clear that different spatial filters have different abilities to reduce the travelling and non-travelling parts of signals. Since crosstalk is mainly due to the non-travelling components, the detection system that results in the best suppression of non-travelling components will also result in the best crosstalk rejection. Table 6.1 shows the results obtained. The NDD detection system performed best in most of the simulated conditions. The only exceptions were a set-up with poor skin conductivity where NDD and DD were comparable, and the two simulations in which the muscle geometry was varied. Here, the DD filter performed best, with NDD being the second choice.

The study further investigated the effect of different anatomical and detection system parameters on crosstalk reduction. It can be summarised as follows: the selectivity with respect to crosstalk in an sEMG measurement is decreased by increasing the thickness of the fat layer, increasing the skin conductivity, decreasing the fibre length, increasing the IED of the detection system, placing the detection electrodes directly above the end-plate area or simulating a shorter muscle (with increased diameter). Crosstalk selectivity is

increased by the opposite situations from those mentioned above, while varying the contraction force strength or placing the electrodes directly above the tendon area has no influence on it.

Table 6.1. Effect of different anatomical and detection system parameters on crosstalk selectivity in an sEMG measurement

Experimental set-up	Detection system	Effect on crosstalk selectivity
Thick fat layer	NDD	Decrease
Thin fat layer	NDD	Increase
Good skin conductivity	NDD	Decrease
Poor skin conductivity	DD / NDD	Increase
Long fibre length	NDD	Increase
Short fibre length	NDD	Decrease
5 mm IED	NDD	Increase
10 mm IED	NDD	Decrease
Electrodes on end-plate	NDD	Increase
Electrodes on tendon	NDD	No effect
Longer muscle	DD	Increase
Shorter muscle	DD	Decrease
Low contraction force	NDD	No effect
High contraction force	NDD	No effect

6.2. Critical review

The validity of the model is confirmed by comparing the results obtained with other experimental and modelling results. The SFAP model was tested extensively with satisfactory results (Farina et al. 2002a; Farina et al. 2002e).

General trends observed with the complete muscle model, such as decreasing selectivity with increasing fat layer thickness or increasing IED, have been confirmed by experimental (Farina et al. 2002e) and other modelling studies (Lowery 2003b).

The increased spatial selectivity of 2-D spatial filters allows the noninvasive detection of single MU CV, impulse response, firing rate and recruitment (Disselhorst-Klug 1999b; Farina et al. 2003c; Rau 1997; Rau & Disselhorst-Klug 1997). An experimental (Van Vlugt & Van Dijk 2000) and two modelling studies (Dimitrov et al. 2003; Farina et al. 2002a), however, found that DD (a 1-D filter) is more selective for crosstalk rejection than NDD. This contradicts the general findings of the current model. Van Vlugt and Van Dijk (2001) lowered the skin impedance by shaving, abrading, cleaning and moistening it and used both stimulation and MVC to estimate crosstalk rejection. In the MVC study some 2-D filters were able to reduce the amount of crosstalk, although DD still performed better. The modelling experiment of Farina et al. (2002a) was based on SFAPs, which may explain the differences from the current model. Dimitrov et al. (2003) simulated MUAPs, but only from MUs located at different depths. Their model did not take peripheral MU location into account, which results in an unfair advantage for the DD system and may explain its better performance.

In the current study, NDD was found to be more selective than DD with respect to crosstalk rejection for most of the simulated conditions. One of the exceptions was the case where a lower value of skin conductivity was simulated. Here, DD and NDD showed a similar ability for crosstalk rejection. Human skin conductivity can vary between $1 \cdot 10^{-5}$ and $1 \cdot 10^{2}$ S/m (Gabriel et al. 1996), depending on factors such as humidity, stress level, stimulation frequency (if applicable) etc. The current values used (0.1 and 1 S/m) are between the extreme limits and have been used in previous simulation models (Farina & Merletti 2000; Roeleveld 1997a). It is, however, not clear if these are accurate values to use when comparing simulated and modelled EMG signals. Roeleveld et al. (1997a) stated that it is necessary to include a high conductivity skin layer in the volume conductor model to obtain an accurate spread of potentials. The authors used a value of 1 S/m for skin conductivity, but stated that it might be higher than physiologically obtained values. The current increased crosstalk selectivity of NDD may thus be explained by the high value of skin conductivity used in the simulation. The results obtained with the lower value seem more comparable with experimental results, which may indicate that physiological skin conductivity during sEMG measurements is lower than was assumed.

It is furthermore clear that crosstalk selectivity is rather dependent on the muscle and limb geometry. In the experiment where the muscle is shortened (section 5.1), DD had the best crosstalk rejection. The model used for these simulations had a larger radius than the one

used in chapter 4. Combined with the other geometrical changes introduced in chapter 5, this might explain the improved crosstalk rejection of DD compared to NDD. The model parameters in chapter 4 are averages obtained from measurements from the general population. The models in chapter 5 are based on values computed from a Gaussian equation to ensure a constant muscle volume with muscle shortening. The results obtained with this model seem more comparable with experimental results.

As stated by Farina et al. (2004c) the volume conductor parameters significantly affect the selectivity of the spatial filters. This is clear from the current results, and indicates that care should be taken in simulations to ensure the model parameters accurately reflect the situation being simulated.

The hypothesis that 2-D filters perform better with respect to crosstalk rejection is thus accepted within certain limits. A significant reduction of the skin conductivity or certain geometrical muscle changes may cause the DD system to result in better crosstalk rejection than NDD.

To minimise the influence of crosstalk on an EMG measurement, the study concludes that one should use an NDD detection system, a site with the minimum fat layer, a high skin conductivity, long muscle fibers, an IED of 5 mm, and place the detection electrodes halfway between the IZ and tendon area.

6.3. Further work

It is clear from the current study that skin conductivity has a large influence on spatial filter selectivity. Since noticeable interperson variations exist for this parameter and it is dependent on several external factors, it may prove useful to conduct a study on skin conductivity in sEMG measurements. The exact effect of skin conductivity on spatial filter selectivity can be determined, as well as the average skin conductivity detected in sEMG measurements.

A simulation experiment like the one in the current study can be performed, using anatomical data obtained from a test candidate. Experimental measurements can then be recorded from this same candidate and compared to the simulations. This should enable a more accurate conclusion on the effects of different parameters on crosstalk rejection, as

well as provide a definite estimate of skin conductivity. Different muscle geometries can also be measured experimentally on test candidates and then simulated.

The dynamic models used were quite elementary and rough, and a more detailed model of dynamic muscle contraction might yield different results.

This study provided some new insight into the modelling of a complete muscle for sEMG crosstalk estimates. It is clear that all the factors affecting crosstalk are not fully understood yet, and more studies are necessary to expand knowledge on the subject. The current research provides the next step in the invaluable field of sEMG simulation.

References

Andreassen, S. & Arendt-Nielsen, L. 1987, 'Muscle fiber conduction velocity in motor units of the human anterior tibial muscle: a new size principle parameter', *Journal of Physiology*, vol. 391, pp. 561-571.

Basmajian, J. V. & De Luca, C. J. 1985, *Muscles Alive: Their function revealed by electromyography*, Williams & Williams, Baltimore.

Bhullar, H. K., Loudon, G. H., Fothergill, J. C. & Jones, N. B. 1990, 'Selective noninvasive electrode to study myoelectric signals', *Medical & Biological Engineering and Computing*, vol. 28, pp. 581-586.

Blok, J. H., Stegeman, D. F. & Van Oosterom, A. 2002, 'Three-layer volume conductor model and software package for applications in surface electromyography', *Annals of Biomedical Engineering*, vol. 30, pp. 566-577.

Broman, H., Bilotto, G. & De Luca, C. J. 1985, 'A note on the noninvasive estimation of muscle fiber conduction velocity', *IEEE Transactions on Biomedical Engineering*, vol. 32, pp. 341-344.

Bullen, F., Pfaeffle, J., Stabile, K., Gabriel, M., Tomaino, M. & Fischer, K., *Computer-aided interosseous ligament reconstruction planning*, [Online], Musculoskeletal Research Center, Department of Orthopaedic Surgery, University of Pittsburgh Medical Center, PA, Available from: <http://www.pitt.edu/~msrc/summer/2000/fiona_doc.html> [2004, 29 March].

Day, S. *Important factors in surface EMG measurement*, Bortec Biomedical, Available from:

http://www.bortec.ca/Images/pdf/EMG%20measurement%20and%20recording.pdf [2005, April 13].

De Luca, C. J. & Merletti, R. 1988, 'Surface myoelectric signal cross-talk among muscles of the leg', *Electroencephalography and Clinical Neurophysiology*, vol. 69, pp. 568-575.

De Luca, C. J. 2002, '*Surface electromyography: Detection and recording'*, DELSYS Incorporated.

Devasahayam, S. R. 2000, *Signals and Systems in Biomedical Engineering*, Kluwer Academic/Plenum, New York.

Dimitrov, G. V., Disselhorst-Klug, C., Dimitrova, N. A., Schulte, E. & Rau, G. 2003, 'Simulation analysis of the ability of different types of multi-electrodes to increase selectivity of detection and to reduce crosstalk', *Journal of Electromyography and Kinesiology*, vol. 13, pp. 125-138.

Dimitrova, N. A., Dimitrov, G. V. & Lateva, Z. C. 1991, 'Influence of the fiber length on the power spectra of single muscle fiber extracellular potentials', *Electromyography and Clinical Neurophysiology*, vol. 31, no. 7, pp. 387-398.

Dimitrova, N. A., Dimitrov, G. V. & Nikitin, O. A. 2002, 'Neither high-pass filtering nor mathematical differentiation of the EMG signals can considerably reduce cross-talk', *Journal of Electromyography and Kinesiology*, vol. 12, pp. 235-246.

Disselhorst-Klug, C., Blanc, Y. & Rau, G. 1999a, *Examination of the reduction of crosstalk between leg muscles by spatial filtering techniques*, Roessingh Research and Development, Enschede, The Netherlands.

Disselhorst-Klug, C., Rau, G., Schmeer, A. & Silny, J. 1999b, 'Non-invasive detection of the single motor unit action potential by averaging the spatial distribution triggered on a spatially filtered motor unit action potential', *Journal of Electromyography and Kinesiology*, vol. 9, pp. 67-72.

Disselhorst-Klug, C., Silny, J. & Rau, G. 1997, 'Improvement of spatial resolution in surface-EMG: A theoretical and experimental comparison of different spatial filters', *IEEE Transactions on Biomedical Engineering*, vol. 44, no. 7, pp. 567-574.

Duchêne, J. & Hogrel, J. Y. 2000, 'A model of EMG generation', *IEEE Transactions on Biomedical Engineering*, vol. 47, no. 2, pp. 192-201.

Elfving, B., Liljequist, D., Mattsson, E. & Németh, G. 2002, 'Influence of interelectrode distance and force level on the spectral parameters of surface electromyographic recordings from lumbar muscles', *Journal of Electromyography and Kinesiology*, vol. 12, pp. 295-304.

Farina, D., Arendt-Nielsen, L., Merletti, R., Indino, B. & Graven-Nielsen, T. 2003a, 'Selectivity of spatial filters for surface EMG detection from the tibialis anterior muscle', *IEEE Transactions on Biomedical Engineering*, vol. 50, no. 3, pp. 354-364.

Farina, D., Cescon, C. & Merletti, R. 2002a, 'Influence of anatomical, physical and detection-system parameters on surface EMG', *Biological Cybernetics*, vol. 86, pp. 445-456.

Farina, D. & Cescon, C. 2001a, 'Concentric-ring electrode system for noninvasive detection of single motor unit activity', *IEEE Transactions on Biomedical Engineering*, vol. 48, no. 11, pp. 1326-1334.

Farina, D., Fattorini, L., Felici, F. & Filligoi, G. 2002b, 'Nonlinear surface EMG analysis to detect changes of motor unit conduction velocity and synchronization', *Journal of Applied Physiology*, vol. 93, November, pp. 1753-1763.

Farina, D., Fosci, M. & Merletti, R. 2002c, 'Motor unit recruitment strategies investigated by surface EMG variables', *Journal of Applied Physiology*, vol. 92, January, pp. 235-247.

Farina, D., Madeleine, P., Graven-Nielsen, T., *et al.* 2002d, 'Standardising surface electromyogram recordings for assessment of activity and fatigue in the human upper trapezius muscle', *European Journal of Applied Physiology*, vol. 86, pp. 469 – 478.

Farina, D., Merletti, R., Indino, B., Nazzaro, M. & Pozzo, M. 2002e, 'Surface EMG crosstalk between knee extensor muscles: experimental and model results', *Muscle & Nerve*, vol. 26, pp. 681-695.

Farina, D., Merletti, R., Indino, T. & Graven-Nielsen, T. 2004a, 'Surface EMG crosstalk evaluated from experimental recordings and simulated signals. Reflections on crosstalk interpretation, quantification and reduction', *Methods of Information in Medicine*, vol. 43, pp. 30-35.

Farina, D. & Merletti, R. 2000, 'Comparison of algorithms for estimation of EMG variables during voluntary isometric contractions', *Journal of Electromyography and Kinesiology*, vol. 10, pp. 337-349.

Farina, D. & Merletti, R. 2001b, 'A novel approach for precise simulation of the EMG signal detected by surface electrodes', *IEEE Transactions on Biomedical Engineering*, vol. 48, no. 6, June, pp. 637-646.

Farina, D. & Merletti, R. 2003b, 'A novel approach for estimating muscle fiber conduction velocity by spatial and temporal filtering of surface EMG signals', *IEEE Transactions on Biomedical Engineering*, vol. 50, no. 12, pp. 1340-1351.

Farina, D., Mesin, L., Marina, S. & Merletti, R. 2004b, 'A surface EMG generation model with multilayer cylindrical description of the volume conductor', *IEEE Transactions on Biomedical Engineering*, vol. 51, no. 3, pp. 415-426.

Farina, D., Mesin, L., Martina, S. & Merletti, R. 2004c, 'Comparison of spatial filter selectivity in surface myoelectric signal detection: influence of the volume conductor model', *Medical & Biological Engineering and Computing*, vol. 42, pp. 114-120.

Farina, D. & Rainoldi, A. 1999, 'Compensation of the effect of sub-cutaneous tissue layers on surface EMG: a simulation study', *Medical Engineering and Physics*, vol. 21, pp. 487-496.

Farina, D., Schulte, E., Merletti, R., Rau, G. & Disseldorst-Klug, C. 2003c, 'Single motor unit analysis from spatially filtered surface electromyogram signals. Part 1: spatial selectivity', *Medical and Biological Engineering and Computation*, vol. 41, pp. 330-337.

Foster, K. R. & Swan, H. P. 1986, 'Dielectrical properties of tissues', in *CRC Handbook of Biological Effects of Electromagnetic Field*, ed. C. P. Eds, CRC Press, pp. 26-95.

Fuglevand, A. J., Winter, D. A. & Patla, A. E. 1993, 'Models of Recruitment and Rate Coding Organization in Motor-Unit Pools', *Journal of Neurophysiology*, vol. 70, no. 6, December, pp. 2470-2488.

Gabriel, C., Gabriel, S. & Corthout, E. 1996, 'The dielectric properties of biological tissues: I. Literature', *Physics in Medicine and Biology*, vol. 41, pp. 2231-2249.

Garner, B. A. & Pandy, M. G. 2003, 'Estimation of musculotendon properties in the human upper limb', *Annals of Biomedical Engineering*, vol. 31, pp. 207-220.

Geddes, L. A. & Baker, L. E. 1967, 'The specific resistance of biological material - a compendium of data for the biomedical engineer and physiologist', *Medical & Biological Engineering and Computing*, vol. 5, pp. 271-293.

Ghori, G. M., Donne, B. & Luckwill, R. G. 1995, 'Relationship between torque and EMG activity of a knee extensor muscle during isokinetic concentric and eccentric actions', *Journal of Electromyography and Kinesiology*, vol. 5, no. 2, pp. 109-115.

Gootzen, T., Stegeman, D. F. & Van Oosterom, A. 1991, 'Finite limb dimensions and finite muscle length in a model for the generation of electromyographic signals', *Electroencephalography and Clinical Neurophysiology*, vol. 81, pp. 152-162.

Hall, E. L. 1979, *Computer image processing and recognition*, University of Tennessee, Knoxville, Tennissee.

Hogrel, J. Y., Duchene, J. & Marini, J. F. 1998, 'Variability of some sEMG parameter estimates with electrode location', *Journal of Electromyography and Kinesiology*, vol. 8, pp. 305-315.

Houtman, C. J., Stegeman, D. F., Van Dijk, J. P. & Zwarts, M. J. 2003, 'Changes in muscle fiber conduction velocity indicate recruitment of distinct motor unit populations', *Journal of Applied Physiology*, vol. 95, pp. 1045-1054.

Kamen, G. & Caldwell, G. E. 1996, 'Influences of muscle length on the EMG signals', *Physiology and Interpretation of the Electromyogram*, vol. 13, no. 5, pp. 366-384.

Klein, C. S., Marsh, G. D., Petrella, R. J. & Rice, C. L. 2003, 'Muscle fiber number in the biceps brachii muscle of young and old men', *Muscle & Nerve*, vol. 28, no. 1, pp. 62-70.

Knaflitz, M., Merletti, R. & De Luca, C. J. 1990, 'Inference of motor unit recruitment order in voluntary and electrically elicited contractions', *Journal of Applied Physiology*, vol. 68, pp. 1657-1667.

Koh, T. J. & Grabiner, M. D. 1992, 'Cross talk in surface electromyograms of human hamstring muscles', *Journal of Orthopaedic Research*, vol. 10, pp. 701-709.

Koh, T. J. & Grabiner, M. D. 1993, 'Evaluation of methods to minimize cross talk in surface electromyography', *Journal of Biomechanics*, vol. 26, suppl 1, pp. 151-157.

Kossev, A., Gydikov, A., Trayanova, N. & Kosarov, D. 1988, 'Configuration and selectivity of the branched EMG electrodes', *Electromyography and Clinical Neurophysiology*, vol. 28, pp. 397-403.

Lange, F., Van Weerden, T. W. & Van der Hoeven, J. H. 2002, 'A new surface electromyography analysis method to determine spread of muscle fiber conduction velocity', *Journal of Applied Physiology*, vol. 93, pp. 759-764.

Lindstrom, L. H. & Magnusson, R. I. 1977, 'Interpretation of myoelectric power spectra: a model and its applications', *Proceedings of the IEEE*, vol. 65, no. 5, May, pp. 653-662.

Lindstrom, L., Magnusson, R. & Petersen, I. 1970, 'Muscular fatigue and action potential conduction velocity changes studied with frequency analysis of EMG signals', *Electromyography*, vol. 10, pp. 341-356.

Lowery, M. M., Stoykov, N. S. & Kuiken, T. A. 2003a, 'A simulation study to examine the use of cross-correlation as an estimate of surface EMG cross talk', *Journal of Applied Physiology*, vol. 94, pp. 1324-1334.

Lowery, M. M., Stoykov, N. S. & Kuiken, T. A. 2003b, 'Independence of myoelectric control signals examined using a surface EMG model', *IEEE Transactions on Biomedical Engineering*, vol. 50, no. 6, pp. 789-793.

Lowery, M. M., Stoykov, N. S., Taflove, A. & Kuiken, T. A. 2002, 'A multiple-layer finite-element model of the surface EMG signal', *IEEE Transactions on Biomedical Engineering*, vol. 49, no. 5, pp. 446-454.

Marieb, E. 1991, *Human anatomy and physiology*, Benjamin / Cummings, Redwood City, CA.

Halyard, M. &. 2001, *Fundamentals of Anatomy & Physiology*, Addison-Wesley / Benjamin Cummings.

Masuda, T. & De Luca, C. J. 1991, 'Recruitment threshold and muscle fiber conduction velocity of single motor units', *Journal of Electromyography and Kinesiology*, vol. 1, no. 2, pp. 116-123.

Masuda, T., Sadoyama, T. & Shiraishi, M. 1996, 'Dependence of average muscle fiber conduction velocity on voluntary contraction force', *Journal of Electromyography and Kinesiology*, vol. 6, no. 4, pp. 267-276.

Matthews, B. H. C. 1934, 'A special purpose amplifier', *Journal of physiology*, vol. 81, pp. 28-33.

Maurel, W. , *Muscle Action Modeling*, [Online], Laboratoire d'Infographie, Lausanne, Switzerland, Available from: <http://ligwww.epfl.ch/~maurel/Publish/PhD98/pdfs/Chap3.pdf> [2004, 29 March].

Merletti, R., Farina, D. & Gazzoni, M. 2003, 'The linear electrode array: a useful tool with many applications', *Journal of Electromyography and Kinesiology*, vol. 13, pp. 37-47.

Merletti, R., Knaflitz, M. & De Luca, C. J. 1990, 'Myoelectric manifestations of fatigue in voluntary and electrically elicited contractions', *Journal of Applied Physiology*, vol. 69, pp. 1810-1820.

Merletti, R., Lo Conte, L., Avignone, E. & Guglielminotti, P. 1999a, 'Modeling of surface myoelectric signals - Part I: Model implementation', *IEEE Transactions on Biomedical Engineering*, vol. 46, no. 7, pp. 810-820.

Merletti, R. & Parker s.a., P. *Electromyography*, John Wiley & Sons, Inc, New York.

Merletti, R., Rainoldi, A. & Farina, D. 2001, 'Surface electromyography for noninvasive characterization of muscle', *Exercise and Sport Science Review*, vol. 29, no. 1, pp. 20-25.

Merletti, R., Roy, S. H., Kupa, E., Roatta, S. & Granata, A. 1999b, 'Modelling of Surface Myoelectric Signals - Part II: Model - Based Signal Interpretation', *IEEE Transactions on Biomedical Engineering*, vol. 46, no. 7, July, pp. 821-829.

Mesin, L., Joubert, M., Hanekom, T., Merletti, R., Farina, D. 2005, 'a Finite element model for describing the effect of muscle shortening on surface EMG', submitted to: *IEEE Transactions on Biomedical Engineering*.

Miyatani, M., Kanehisa, H., Masuo, Y., Ito, M. & Fukunaga, T. 2001, 'Validity of estimating limb muscle volume by bioelectrical impedance', *Journal of Applied Physiology*, vol. 91, no. 1, pp. 386-394.

Mogk, J. P. M. & Keir, P. J. 2003, 'Crosstalk in surface electromyography of the proximal forearm during gripping tasks', *Journal of Electromyography and Kinesiology*, vol. 13, pp. 63-71.

Morrenhof, J. W. & Abbink, H. J. 1985, 'Cross-correlation and cross-talk in surface electromyography', *Electromyography and Clinical Neurophysiology*, vol. 25, pp. 73-79.

Okada, M. 1987, 'Effect of muscle length on surface EMG wave forms in isometric contractions', *European Journal of Applied Physiology and Occupational Physiology*, vol. 56, no. 4, pp. 482-486.

Orcholl, J. L., Scholar, M. & Hudson, J., *Diagnostic criteria for the comparison of human and American black bear skeletal elements*, [Online] , Available from: <http://www.uwm.edu/Dept/Grad_Sch/McNair/Summer01/jackieorcholl.htm > [2004, 29 March].

Perry, J., Easterday, C. S. & Antonelli, D. J. 1981, 'Surface versus intramuscular electrodes for electromyography of superficial and deep muscles', *Physical Therapy*, vol. 61, no. 1, pp. 7-15.

Plonsey, R. & Barr, R. C. 2000, *Bioelectricity, A Quantitative Approach*, Kluwer Academic / Plenum, New York.

Plonsey, R. 1984, 'Quantitative formulations of electrophysiological sources of potential fields in volume conductors', *IEEE Transactions on Biomedical Engineering*, vol. 31, no. 12, pp. 868-872.

Rainoldi, A., Galardi, G., Maderna, L., Comi, G., Lo Conte, L. & Merletti, R. 1999, 'Repeatability of surface EMG variables during voluntary isometric contractions of the biceps brachii muscle', *Journal of Electromyography and Kinesiology*, vol. 9, pp. 105-119.

Rainoldi, A., Nazzaro, M., Merletti, R., Farina, D., Caruso, I. & Gaudenti, S. 2000, 'Geometrical factors in surface EMG of the vastus medialis and lateralis muslces', *Journal of Electromyography and Kinesiology*, vol. 10, pp. 327-336.

Rau, G., Disselhorst-Klug, C. & Silny, J. 1997, 'Noninvasive approach to motor unit characterization: muscle structure, membrane dynamics and neuronal control', *Journal of Biomechanics*, vol. 30, no. 5, pp. 441-446.

Rau, G. & Disselhorst-Klug, C. 1997, 'Principles of High-Spatial-Resolution Surface EMG (HSR-EMG): Single Motor Unit Detection and Application in the Diagnosis of Neuromuscular Disorders', *Journal of Electromyography and Kinesiology*, vol. 7, no. 4, pp. 233-239.

Reucher, H., Rau, G., Silny, J. 1987a, 'Spatial filtering of noninvasive multielectrode EMG: part 1- Introduction to measuring technique and applications', *IEEE Transactions on Biomedical Engineering*, vol. 34, no. 2, pp. 98-105.

Reucher, H., Silny, J. & Rau, G. 1987b, 'Spatial filtering of noninvasive multielectrode EMG: part 2 - Filter performance in theory and modeling', *IEEE Transactions on Biomedical Engineering*, vol. 34, no. 2, pp. 106-113.

Roeleveld, K., Blok, J. H., Stegeman, D. F. & Van Oosterom, A. 1997a, 'Volume conduction models for surface EMG; confrontation with measurements', *Journal of Electromyography and Kinesiology*, vol. 7, no. 4, pp. 221-232.

Roeleveld, K., Blok, J., Arends, T., Stegeman, D. & Vingerhoets, D. 1997b, 'Long distance spread of surface EMG over the skin: a new hypothesis', *Electroencephalography and Clinical Neurophysiology*, vol. 103, no. 1, p. 221-221.

Roeleveld, K., Stegeman, D. F., Vingerholets, H. M., Van Oosterom, A. 1997c, 'Motor unit potential contribution to surface electromyography', *Acta Physiologica Scandinavica*, vol 160, no 2, p. 175 – 183.

Roeleveld, K., Sandberg, A., Stalberg, E. V. & Stegeman, D. F. 1998, 'Motor unit size estimation of enlarged motor units with surface electromyography', *Muscle and Nerve*, vol. 21, no. 7, pp. 878-886.

Sadoyama, T., Masuda, T., Miyata, H. & Katsuta, S. 1988, 'Fiber conduction velocity and fiber composition in human vastus lateralis', *European journal of Applied Physiology and Occupational Physiology*, vol. 57, pp. 767-771.

Sale, D. G. 2002, *Strength training: Neural adaptation*, [Online], Department of Kinesiology, McMaster University, Hamilton, Canada, Available from: <http://www.sportsci.org/encyc/drafts/Strength_neural_mech.doc> [2004, 29 March].

Saitou, K., Okada, M. & Sadoyama, T. 1990, 'Effect on surface EMG waveforms of electrode location with respect to the neuromuscular junctions: its significance in EMG-muscle length relation', *Proceedings of the 8th Congress of ISEK*, Baltimore, pp. 27-30.

Schneider, J., Silny, J. & Rau, G. 1991, 'Influence of tissue inhomogeneities on noninvasive muscle fiber conduction velocity measurements - investigated by physical and numerical modeling', *IEEE Transactions on Biomedical Engineering*, vol. 38, no. 9, pp. 851-860.

Schulte, E., Farina, D., Merletti, R., Rau, G. & Disselhorst-Klug, C. 2004, 'Influence of muscle fibre shortening on estimates of conduction velocity and spectral frequencies from surface electromyographic signals', *Medical & Biological Engineering and Computing*, vol. 42, pp. 477-486.

Solomonow, M., Baratta, R., Bernardi, M., Zhou, B., Lu, Y., Zhu, M. & Acierno, S. 1994, 'Surface and wire EMG crosstalk in neighbouring muscles', *Journal of Electromyography and Kinesiology*, vol. 4, no. 3, pp. 131-142.

Stalberg, E. & Antoni, L. 1980, 'Electrophysiological cross section of the motor unit', *Journal of Neurology, Neurosurgery and Psychiatry*, vol. 43, pp. 469-474.

Stegeman, D. F., Blok, J. H., Hermens, H. J. & Roeleveld, K. 2000, 'Surface EMG models: properties and applications', *Journal of Electromyography and Kinesiology*, vol. 10, pp. 313-326.

Stegeman, D. F., Dumitru, D., King, J. C. & Roeleveld, K. 1997, 'Near- and Far-Fields: Source Characteristics and the Conducting Medium in Neurophysiology', *American Clinical Neurophysiology Society*, vol. 14, no. 5, pp. 429-442.

Sun, T. Y., Lin, T. S. & Chen, J. J. 1999, 'Multielectrode surface EMG for noninvasive estimation of motor unit size', *Muscle and Nerve*, vol. 22, no. 8, pp. 1063-1070.

The Baltimore Longitudinal Study of Aging, T. B. 1998, *Data elements found in body composition*, [Online], Gerontology Research Center, Baltimore, Maryland, 2004, Available from: <http://blswww.grc.nia.nih.gov/i161/info161.htm> [2004, 29 March].

Troni, W., Cantello, R. & Tainero, I. 1983, 'Conduction velocity along human muscle fibers in situ', *Neurology*, vol. 33, pp. 1453-1459.

Van Steenwijk, R. 1986, 'Concept of local resolution in the design of lead-off electrode systems', *Medical & Biological Engineering and Computing*, vol. 24, pp. 616-624.

Van Vlugt, J. P. P. & Van Dijk, J. G. 2000, 'A convenient method to reduce crosstalk in surface EMG', *Clinical Neurophysiology*, vol. 112, pp. 583-592.

Webster, J. G. 1998, *Medical instrumentation. Application and design*, John Wiley and Sons, Inc., New York.

Winter, D. A., Fuglevand, A. J. & Archer, S. E. 1994, 'Crosstalk in surface electromyography: Theoretical and practical estimates', *Journal of Electromyography and Kinesiology*, vol. 4, no. 1, pp. 15-26.

Zhao, X., Kinouchi, Y., Yasuno, E., Gao, D., Iritani, T., Morimoto, T. & Takeuchi, M. 2004, 'A new method for noninvasive measurement of multilayer tissue conductivity and structure using divided electrodes', *IEEE Transactions on Biomedical Engineering*, vol. 51, no. 2, pp. 362-370.

Zwarts, M. J., Drost, G. & Stegeman, D. F. 2000, 'Recent progress in the diagnostic use of surface EMG for neurological diseases', *Journal of Electromyography and Kinesiology*, vol. 10, pp. 287-291.